INFORMATION TO USERS

This manuscript has been reproduced from the microfilm master. UMI films the text directly from the original or copy submitted. Thus, some thesis and dissertation copies are in typewriter face, while others may be from any type of computer printer.

The quality of this reproduction is dependent upon the quality of the copy submitted. Broken or indistinct print, colored or poor quality illustrations and photographs, print bleedthrough, substandard margins, and improper alignment can adversely affect reproduction.

In the unlikely event that the author did not send UMI a complete manuscript and there are missing pages, these will be noted. Also, if unauthorized copyright material had to be removed, a note will indicate the deletion.

Oversize materials (e.g., maps, drawings, charts) are reproduced by sectioning the original, beginning at the upper left-hand corner and continuing from left to right in equal sections with small overlaps.

Photographs included in the original manuscript have been reproduced xerographically in this copy. Higher quality 6" x 9" black and white photographic prints are available for any photographs or illustrations appearing in this copy for an additional charge. Contact UMI directly to order.

ProQuest Information and Learning
300 North Zeeb Road, Ann Arbor, MI 48106-1346 USA
800-521-0600

NULL STEERING AND PATTERN CONTROL IN SMART ANTENNA ARRAYS

BY

NADEEM ATHER

A Thesis Presented to the

DEANSHIP OF GRADUATE STUDIES

KING FAHD UNIVERSITY OF PETROLEUM & MINERALS

DHAHRAN, SAUDI ARABIA

In Partial Fulfillment of the
Requirements for the Degree of

MASTER OF SCIENCE

In

ELECTRICAL ENGINEERING

March 2001

UMI Number: 1406107

Bell & Howell Information and Learning Company
300 North Zeeb Road
P.O. Box 1346
Ann Arbor, MI 48106-1346

KING FAHD UNIVERSITY OF PETROLEUM & MINERALS
DHAHRAN 31261, SAUDI ARABIA

DEANSHIP OF GRADUATE STUDIES

This thesis, written by **NADEEM ATHER** *under the direction of his Thesis Advisor and approved by his Thesis Committee, has been presented to and accepted by the Dean, Deanship of Graduate Studies, in partial fulfillment of the requirements for the degree of*

MASTER OF SCIENCE *in* **ELECTRICAL ENGINEERING.**

Thesis Committee

Mahmoud M. Dawoud 19/5/2001
Prof. Mahmoud M. Dawoud (Chairman)

19/5/2001
Dr. Samir Abdul-Jauwad (Member)

21/5/2001
Dr. Al-Jamid, Hussain A. (Member)

22/5/2001
Dr. Samir A. Al-Baiyat
(Department Chairman)

Prof. Osama A. Jannadi
(Dean, Deanship of Graduate Studies)

Date: 23/5/2001

عمادة الدراسات العليا
DEANSHIP OF GRADUATE STUDIES

Dedicated to

My Parents

whose prayers and perseverance led to this accomplishment

Acknowledgements

All praise and glory be to Allah, the cherisher and sustainer of the worlds, most gracious and most merciful, whose boundless guidance and support has led to this accomplishment. May peace and blessings of Allah be upon Prophet Muhammad.

I acknowledge the support of King Fahd University of Petroleum and Minerals during the tenure of this research. My cordial thanks are due to my thesis advisor Prof. Mahmoud M. Dawoud for the knowledge, guidance and encouragement he has provided throughout this research. Thanks are also due to my committee members Dr. Samir Abdul-Jauwad and Dr. Al-Jamid, Hussain A. for their helpful suggestions, appreciation and kind cooperation.

I am also grateful to the department chairman Dr. Samir Al-Baiyat for his kind cooperation. I express my heartfelt thanks to the faculty members, staff and my friends form the research community who made my stay at KFUPM a vivacious and memorable one.

My profound acknowledgements are to my parents and family members for their motivation and source of moral support during hard times.

Contents

List of Figures

List of Tables

Abstract

Name: **Nadeem Ather**

Title: **Null Steering and Pattern Control in Smart Antenna Arrays**

Major Field: **Electrical Engineering**

Date of Degree: **March 2001**

Smart Antennas are used in modern mobile communication systems to enhance the desired signal and suppress the interference arising due to Co-Channel Interference (CCI), Adjacent Channel Interference (ACI) and multipath. Null Steering and Pattern Control in Tracking Beam Smart Antenna Arrays is carried out to combat these interferences. A Numerical Pattern synthesis algorithm is used to synthesize the desired pattern with main beam in the direction of the desired signal and nulls in the direction of the interferences. Complex weight (Amplitude and Phase) perturbations are used to achieve the desired Array Pattern. The ESPRIT algorithm is used to estimate the Direction Of Arrival (DOA) of the signals. In the DOA estimation, signal environments wherein, signals uncorrelated with each other and signals completely correlated (Coherent multipath) are considered. Simultaneous estimation of both DOA and frequency is also done to deal with ACI. The effect of change in number of elements of the array, SNR of the signals and separation between the signals is also studied. It is seen that in the estimation of DOA the ESPRIT algorithm outperformed the most widely used MUSIC algorithm for real time implementation.

Master of Science Degree

King Fahd University of Petroleum and Minerals

Dhahran, Saudi Arabia

March 2001

ملخص الرسالة

الاسم : نديم اقمر

العنوان : توجيه أصفار وتحكم شكل الإشعاع في مصفوفات الهوائيات الذكية

الدرجة : ماجستير

التخصص: الهندسة الكهربائية

التاريخ : ذو الحجة ١٤٢١هـ

تستخدم الهوائيات الذكية في نظم الاتصالات المتحركة الحديثة لتحسين الإشارات المرغوب فيها وإخماد التداخلات الناتجة عن كل من : تداخل من القنوات المختلطة (CCI) ، تداخل من القنوات المتجاورة (ACI) والطرق المتعددة. الأصفار وتحم مشكل الإشعاع في مصفوفات الهوائيات الذكية ذات أحزمة متعقبة لمواجهة هذه التداخلات. واستخدم خوارزميات تركيب مشكل الإشعاع العددي لتركيب شكل ذات حزمة رئيسية في اتجاه الإشارة المرغوبة وأصفار في اتجاه التداخل. تستخدم اضطرابات ذات أثقال مركبة (المدى والزاوية) للوصول إلى شكل إشعاع المصفوفة المرغوبة. وتستخدم خوارزميات الاسبريت لتقدير اتجاه وصول الإشارة (DOA). في حالة تقدير اتجاه وصول درجة كل من المحيط الذي فيه الإشارة ، الإشارات غير المترابطة مع بعضها البعض ، وكذلك الإشارات المترابطة بشكل كامل (ترابط متعدد الطرق). ودرس كذلك التقدير المتزامن لكم من اتجاه الوصول (DOA) والتردد للتعامل مع تداخل القنوات المتجاورة (ADI). ونقش كذلك تأثير التغير في عدد العناصر في المصفوفة ونسبة الإشارة إلى الضوضاء (SNR) والفواصل بين الإشارات. ولقد وجد أن تقدير اتجاه الوصول في الاسبريت (ESPRIT) تتفوق في الأعداد على خوارزميات ميوزيك (MUSIC) واسعة الاستخدام في تنفيذ الزمن الحقيقي.

درجة الماجستير في العلوم

جامعة الملك فهد للبترول والمعادن

الظهران – المملكة العربية السعودية

ذو الحجة ١٤٢١هـ

CHAPTER 1

INTRODUCTION

1.1 Background

The demand for wireless communication has experienced an unprecedented growth in the past few years and future predictions show no sign of saturation [1]. The anticipation is to provide anyone, anywhere and anytime with mobile communication service at low cost, high quality and high data rates. Therefore it requires a state of art communication technique. Smart Antennas have to be generally employed in such cases. Smart Antennas open a new dimension "*Space*" along with multiple access in Frequency, Time or Code. Spatially selective transmission and reception of RF energy offers enormous potential to improve performance including range and capacity. Thus spatial processing introduces a new degree of freedom in the system design.

The main impediments to the high performance wireless communications are Inter Symbol Interference (ISI) due to the signal delay of going through the multipath channel and Co-Channel Interference (CCI) due to multiple access. Co-Channel Interference

limits the system capacity and Inter Symbol Interference has a profound effect on the performance of the Bit Error Rate (BER). Also the system capacity can be affected by Adjacent Channel Interference (ACI) due to signals adjacent in frequency to the desired signal. However since these interferences arrive at the receiver from different directions, spatial processing can be used to mitigate them. Signals separated in the spatial domain possess distinct *Spatial Signatures*. This is the *fundamental* property exploited by Smart Antenna Systems (SAS).

The purpose of this study is to investigate the capability of Smart Antenna Systems with regard to the estimation of the Directions Of Arrival of the signals and synthesizing the array pattern with maximum gain in the desired direction and steering the nulls to the directions of interferers.

1.2 Introduction to Smart Antenna Systems

1.2.1 General Concept

In truth antennas are not smart but antenna systems are smart. Generally co-located with a base station, a Smart Antenna System combines an antenna array with a real time signal processing capability to transmit and receive in an adaptive, spatially selective manner [2]. In other words, such a system can automatically change the direction of its radiation pattern in response to its signal environment. A typical functional diagram of a SAS is shown in Figure 1.2-1.

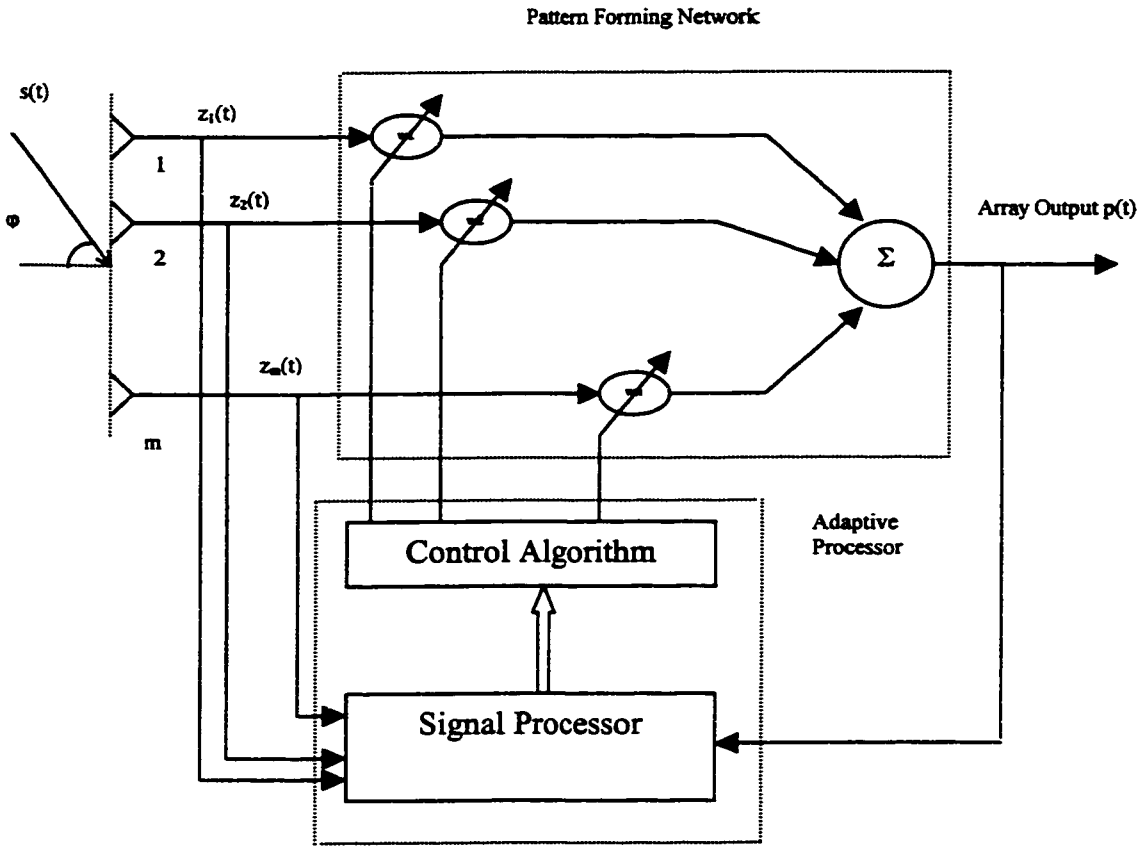

Figure 1.2-1: Functional diagram of a Smart Antenna System

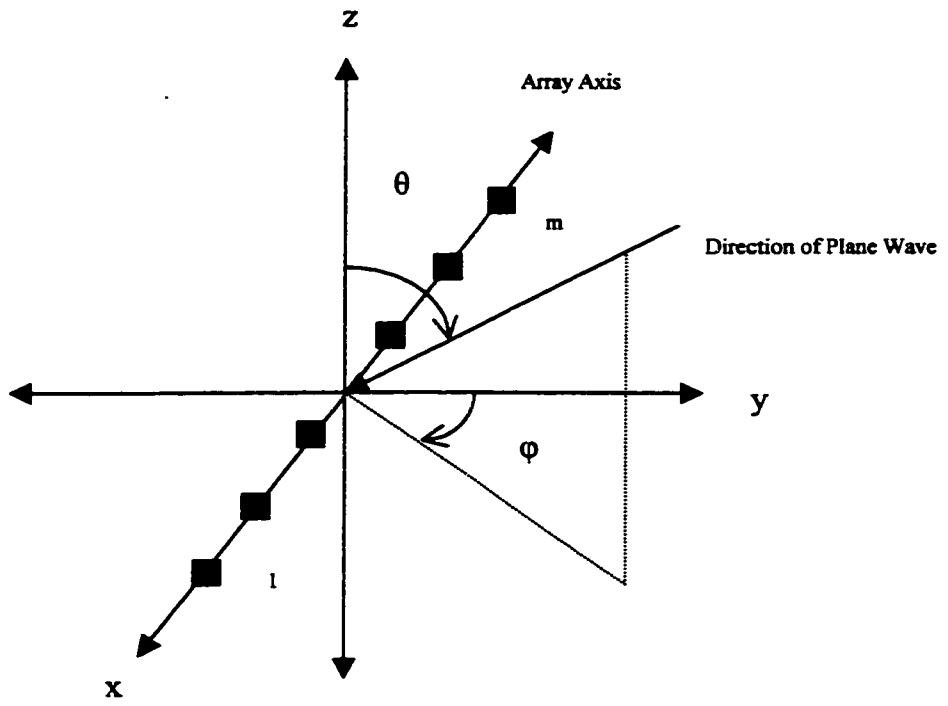

Figure 1.2-2: A plane wave incident on a Linear Equally Spaced (LES) Array

Figure 1.2-2 shows a plane wave incident on an *m* element Linear Equally Spaced array of isotropic elements. The direction of arrival of the plane wave is given by the angle (θ, φ). θ is the elevation angle and φ represents the azimuth angle. For a plane wave incident in the x-y plane, which represents the horizon, $\theta = 90^0$. This is a valid assumption for most of the cellular smart antenna applications. In such a case the azimuthal angle φ gives the true DOA of the incident wave.

For an incident signal wave front s(t), the received signal at the antenna element *i* (assumed to be noiseless) is given by

$$z_i(t) = Cs(t)e^{-jk(i-1)d\sin(\varphi)\sin(\theta)} \qquad (1.1)$$

Where,

C = Arbitrary gain constant

$k = 2\pi / \lambda$ is the phase propagation factor

d = Distance between the elements

λ = Wavelength corresponding to carrier frequency (f)

The signal p(t) at the array output is given by

$$p(t) = Cs(t) \sum_{i=1}^{m} w_i e^{-jk(i-1)d\sin(\varphi)\sin(\theta)} \quad (1.2)$$

$$= Cs(t)f(\theta, \varphi) \quad (1.3)$$

The term $f(\theta, \varphi)$ is called the *array factor*. The array factor determines the ratio of the received signal available at the array output, p(t) to the signal Cs(t) measured at the reference element, as a function of the Direction of Arrival (θ, φ). In the plane representing the horizon, $\theta = 90^0$, array factor can be written as $f(90^0, \varphi)$ which can be as well represented as $f(\varphi)$ without loss of generality. By adjusting the set of complex weights $\{w_i\}$, it is possible to direct the maximum of the main beam of the array factor in any direction φ_0. To see how the weights $\{w_i\}$ can be used to change the antenna pattern of the array, the i^{th} weight is given by

$$w_i = e^{jk(i-1)d\sin(\varphi_0)} \quad (1.4)$$

Then the array factor reduces to

$$f(\theta) = \sum_{i=1}^{m} e^{-jk(i-1)d\,(\sin(\varphi) - \sin(\varphi_o))} \tag{1.5}$$

$$= \frac{\sin\left(\frac{\beta md}{2}(\sin(\varphi) - \sin(\varphi_o))\right)}{\sin\left(\frac{\beta d}{2}(\sin(\varphi) - \sin(\varphi_o))\right)} e^{-j\frac{\beta d}{2}(\sin(\varphi) - \sin(\varphi_o))} \tag{1.6}$$

Thus by varying a single parameter φ_o, the beam can be steered to any desired direction.

In general working with array antennas, it is very convenient to make use of vector notation. Defining the weight vector as

$$w = [w_1 \ \ldots\ldots \ w_m]^T \tag{1.7}$$

where, the superscript T represents transpose.

The signals from antenna elements are grouped in a data vector

$$z(t) = [z_1 \ \ldots\ldots \ z_m]^T \tag{1.8}$$

Then the array output p(t) can be expressed as the inner product of the array weight vector w, and the data vector z(t).

$$p(t) = w^T z(t) \tag{1.9}$$

The array factor in the direction of φ is

$$f(\varphi) = w^T a(\varphi) \tag{1.10}$$

The vector a(φ) is called the *"steering vector"* in the direction φ. Given a plane wave incident from a direction φ as illustrated in Figure 1.2-2, the steering vector a(φ) describes the phase of the signals available at each antenna element relative to the phase of the signal at the reference element (element 1). The steering vector can be expressed as

$$a(\varphi) = [1, a_1(\varphi)...a_m(\varphi)]^T \tag{1.11}$$

Where,

$$a_i(\varphi) = e^{-jk(i-1)d\sin(\varphi)} \tag{1.12}$$

A set of steering vectors either measured or calculated over all the values of φ is called *"array manifold"*. In addition to being useful in the analysis of arrays, knowledge of the array manifold is critical in direction finding, downlink Beamforming and other aspects of array operation. As stated above the angle φ is called the Direction of Arrival (DOA) of the received plane wave. It is also assumed that the multipath components arrive at the base station in the horizontal plane so that the azimuthal direction φ completely specifies the DOA.

Just as analyzed in the previous discussion, a discrete model is used to characterize the channel in the presence of multipath. Each multipath component is considered to be a plane wave arriving from a discrete direction at a discrete time delay. For a particular subscriber the channel between the portable transmitter and the base station receiver is modeled using the *Vector Channel Impulse Response* (VCIR).

$$h(\tau, t) = \sum_{i=1}^{L} a(\varphi_i)\alpha_i(t)\delta(\tau - \tau_i) \tag{1.13}$$

where, α_i, τ_i, and φ_i are the complex amplitude, path delay and DOA of the i^{th} multipath component. There are total L multipath components.

The vector channel impulse response relates the transmitted signal to the signal received at each antenna element of the array. Given a transmitted signal s(t), the data vector is given by:

$$z(t) = [z_1 \ \ldots\ldots \ z_m]^T$$

$$= s(t)*h(\tau, t) + n(t) \tag{1.14}$$

$$= \sum_{i=1}^{L} a(\varphi_i)\alpha_i(t)s(t - \tau_i) + n(t) \tag{1.15}$$

where, n(t) is the vector representing the noise introduced at each antenna element.

The concepts outlined in this section form the fundamental basis for both spatial processing receivers and transmission beamforming systems. When arrays are used at the base station, spatial processing receivers are used to enhance and separate reverse link signals. Spatial processing, when used for transmission at the base station is called down link Beamforming or forward link beamforming.

1.2.2 Types of Smart Antenna Systems

Terms commonly heard today that embrace various aspects of a smart antenna technology include intelligent antennas, phased array, SDMA, spatial processing, adaptive antenna systems etc. However, Smart Antenna Systems are customarily categorized as either Switched beam SAS or Tracking Beam (Adaptive Array) SAS. Both systems attempt to increase the gain according to the location of the user. However, only the adaptive system provides optimal gain while simultaneously identifying, tracking and minimizing interfering signals. It's the adaptive systems active interference strategy and additional gain that provide substantial performance advantages and flexibility over the more passive switched beam approach. The following are distinctions between the two major categories of smart antennas regarding the choices in transmit strategy.

Switched Beam SAS

The traditional switched beam approach is an extension of the current cellular sectorization method in which a typical sectorized cell site has three 120 degree macro sectors. The switched beam approach further subdivides macro-sectors into several micro sectors. Each micro sector contains a predetermined fixed beam pattern with the greatest sensitivity located in the center of the beam and less sensitivity elsewhere. The switched beam system establishes certain choices of beam patterns before deployment and selects from one of several choices during operation. When the mobile user enters a particular macro sector, the switched beam system selects the micro sector containing the strongest signal. Through out the call, the system monitors signal strength and switches to other fixed micro sectors as required.

There are however limitations to switched beam system. Because the beams are predetermined, the signal strength varies as the user moves through the sector. As a mobile unit moves towards the far azimuth edges of a beam, the signal strength can degrade rapidly before the user is switched to another micro sector. This phenomenon is called *"scalloping"*. Also the interference entering through the side lobes cannot be nulled. This is shown in Figure 1.2-3.

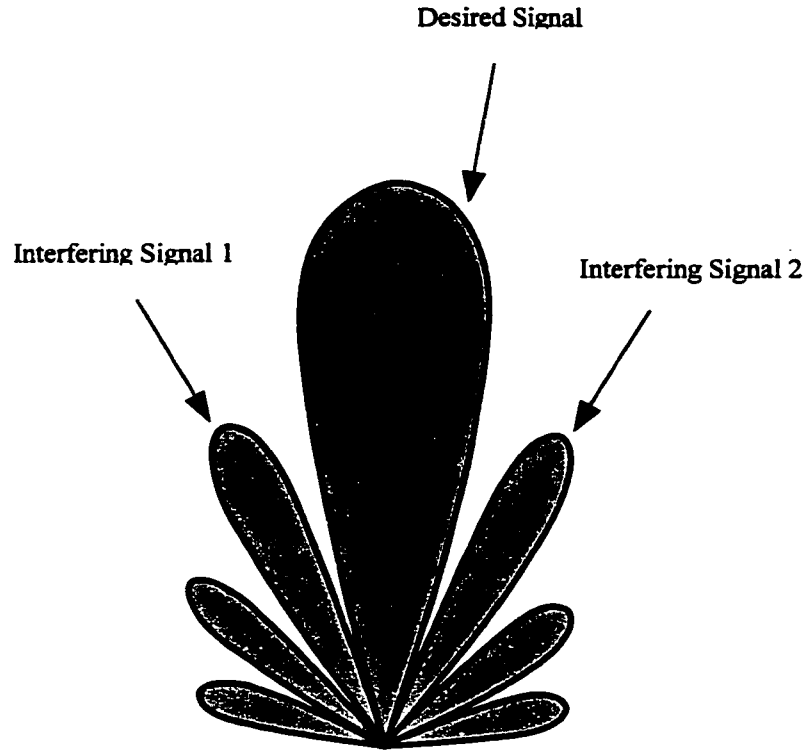

Figure 1.2-3: Typical beam selection in Switched Beam SAS. Desired direction lying along the sloping edge of the main beam and interferers lying along the side lobes

Adaptive Array SAS

The adaptive array systems take a different approach. By adjusting to an RF environment as it changes, adaptive antenna technology can dynamically alter the radiation pattern to optimize the performance of the wireless system. The adaptive approach utilizes

sophisticated signal processing algorithms to continuously distinguish between desired signals, multipath and interfering signals as well as calculate their directions of arrival. The adaptive approach continuously updates its beam pattern based on the changes in both desired and interfering signal locations. The ability to smoothly track users with main lobes and interferers with nulls insures that the link budget is constantly maximized. A typical beam forming strategy is shown in Figure 1.2-4.

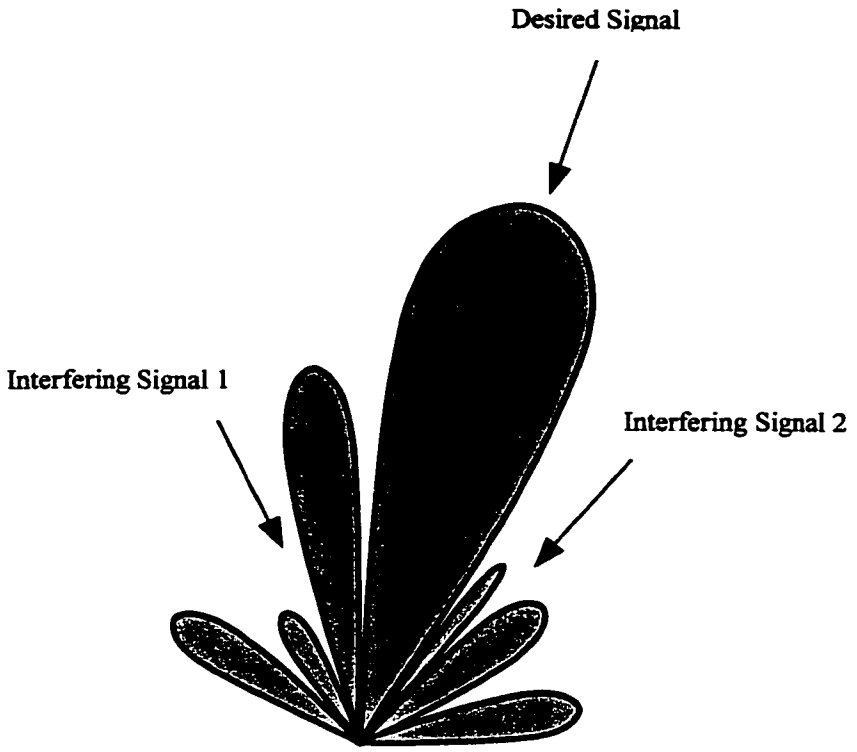

Figure 1.2-4:Typical beam formation in Adaptive SAS. Desired direction along the main beam direction and nulls along the interfering directions

1.2.3 Smart Antenna Benefits

Smart Antennas offer a broad range of ways to improve wireless system performance. In general Smart Antennas have the potential to provide enhanced range and reduced

infrastructure costs in early deployments and increased long term system capacity. These two major benefits are discussed below.

Range Extension

Smart Antennas provide enhanced coverage through range extension. Given the same transmitted power output at the base station and subscriber unit, smart antennas can increase range by increasing the gain of the base station antenna. The uplink power received from a mobile unit at a base station is given by

$$P_r = P_t + G_s + G_b - PL \tag{1.16}$$

Where,

P_r = Power received at the base station (dBW)

P_t = Power transmitted by the subscriber (dBW)

G_s = Gain of the subscriber unit (dB)

G_b = Gain of the base station antenna (dB)

PL = Path Loss (dB)

On the uplink, if a certain received power $P_{r\text{-}min}$ is required at the base station, by increasing the gain of the base station G_b, the link can tolerate greater path loss PL (PL is proportional to distance between base station and subscriber unit). Thus by increasing the tolerable path loss, the reception range of the base station can be increased. Smart

Antenna systems can increase the base station range form 20 – 200 per cent depending on environmental circumstances and hardware/software used [3].

Capacity Enhancement

Smart Antennas can improve system capacity. Smart Antennas can be used to allow the subscriber and base station to operate at the same range as a conventional system, but at lower power. This may allow FDMA and TDMA systems to be rechannelized to reuse frequency channels more often than systems using conventional fixed antennas, since the carrier-to-interference ratio is much greater when smart antennas are used. In CDMA systems, if Smart Antennas are used to allow subscribers to transmit less power for each link, then the Multiple Access Interference is reduced, which increases the number of simultaneous subscribers that can be supported in each cell.

Smart Antennas can also be used to spatially separate signals, allowing different subscribers to share the same spectral resources, provided that they are spatially separable at the base station. This *Space Division Multiple Access* (SDMA) allows multiple users to operate in the same cell on the same frequency/time slot provided, using Smart Antennas to separate the signals. Since this approach allows more users to be supported within a limited spectrum allocation, compared with conventional antennas, SDMA can lead to improved capacity.

1.3 Literature Review

1.3.1 Smart Antenna Implementation

Many authors have given contributions to the field of adaptive antenna arrays for wireless communications. Godara's papers [4, 5] form an excellent review and introduction to the topic in a comprehensive way with many references. The textbooks by Compton [6], Mozingo/Miller [7], Hudson [8] and the reference paper by W.F Gabriel [9] provide excellent introductions to the general theory of adaptive antenna arrays. A lot of research is going on in implementing Smart Antennas in the existing 2nd Generation mobile communications and future 3rd Generation systems. Roy [10] gave a brief description of some of the current technical challenges facing wireless service providers. Historical attempts to address these challenges and Smart Antenna technology as a solution are presented. In [11] the experimental results demonstrating the efficacy of Smart Antenna technology involving SDMA in improving the capacity and coverage is given. The use of spatial and temporal processing in improving the performance in mobile radio communications is presented in [12, 13].

Application of Smart Antennas in wireless systems using CMDA, GSM and IS – 136 in different environments and performance analysis is carried out by Jack H. Winters in [14]. Rappaport and Liberti Jr. [2] gave in depth concepts of use of Smart Antennas in IS – 95 and Third Generation CDMA applications. A thorough investigation of the comparison of Tracking Beam Array and Switching Beam Array is done by Choi et al in [15].

Focusing our attention on the interference suppression techniques in Smart Antenna System, various beamforming and null steering strategies have been proposed to combat interference. One of the earliest forms of quasi-adaptive generic arrays is the side lobe canceller (SLC) discussed in [16]. Sng et al [17] suggested a new Generalized Sidelobe Canceller (GSC) beam forming structure where in the weight updates are calculated based on the steering vectors corresponding to the DOAs of the jammers. This research was further extended in [22] to reduce the adaptive dimension of the array. Zooghby et al in their recent research paper [18] carried out multiple source tracking with neural network based Smart Antennas. The proposed neural multiple source tracking (N-MUST) algorithm is used to perform DOA. The experimental validation of this proposed work is presented in [19]. Zetterberg and Ottersen [20] investigated the spectrum efficiency gain using transmitting antenna arrays at the base station. The proposed system estimates the angular positions of the mobiles from the received data and allows multiple mobiles to be allocated to the same channel within the cell. Ponnikanti and Sali [21] devised an effective adaptive antenna scheme to prevent the desired signal cancellation in optimal weight vector computation of the beamformer.

Kozick et al [23] investigated the effect of steering the individual element pattern along with adjusting complex weights to improve the performance of adaptive arrays. Choi et al [24] proposed a new technique based on Lagrange formula to calculate the weight vector in a Smart Antenna System. They showed a decrease in computational load in computing the weight vector.

Effective interference cancellation scheme based on smart antennas is suggested in [25]. Haimovic and Shah [26] suggested suppression of narrow band interference in CDMA communications using spatial processing. Ibars et al [27] used Smart Antennas to mitigate Co-Channel interference arising as a result of decreasing the frequency re-use factor (from 7 to 3). Also in another paper [28] Saleeb and Adel designed a smart antenna to suppress Co- Channel interference. They showed a 75 per cent increase in number of channels per cell.

1.3.2 DOA Estimation Techniques

Array based Direction Of Arrival estimation can be broadly classified into the following categories.

- Conventional techniques
- Subspace based techniques

Conventional techniques

These are also called Spectral Estimation techniques. DOA are estimated by computing the spatial spectrum and then determining local maxima or peaks [29, 30]. One of the earliest spectral estimation methods is the Barlett method [31]. Capon [32] suggested a minimum variance method with better resolution properties than Barlett method. Burg [33] suggested a method that finds the power spectrum such that its Fourier transform equals the measured correlation subjected to the constraint that its entropy is maximized.

Subspace based techniques

One of the earliest and most popular subspace based technique for direction finding is the MUltiple Signal Classification (MUSIC) algorithm, the one proposed by Schnidt in 1979 [34, 35]. Here the space is divided into Signal and Noise subspace. The noise subspace is spanned by the eigen vectors corresponding to the smallest Eigenvalues of the data correlation matrix. The steering vectors corresponding to the directions of the incident signals will be orthogonal to the noise subspace which are reflected as peaks in the MUSIC spectra. As such the entire Array Manifold $a(\omega)$ has to be searched before all the peaks corresponding to the true DOA are estimated. Therefore the process is time consuming. The MUSIC algorithm has been implemented and its performance experimentally verified in [36]. Various modifications have been made to the MUSIC algorithm to increase the resolution and decrease the computational complexity. Cyclic MUSIC, which exploits the spectral coherence properties of the signals to improve the performance of the conventional MUSIC algorithm has been proposed in [37]. Barabell [38] developed the Root MUSIC algorithm based on polynomial rooting and provides higher resolution.

The Estimation of Signal Parameters via Rotational Invariance Technique (ESPRIT) algorithm is another subspace-based DOA estimation technique developed by Roy et al. [39-42]. ESPRIT dramatically reduces the computational and storage requirements of MUSIC and does not involve an exhaustive search through all possible steering vectors to estimate the DOA. Chen and Chen [48] used ESPRIT algorithm along with marked subspace technique to perform joint estimates of both DOA and frequency. The

parameters (frequencies and powers) of cissoids (Complex Sinusoids) in noise were estimated using ESPRIT by Roy et al [50].

DOA Estimation under coherent signal conditions

Only under uncorrelated conditions does the source covariance matrix satisfy the full rank condition, which is the basis of the subspace-based algorithms. Under the presence of highly correlated or coherent signals the performance of these algorithms degrades rapidly. The situation can be dealt with by modification of the covariance matrix through a preprocessing scheme called *spatial smoothing*. One method of spatial smoothing proposed by Evans et al [43] and further expanded by Shan et al [44] is based on averaging the covariance matrix of overlapping identical arrays. Pillai and Kwon presented a forward backward spatial smoothing technique in [49] An adaptive spatial smoothing technique was proposed by Takao and Kikuma [45]. The technique is based on the spatial averaging of the correlation matrices obtained by the subarrays that are extracted from the full array and partially overlapped with each other. Another form of spatial smoothing proposed by Haber and Zoltowski [46] involves moving the entire array structure during the time interval in which the covariances are estimated. Li and Compton [47] proposed a similar technique in which the Angle of Arrival of coherent signals is estimated using ESPRIT algorithm along with a single pair of antennas in motion. The approach exploits the Doppler frequency shifts caused by the doubler in motion.

1.3.3 Null Steering Techniques

The objective of steering nulls in the antenna array pattern in a particular direction is to mitigate the interferences arriving in that direction. This can be achieved by controlling

the amplitude and/or phase of the current induced on the elements of the array or by controlling the position of the elements of the array such that the array factor in that direction is zero (practically to a required depth, e.g. –60 dB with respect to the normalized maximum array factor of 0 dB). This mitigation is necessary in today's mobile communication environment in order to combat the various sources of interferences like Co-Channel interference, Adjacent channel interference etc. Null steering involving the above mentioned controllable variables are briefed below.

Element position perturbation method

This technique was developed by Ismail and Dawoud [51], where null steering is carried out by controlling the positions of the antenna array elements. This avoids the complicated use of amplitude and/or phase control systems and frees the phase shifters solely for steering the main beam towards the direction of the desired signal. An experimental verification was done in [52] wherein, null steering was achieved for an eight-element monopole over a ground plane. Single and double nulls were realized in the side lobe region. Dawoud et al [53] applied genetic algorithm and compared the results with analytical solution for array pattern nulling by element position perturbation. Null steering in scanned arrays by using position perturbations was carried out in [54].

Amplitude only control method

In this method the Amplitudes of the induced currents are controlled to achieve Null Steering. Mismer and Ismail [59] employed the method of amplitude only control to perform null steering by a linear programming technique using minimax approximation.

Liao and Chu [57] investigated the technique to steer the array nulls for planar arrays by controlling only the excitation current amplitudes based on genetic algorithms. Implementation was done in rectangular and circular planar arrays.

Phase only control method

In this method, only the phases of the currents induced on the elements are varied. Liao and Chu [56] used phase only null steering in linear arrays using a modified genetic algorithm to speed up the convergence rate. Numerical results for 20-element linear array with one to four imposed interferences were demonstrated. Ismail and Mismer [60] presented a new antenna configuration of dual phase shifters to steer multiple nulls by controlling the arbitrary phase perturbations. Steyskal demonstrated pattern nulling by phase perturbations in [61].

Complex weight control method

Here pattern synthesis is carried out by perturbing both phase and amplitude of the array elements. This is much efficient technique. The number of degrees of freedom in this case is twice the number of array elements resulting in better control of null steering. Mitchell et al [58] carried out array pattern synthesis with performance constraints in complex plane where genetic algorithm was applied on the roots of the array polynomial. Also Compton et al [55] presented a numerical technique to arrive at the complex weights, which gives a desired side lobe level in linear arrays.

1.4 Objectives of work

The objective of this work is to investigate and combine the techniques for Direction of Arrival and Null steering for suitable implementation in a Smart Antenna System. The proposed objectives of the work can be summarized as follows.

- Null Steering and Pattern Control in Tracking Beam (or Adaptive) Smart Antenna System is carried out. The linear array is employed.

- A Numerical Pattern Synthesis Algorithm is used for Null Steering and Pattern Synthesis. Complex weight (Amplitude and Phase) perturbations are used to achieve the desired Array Pattern.

- A comparison of DOA estimation by ESPRIT algorithm and by the most widely used MUSIC algorithm is carried out to choose the most suitable algorithm for our application.

- ESPRIT Algorithm is used for the Direction Of Arrival (DOA) estimation of the signals (Desired signal and Interfering signals).

- In the DOA estimation, signal environments wherein, signals uncorrelated with each other and signals completely correlated with each other (like coherent multipath) are studied.

- Simultaneous estimation of DOA and Frequency of signals is also carried out to combat Adjacent Channel Interference (ACI).

- The effect of SNR, separation between the signals and the number of elements of the array on the parameter estimation by ESPRIT is also carried out.

CHAPTER 2

DIRECTION OF ARRIVAL ESTIMATION

2.1 Introduction

This chapter provides a detailed overview of the Estimation of Signal Parameter via Rotational Invariance Techniques (ESPRIT) algorithm used for the Direction Of Arrival estimation of RF Signals in wireless systems using an antenna array. This is a subspace based DOA estimation technique, which exploits the Eigen structure of the array data covariance matrix. The subspace-based methods in general rely on the following properties of the data covariance matrix.

- The space (m dimensional) spanned by the array data covariance matrix is partitioned into two subspaces namely the Signal subspace (n dimensional) and the Noise subspace (m-n dimensional).
- The Signal subspace is spanned by Eigenvectors associated with larger Eigenvalues (corresponding to Signals) and the Noise subspace is spanned by Eigenvectors associated with smaller Eigenvalues (corresponding to noise).

- The Signal subspace and the Noise subspace are Orthogonal to each other.
- The Steering vectors Corresponding to the directional sources span the Signal subspace orthogonal to the Noise subspace.

ESPRIT reduces the computational and storage requirement inherent in other Subspace based algorithms (like MUSIC) and does not involve an exhaustive search through all possible steering vectors (in the Subspace) to estimate the DOA. ESPRIT derives its advantages by requiring that the sensor array have a structure that can be decomposed into two equal-sized identical sub-arrays with the corresponding elements of the two sub-arrays displaced from each other by a fixed translational distance. That is the array should possess displacement (translational) invariance and the sensors should occur in matched pairs with identical displacement. A typical array geometry illustrating the concept of sub-arrays is shown in Figure 2.1-1 Thus a Uniform Linear Array with four identical elements with inter element spacing d may be thought of as two sub-arrays one with first three elements and the other with the last three elements, where the corresponding elements of the two sub-arrays are separated by the distance d. The way ESPRIT exploits the sub-array structure to estimate the DOA is briefly described below. The flow chart of the implementation of the ESPRIT algorithm for the estimation of DOA and Frequency is shown in Figure 4.2-2 and Figure 4.3-2.

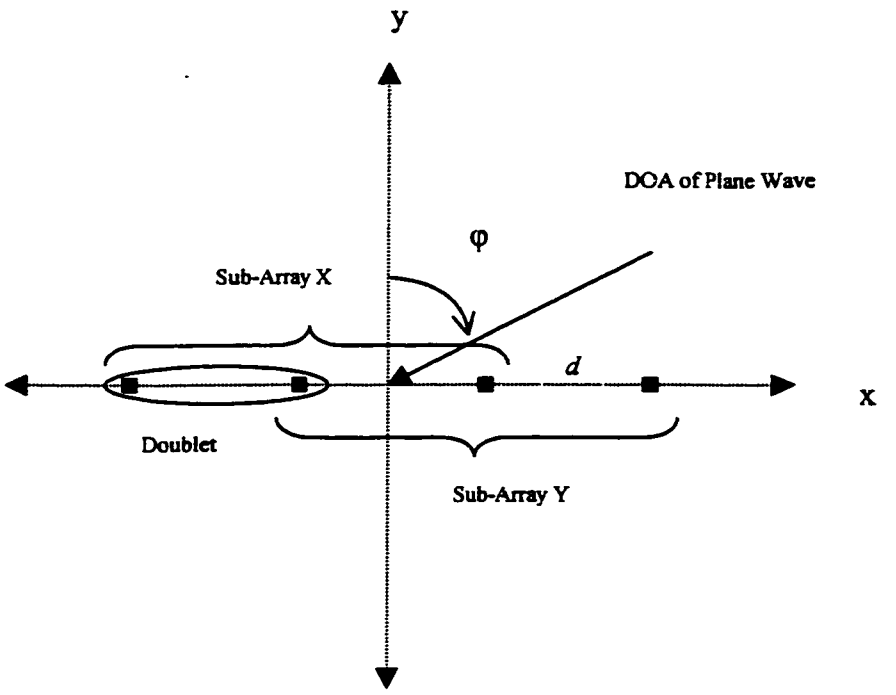

Figure 2.1-1: Illustration of ESPRIT Array Geometry

2.2 The ESPRIT Algorithm

Let the signals induced on the i^{th} doublet due to a narrow band source s(t) in the direction of φ be denoted by $x_i(t)$ and $y_i(t)$. The phase difference between the signals received at these two sensors of the doublet depends on the time taken by the plane wave arriving in a particular direction to travel from one sensor to another, which in turn depends on the distance between the sensors *'d'* and the DOA of the wave *'φ'*.

In general if there are *'n'* ($n \leq m$, where m is the number of sensors in the Array) narrow band sources, then the received signals at the Sub-Arrays X and Y (m-1 elements in each) are given by,

$$X(t) = AS(t) + N_X(t) \tag{2.1}$$

$$Y(t) = A\Phi S(t) + N_Y(t) \tag{2.2}$$

Where,

$X(t) = [x_1(t) \ldots x_{m-1}(t)]^T$ is a m-1 x 1 Vector at Sub-Array X

$Y(t) = [y_1(t) \ldots y_{m-1}(t)]^T$ is a m-1 x 1 Vector at Sub-Array Y

$N_X(t) = [u_1(t) \ldots u_{m-1}(t)]^T$ is a m-1 x 1 Vector of noise at Sub-Array X

$N_Y(t) = [v_1(t) \ldots v_{m-1}(t)]^T$ is a m-1 x 1 Vector of noise at Sub-Array Y

$S(t) = [s_1(t) \ldots s_n(t)]^T$ is a n x 1 Vector of impinging sources

$$\Phi = \begin{bmatrix} e^{(j\omega d \sin(\theta_1)/c)} & . & 0 \\ . & . & . \\ 0 & . & e^{(j\omega d \sin(\theta_n)/c)} \end{bmatrix} \text{ is a diagonal n x n matrix} \tag{2.2a}$$

$$A = [a(\varphi_1) \quad \ldots \quad a(\varphi_n)] \text{ is a m-1 x n Steering Vector matrix} \tag{2.2b}$$

Φ is a unitary matrix relating the measurements at Sub-Array X and Sub-Array Y and is aptly called as a *"rotation"* operator (which gives the name of the algorithm). $a(\varphi_i)$ is the Steering Vector corresponding to the direction of i^{th} source. $a(\varphi_i)$ is same as defined in Equation 1.11.

The auto covariance of the source matrix S is given by

$$R_{SS} = E\{S(t)S^*(t)\} \tag{2.3}$$

R_{SS} possesses a full rank n if all the signals are uncorrelated. The rank will be less than n if correlated signals are present. Also in the absence of noise, the number of non-zero Eigenvalues will be equal to the rank of R_{SS}.

The ESPRIT algorithm processing the data received at Sub-Arrays X and Y simultaneously is explained. With X(t) and Y(t) as defined in Equations 2.1 and 2.2, the total data matrix Z(t) (of length m) can be constructed as,

$$Z(t) = \begin{bmatrix} X(t) \\ Y(t) \end{bmatrix} \tag{2.4}$$

$$= \begin{bmatrix} A \\ A\Phi \end{bmatrix} S(t) + \begin{bmatrix} N_X(t) \\ N_Y(t) \end{bmatrix} \tag{2.5}$$

$$= \overline{A} S(t) + N(t) \tag{2.6}$$

where, $\overline{A}$ and N(t) are of dimensions (m x n) and (m x 1) respectively. Then the data covariance matrix

$$R_{ZZ} = E\{Z(t)Z^{*}(t)\}$$

$$= \overline{A} R_{SS} \overline{A}^{*} + \sigma^2 I \tag{2.7}$$

σ^2 is the variance of Additive uncorrelated white noise present at all sensors

I is the m x m Identity matrix.

$(.)^*$ denotes the complex conjugate transpose.

if $n \leq m$, then the $m - n$ Eigenvalues of R_{ZZ} are equal to σ^2. The n eigenvectors V_s corresponding to the n largest Eigenvalues satisfy the relation,

$$Range\{V_x\} = Range\{\bar{A}\} \tag{2.8}$$

Equation 2.8 states that V_s and $\bar{A}$ span the same n dimensional signal space. Now, since *Range* $\{V_s\}$ = *Range* $\{\bar{A}\}$, there must exist a unique nonsingular matrix T (n x n) such that

$$V_x = \bar{A}T \tag{2.9}$$

Further, the invariance structure (due to translational displacement of Sub-Arrays) of the array allows the decomposition of V_s into V_0 and V_1 such that

$$V_0 = AT \tag{2.10}$$

$$V_1 = A\Phi T \tag{2.11}$$

This implicates that

$$Range\ \{V_0\} = Range\ \{V_1\} = Range\ \{A\} \tag{2.12}$$

Since V_0 and V_1 also span the same n dimensional signal space, they can be mapped by a unique nonsingular transformation matrix Ψ.

$$V_0 \Psi = V_1 \tag{2.13}$$

Substituting Equations 2.10 and 2.11 in Equation 2.13, we get,

$$AT\Psi = A\Phi T \tag{2.14}$$

$$AT\Psi T^{-1} = A\Phi \tag{2.15}$$

Now assuming A to be full rank (i.e., non-singular), implies that,

$$T\Psi = \Phi T \tag{2.16}$$

From Equation 2.16, its evident that the Eigenvalues of Ψ must be equal to the diagonal elements of Φ and the column vectors of T are the Eigenvectors of Ψ. The DOA are obtained as non-linear functions of Eigenvalues of the operator Ψ that maps (rotates) one set of vectors V_0 that span the signal subspace to another set of vectors V_1.

In practice with only a finite number of noisy measurements $\hat{(.)}$ available, the conditions in Equations 2.8 and 2.12 are not satisfied. Hence finding a Ψ such that $\hat{V}_0 \Psi = \hat{V}_1$ is not possible. Therefore one must resort to Total Least Squares solution given by

The Total Least Squares solution

Having estimated $\hat{V}_0$ and $\hat{V}_1$ from the measured $\hat{R}_{zz}$ Ψ can be obtained from Equation 2.13 using the Total Least Squares criterion as follows

Compute the Eigen decomposition of

$$\hat{V}_{01}^{*}\hat{V}_{01} = \begin{bmatrix} \hat{V}_0^{*} \\ \hat{V}_1^{*} \end{bmatrix} \begin{bmatrix} \hat{V}_0 & \hat{V}_1 \end{bmatrix} = V\Lambda V^{*} \tag{2.17a}$$

and partition V into n x n submatrices

$$V = \begin{bmatrix} V_{11} & V_{12} \\ V_{21} & V_{22} \end{bmatrix} \tag{2.17b}$$

Then Ψ is given by

$$\Psi = -V_{12}V_{22}^{-1} \tag{2.18}$$

Once Ψ is obtained, its Eigenvalues, which correspond to the diagonal elements of Φ can be easily determined. Since the diagonal elements are related to DOA, as seen Equation 2.2a, the DOA can be directly computed.

2.3 DOA Estimation of Coherent Signals

Only under uncorrelated conditions does the source covariance matrix R_{SS} as defined in Equation (2.3) is non-singular and satisfies the full rank condition, which is the basis of the ESPRIT algorithm. Under the presence of highly correlated or coherent signals the performance of the algorithm degrades rapidly. The situation can be dealt with by modification of the covariance matrix through a preprocessing scheme called *spatial smoothing*. One method of spatial smoothing proposed by Evans et al [43] and further

expanded by Shan et al [44] is based on averaging the covariance matrix of overlapping identical arrays. Pillai and Kwon presented a forward backward spatial smoothing technique in [49].

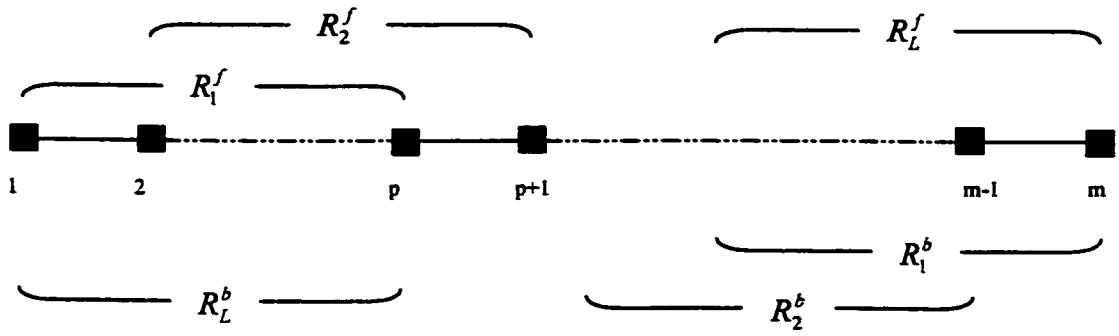

Figure 2.3-1: The forward / backward spatial smoothing scheme

The idea behind the spatial smoothing scheme is to let a linear uniform array with m identical sensors be divided into overlapping forward and backward sub arrays of size 'p' such that the sensor elements {1, ... p} form the first forward subarray and sensors {2, ... p+1} form the second forward subarray etc. similarly the backward subarray can be formulated. The subarray concept is shown in Figure 2.3-1. Let $Z_k(t)$ denote the vector of the received signals at k^{th} forward subarray. Based on the notation of Equation 2.10, we can model the signals received at each subarray as,

$$Z_k^f(t) = AF^{(k-1)}S(t) + N_k(t) \tag{2.19}$$

where, $F^{(k)}$ denote the k^{th} power of the diagonal matrix,

$$F = \text{diag}\{\upsilon_1, \ldots, \upsilon_n\} \tag{2.20}$$

$$\upsilon_i = \exp(-j(2\pi/\lambda)d\sin\varphi_i) \tag{2.21}$$

$$S(t) = [\kappa_1 s_1(t), \kappa_2 s_1(t) \ \ldots \ \kappa_n s_1(t)]^T \tag{2.22}$$

$$\kappa_i = \rho_i e^{j\alpha_i} \tag{2.23}$$

where, ρ_i and α_i are the amplitude attenuation and phase change of i^{th} signal with respect to the 1^{st} signal ($s_1(t)$; $\kappa_1=1$). Thus as seen from Equation 2.22, all the signals are coherent with the 1^{st} signal.

The covariance matrix of the k^{th} forward subarray is given by

$$R_k^f = AF^{(k-1)}R_{SS}F^{*(k-1)}A^* + \sigma^2 I \tag{2.24}$$

As stated earlier, R_{SS} does not satisfy the full rank condition. In fact with S(t) as given in equation 2.22, R_{SS} possesses a rank of 1. However, the application of Spatial Smoothing modifies R_{SS} to possess a full rank *n*. R_{SS} in Equation 2.24 reduces to Equation 2.25 under normalization $E\{|s_1(t)|^2\} = 1$.

$$R_{SS} = \kappa\kappa^* \tag{2.25}$$

$$\kappa = [\kappa_1, \kappa_2 \ \ldots \ \kappa_n]^T \tag{2.26}$$

The forward averaged spatially smoothed covariance matrix R^f is defined as the sample mean of the subarray covariance matrices:

$$R^f = \frac{1}{L}\sum_{1}^{L} R_k^f \tag{2.27}$$

where, L=m-p+1 is the number of subarrays. Now substituting Equation 2.24 in Equation 2.27, we obtain,

$$R^f = A\left(\frac{1}{L}\sum_{1}^{L} F^{(k-1)} R_{SS} (F^{(k-1)})^*\right) A^* + \sigma^2 I$$

$$= A R_{SS}^f A^* + \sigma^2 I \tag{2.28}$$

where, R_{SS}^f is the modified covariance matrix of the signals given by,

$$R_{SS}^f = \left(\frac{1}{L}\sum_{1}^{L} F^{(k-1)} R_{SS} (F^{(k-1)})^*\right) \tag{2.29}$$

Substituting Equation 2.25 in Equation 2.29 results in

$$R_{SS}^f = \frac{1}{L}\left[\kappa, F\kappa, F^2\kappa, \ldots, F^{L-1}\kappa\right]\begin{bmatrix} \kappa^* \\ (F\kappa)^* \\ (F^2\kappa)^* \\ . \\ . \\ (F^{L-1}\kappa)^* \end{bmatrix}$$

$$= \frac{1}{L} CC^{*} \tag{2.30}$$

where

$$C = \left[\kappa, F\kappa, F^{2}\kappa, \ldots, F^{L-1}\kappa\right]$$

$$= \begin{bmatrix} \alpha_1 & & & \\ & \alpha_2 & & \\ & & \ddots & \\ & & & \alpha_n \end{bmatrix} \begin{bmatrix} 1 & \nu_1 & \nu_1^2 & \ldots & \nu_1^{L-1} \\ 1 & \nu_2 & \nu_2^2 & \ldots & \nu_2^{L-1} \\ \vdots & \vdots & \vdots & \ddots & \vdots \\ 1 & \nu_n & \nu_n^2 & \ldots & \nu_n^{L-1} \end{bmatrix}$$

$$= DV \tag{2.31}$$

Clearly the rank of R_{SS}^{f} is equal to the rank of C. Since C=DV and the square matrix D is full rank, the rank of C is same as that of V. Now the rank of (n x L) matrix V is min(n ,L). Hence rank of V is n if and only if $L \geq n$. Thus for $L \geq n$, the covariance matrix R_{SS}^{f} will be non-singular regardless of the coherence of the signals [49].

Just as the array is split into overlapping forward subarrays, it can be split into overlapping backward subarrays such that the first backward subarray is formed using elements {m, m-1, ... n-p+1}, the second subarray is formed using elements {m-1, m-2, ..., m-p} and so on.

Similar to Equation 2.19, the complex conjugate of received signal vector at the k^{th} backward subarray can be expressed as,

$$Z_k^b = AF^{k-1}(F^{m-1}S)^* + N_k^* \tag{2.32}$$

The covariance matrix of the k[th] backward subarray is therefore given by

$$R_k^b = AF^{k-1}\bar{R}_{ss}(F^{k-1})^* A^* + \sigma^2 I \tag{2.33}$$

$$\bar{R}_{ss} = F^{-(m-1)}R_{ss}^*(F^{-(m-1)})^* \tag{2.34}$$

now the spatially smoothed backward subarray matrix R^b can be defiend as

$$R^b = \frac{1}{L}\sum_{k=1}^{L} R_k^b$$

$$= AR_{ss}^b A^* + \sigma^2 I \tag{2.35}$$

Again R_{ss}^b will be non-singular irrespective of the coherence of the signals.

Now the forward / backward smoothed covariance matrix $\hat{R}$ is defined as the mean of R^f and R^b, i.e.,

$$\hat{R} = \frac{R^f + R^b}{2} \tag{2.36}$$

2.4 Simultaneous Estimation of DOA and Frequency

Adjacent channel Interference (ACI) results from signals, which are adjacent in frequency to the desired signal. The cause of this is due to imperfect receiver filters that allow nearby frequencies to leak into the passband. In performing Null Steering in such a case, along with the DOA estimation, the estimation of the frequencies has to be done to extract correct information about the signal environment. This allows the association of DOA with their corresponding frequencies and differentiation of the desired signal can be made based on the estimated frequency. The array geometry for simultaneous estimation of both frequency and DOA is shown in Figure 4.3-1. The angle between the two arrays is ψ, which should not be equal to zero. The implementation of ESPRIT in such a case can be briefly explained as follows.

The data at the first array as shown in Figure 4.3-1 is given by Equations 2.37-2.39 similar to Equations 2.8 - 2.10.

$$Z_1(t) = \begin{bmatrix} X_1(t) \\ Y_1(t) \end{bmatrix} \tag{2.37}$$

$$= \begin{bmatrix} A \\ A\Phi_1 \end{bmatrix} S(t) + \begin{bmatrix} N_{X1}(t) \\ N_{Y1}(t) \end{bmatrix} \tag{2.38}$$

$$= \overline{A}_1 S(t) + N_1(t) \tag{2.39}$$

Similarly, the data at second array with an angular displacement of ψ is given by Equation 2.40 through 2.42.

$$Z_2(t) = \begin{bmatrix} X_2(t) \\ Y_2(t) \end{bmatrix} \tag{2.40}$$

$$= \begin{bmatrix} A \\ A\Phi_2 \end{bmatrix} S(t) + \begin{bmatrix} N_{X2}(t) \\ N_{Y2}(t) \end{bmatrix} \tag{2.41}$$

$$= \overline{A_2} S(t) + N_2(t) \tag{2.42}$$

Where,

$$\Phi_1 = \begin{bmatrix} e^{(j2\pi d \sin(\varphi_1)/\lambda_1)} & . & . \\ . & . & . \\ . & . & e^{(j2\pi d \sin(\varphi_n)/\lambda_n)} \end{bmatrix} \tag{2.43}$$

$$\Phi_2 = \begin{bmatrix} e^{(j2\pi d \sin(\varphi_1 - \psi)/\lambda_1)} & . & . \\ . & . & . \\ . & . & e^{(j2\pi d \sin(\varphi_n - \psi)/\lambda_n)} \end{bmatrix} \tag{2.44}$$

Since there are two unknown variables (φ_i λ_i) involved which are to be determined, the ESPRIT algorithm is applied separately to find Φ_1 and Φ_2. Having obtained the diagonal matrices, the (φ_i λ_i) pair can be obtained by simultaneously solving the corresponding diagonal elements.

The other most widely used subspace based algorithm is the Multiple SIignal Classification (MUSIC) algorithm. The steering vectors corresponding to the directions of the incident signals, which are orthogonal to the noise subspace are reflected as peaks in the MUSIC spectra. As such the entire Array Manifold a(ω) has to be searched before all the peaks corresponding to the true DOA are estimated. Therefore the search process of MUSIC algorithm is time consuming before all the DOA estimated. As seen on the other hand, the ESPRIT algorithm does not involve and exhaustive search through all possible steering vectors of the array manifold to estimate the DOA. Hence ESPRIT dramatically reduces the computational requirements inherent in other Subspace based DOA estimation algorithms. The ESPRIT algorithm has been implemented in this study.

CHAPTER 3

INTERFERENCE CONTROL BY NULL STEERING

3.1 Introduction

Null Steering is an important subset of Smart Antenna System. It is well known that by proper weighting of the array elements its possible to shape the desired beam pattern or in other sense it is possible to place nulls in the prescribed directions. The energy received form the plane waves impinging on the array cancels out at these directions. This property can be used to receive desired signals in the presence of multiple sources of interference. The general approach to the problem of Null Steering is to calculate a set of coefficients (Amplitude and/or Phases) by solving a system of linear equations obtained by equating the Array Factor to Zero in the directions of the desired Nulls. This is the *Analytical method* of Null Steering. Another recently developed technique is the use of *Genetic Algorithms* to achieve the optimum solution. Based on the choice of the control parameter, Null Steering can be broadly classified as follows

- Element position perturbation method
- Amplitude Control method
- Phase Control method
- Complex Weight Control method

The Complex Weight (Amplitude and Phase) Control method, which is selected in this study, is the most efficient technique. The number of degrees of freedom in this case is twice the number of array elements resulting in better control of null steering.

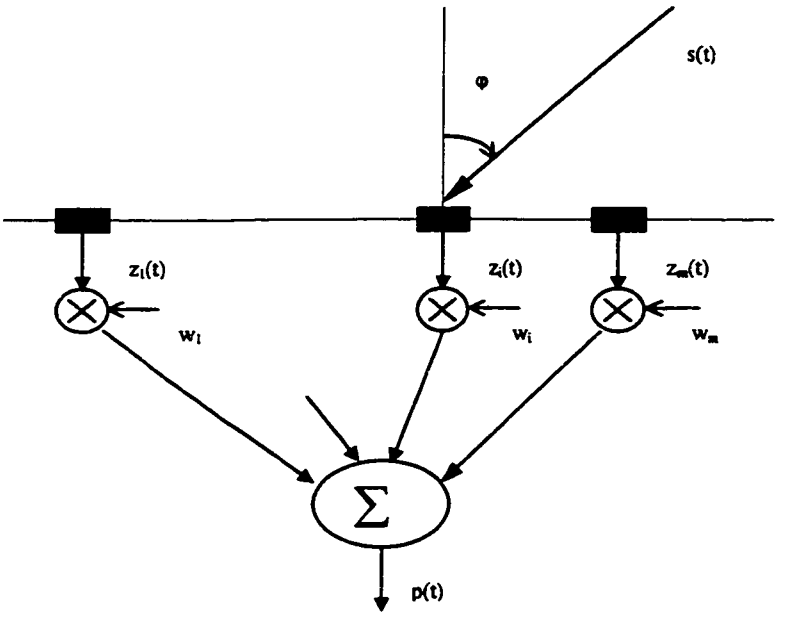

Figure 3.1-1: An m element Linear Array

Consider a *m* element equi-spaced Linear Array as shown in Figure 3.1-1. An array of identical elements all having uniform amplitudes of excitation and each with a

progressive phase shift is referred to as an uniform array. The Array Factor of such an Array is given as

$$AF = \sum_{i=1}^{m} e^{j(i-1)(kdSin\varphi+\beta)} \tag{3.1}$$

where, $k=(2\pi/\lambda)$ is the wave number and $\beta=(-kdsin\varphi_0)$ for phased array with main beam in the direction of φ_0.The perturbed Array Pattern after Complex weight Null Steering method can be given as

$$AF = \sum_{i=1}^{m} w_i e^{j(i-1)(kdSin\varphi+\beta)} \tag{3.2}$$

where w_I is the i^{th} element complex weight (amplitude and phase) $a_i e^{jb_i}$

Since the directions of the interferers and the desired signals are not known a priori and are often time varying due to varying motion of the sources and the array itself, Null Steering needs to be adaptive. The adaptive technique considered in this study consists of two steps. Firstly the Direction Of Arrival of all the plane waves is estimated using the direction finding technique ESPRIT. Secondly a set of complex weights is computed which places nulls in the estimated interference directions.

3.2 The Numerical Pattern Synthesis algorithm

The numerical technique used here for the synthesis of Array Pattern is briefly explained in this section. This technique is based on the one developed in [55] which is based on

Howell – Applebaum Array. The given array elements are assumed to be used as the elements of an adaptive array. The main beam is pointed in the proper direction by choosing the steering vector corresponding to that direction. The algorithm iterates on the interference power until the required null depth is obtained in the directions of the interferences. The flow chart of the algorithm is shown in Figure 4.3-2. The implementation of the algorithm is explained as follows.

Consider the m element linear array as shown in Figure 3.1-1. Let f_i (φ) be the pattern element and d_i is the distance in wavelengths between element i and element i+1 (but for our analysis the elements are taken to be isotropic and distance between the elements is taken as 0.5 λ). Assume a narrow band signal is incident on the array from angle φ, where, φ is measured from broadside as shown in Figure 3.2-1. Let $z_i(t)$ be the received signal on element i and define the signal vector Z(t) as

$$Z = [z_1(t), \ldots z_m(t)]^T \tag{3.3}$$

The array output signal p(t) is obtained by multiplying each $z_i(t)$ by a complex weight w_i and then summing,

$$p(t) = \sum_{i=1}^{m} w_i z_i(t)$$

$$= W^T Z \tag{3.4}$$

Where,

$$W = [w_1, \ldots w_m]^T \tag{3.5}$$

If the incoming signal is at frequency ω_0, Z is given by

$$Z = Ce^{j\omega_0 t}U \tag{3.6}$$

Where C is the signal amplitude, $e^{j\omega_0 t}$ is its time dependence and U is a vector containing the inter-element phase shifts and the element patterns.

$$U = [f_1(\varphi), f_2(\varphi)e^{j\rho_2(\varphi)}, \ldots, f_m(\varphi)e^{j\rho_m(\varphi)}]^T \tag{3.7}$$

Where,

$$\rho_i(\varphi) = 2\pi \sin(\varphi)\sum_{k=1}^{i-1} d_k \tag{3.8}$$

Combining Equations 3.4 and 3.6, gives the array output p(t),

$$p(t) = Ce^{j\omega_0 t}W^T U \tag{3.9}$$

We define the array voltage pattern $P(\varphi)$ as

$$P(\varphi) = |W^T U| \tag{3.10}$$

Assuming that the number of elements m, the element pattern $f_i(\varphi)$ and the element spacing d_i are all given, we want to find a weight vector W for which $P(\varphi)$ has a beam maximum at some angle φ_d and meets the desired null depth specification at other

interfering angles. To do this we imagine that the array is used as an adaptive array. an adaptive array is an antenna system that controls its own pattern by adjusting the weight vector W in response to the signal environment. The weight vector is adjusted to maximize the Signal-to-Interference-plus-Noise Ratio (SINR). Maximum SINR is obtained by maximizing the pattern in the desired direction and minimizing it in the interference directions. The array weights that maximize SINR may be calculated as follows. Suppose a desired signal and an interference signal are incident on the array and each element also contains thermal noise. The total signal vector Z is then given by,

$$Z = Z_d + Z_i + Z_n$$

$$= Z_d + Z_u \tag{3.11}$$

Where Z_d, Z_i and Z_n are the desired, interference, and noise vectors respectively. Z_u is the undesired part of Z. The optimal weights are then given by,

$$W = \phi_u^{-1} U_d^* \tag{3.12}$$

where ϕ_u is the covariance of the undesired signals.

$$\phi_u = E\{Z_u^* Z_u^T\} \tag{3.13}$$

Specifically, if the desired signal is narrow band signal arriving at angle φ_d then,

$$Z_d = C_d e^{(j\omega_0 t + \psi_d)} U_d \tag{3.14}$$

where, A_d is the desired signal amplitude, ψ_d si the carrier phase angle and U_d is given by Equation 3.7 with $\varphi = \varphi_d$. The phase angle, ψ_d is a random variable. Similarly the interference signal can be given as,

$$Z_i = C_i e^{(j\omega_0 t + \psi_i)} U_i \tag{3.15}$$

the noise vector Z_n can be given as,

$$Z_n = [n_1(t), \ldots, n_m(t)]^T \tag{3.16}$$

Where the noise $n_j(t)$ are narrow band random processes, such that,

$$E\{n_i(t) n_j(t)\} = \sigma^2 \delta_{ij} \tag{3.17}$$

Substituting these signal vectors in Equations 3.11 and 3.13, we get,

$$\phi_u = \sigma^2 I + C_i^2 U_i^* U_i^T \tag{3.18}$$

The optimal weight vector can then be calculated from 3.12.

In the implementation of the iterative algorithm, initially the interference is assumed to be zero from the directions of the interferences. The optimal weights and resultant pattern ($P(\varphi, k) = P(\varphi, 0)$) are then calculated. This pattern gives the pattern with main beam in the direction of the desired signal but without nulls in the directions of the interferers. This initial step is referred to as $k = 0^{th}$ iteration. In the next iteration ($k+1$), the interference power for the m^{th} interference coming from φ_m is increased if the pattern

level(P(φ, k)) in the previous iteration (k^{th}) at that direction is more than the desired Null depth (D). And if the pattern level in that direction is below the desired Null depth, then the interference power is decreased. Negative interference powers are not allowed. Therefore if the interference power would become negative, then it is set to zero. Thus for the next iteration ($k+1$), the Interference-to-Noise (ξ_{i_m}) which is actually the interference power when white noise with variance of 1 is taken) power for the m^{th} interferer is given as,

$$\xi_{i_m}(k+1) = \max[0, \Gamma_{i_m}(k)] \tag{3.19}$$

where,

$$\Gamma_{i_m}(k) = \xi_{i_m}(k) + K(P(\varphi,k) - D) \tag{3.20}$$

Where, K is called as the Iteration Gain.

If q interferences are assumed, then,

$$Z_u = Z_n + \sum_{m=1}^{q} Z_{i_m} \tag{3.21}$$

The covariance matrix of these undesired signals is then given by,

$$\phi_u = E\{Z_n^* Z_n^T\} + \sum_{m=1}^{q} E\{Z_{i_m}^* Z_{i_m}^T\}$$

$$= \sigma^2 I + \sum_{m=1}^{q} \xi_{i_m}(k) U_{i_m}^{*} U_{i_m}^{T} \tag{3.22}$$

Solving Equation 3.12 then yields the optimal weight vector for that iteration. This cycle is repeated iteratively until the pattern is judged to meet the required criteria.

CHAPTER 4

IMPLEMENTATION PROCEDURE

4.1 Introduction

In this chapter the actual implementation procedure of the Smart Antenna System combining the techniques detailed in Chapter 2 and Chapter 3 is discussed. The various stages encountered are represented in the form of block diagram. The DOA and complex weight estimation is made from the data sampled from the sensors of the array. For mitigating the Adjacent Channel Interference, which arises due to signals with adjacent carrier frequencies sneaking into an imperfect receiver filter, the knowledge of both Frequency and DOA is needed. In such a case a change in Array geometry is suggested, as there is a need to estimate two variables. The block diagram of Smart Antenna implementation to steer nulls in the directions of interferences is shown in the next section. As the DOA estimation analysis for estimating the interferers with same frequency (CCI and multipath) differs with the one with different frequency (ACI), two separate cases are presented.

4.2 Presence of interfering signals with same carrier frequency as that of desired signal

This scenario is analogous to the presence of Co-Channel Interference and multipath of the desired signals. The implementation then is as shown in Figure 4.2-1. The series of steps involved are as follows.

1) The system continuously updates the data sampled from the sensors of the Array.
2) Processing of this data is conducted at periodic intervals to estimate the DOA and related information of the desired signals as well as interferences via the ESPRIT algorithm.
3) The estimated information is then applied in calculating the complex weights. The snapshots stored in the memory storage and the computed complex weight updates are synchronized.
4) Finally the stored data is weighted with the updated complex weights in a beamformer to give the desired Array Pattern.

The flow chart for the DOA estimation and Null Steering are shown in Figure 4.2-2 and Figure 4.2-3 respectively.

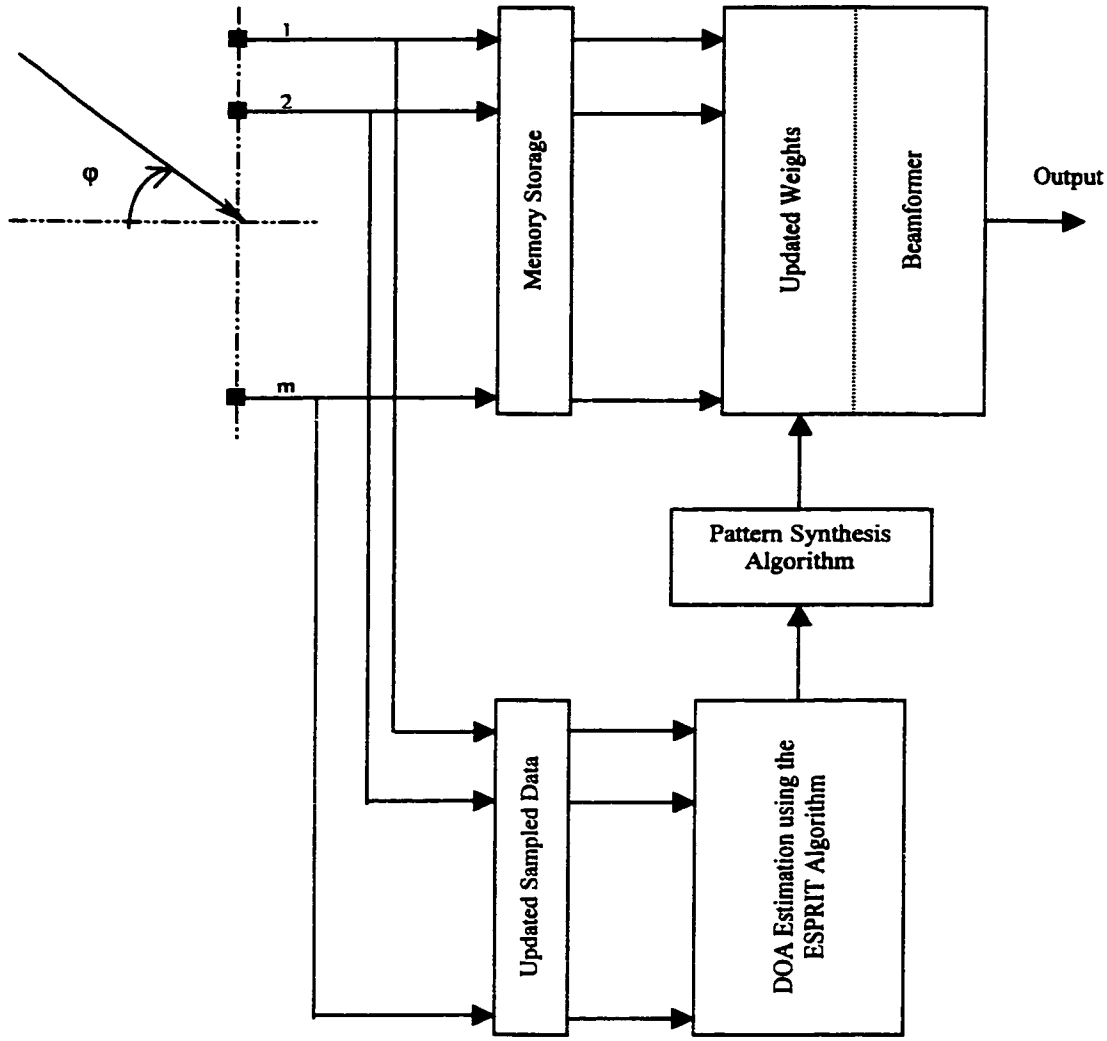

Figure 4.2-1:Array Geometry and SAS Implementation to combat interference with same carrier frequency as the desired signal

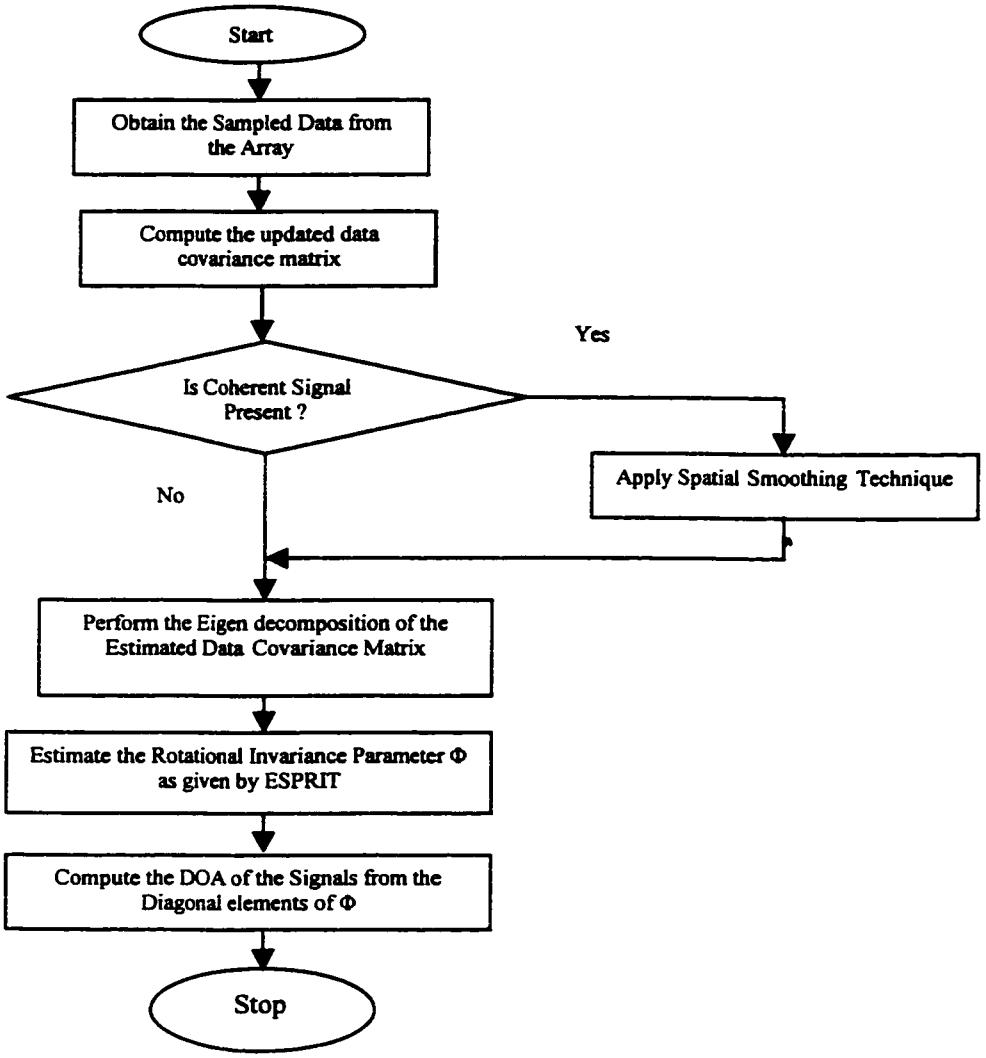

Figure 4.2-2: Flow Chart of DOA Estimation

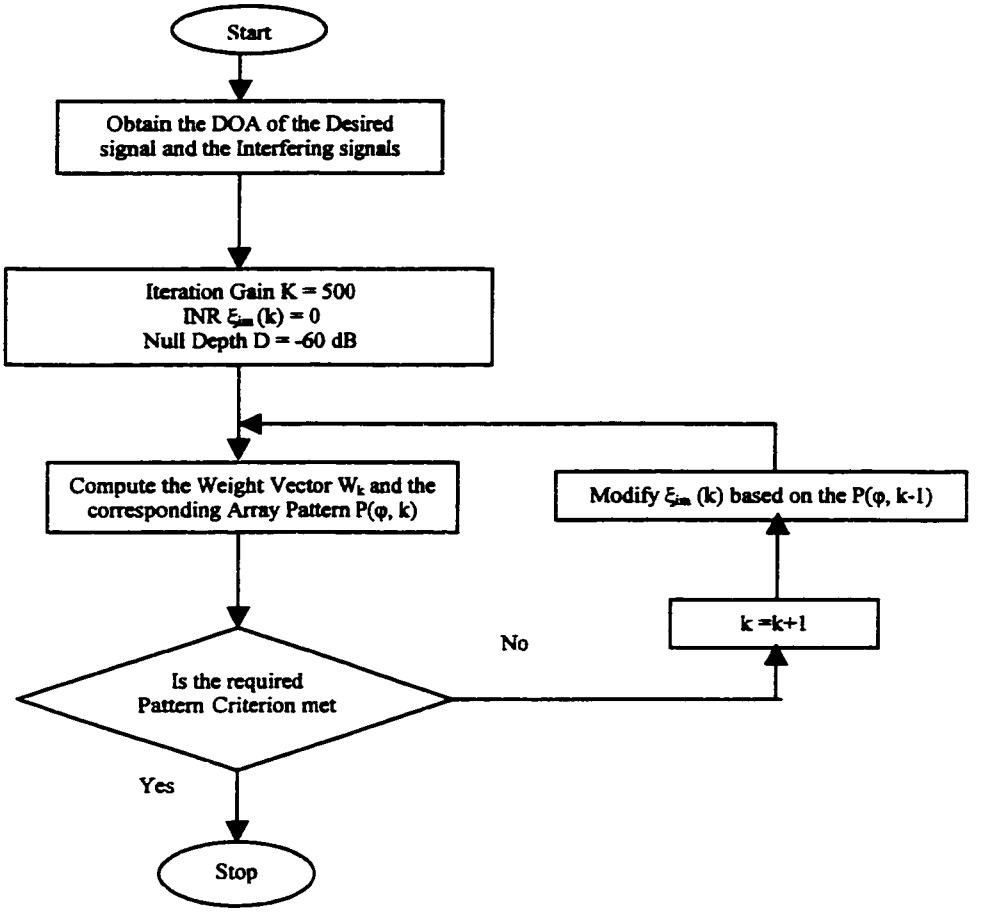

Figure 4.2-3: Flow Chart of Pattern Synthesis Algorithm

4.3 Presence of Interfering signals with carrier frequency adjacent to that of the desired signal

Interference resulting from signals that are adjacent in frequency to the desired signal is called *Adjacent Channel Interference (ACI)*. Adjacent Channel Interference results from imperfect receiver filters that allow nearby frequencies to leak into the passband. Presence of ACI gives rise to a phenomenon called near-far effect. This occurs when a mobile communicating with the base station of a particular cell transmits close to a channel being used by another mobile. Then the base station will have difficulty in discriminating the desired mobile with the Adjacent Channel mobile.

The implementation procedure in such a scenario is similar to the one discussed in Section 4.2 but, simultaneous estimation of both DOA and Frequency is needed. As such a modification of geometry of the array is required as shown in Figure 4.3-1. Data sampled from the second array inclined at an angle of Ψ with respect to the first array is also used in the estimation of the DOA and Frequency as analyzed in Section 2.4. It is important to note that samples from the second array are simply used in the simultaneous estimation of DOA and Frequency unlike the first array, which acts as the actual transmitting and receiving antenna array. For this reason beamforming is done only with data sampled from the first array. The flow chart implementation of simultaneous estimation of DOA and Frequency is presented in Figure 4.3-2.

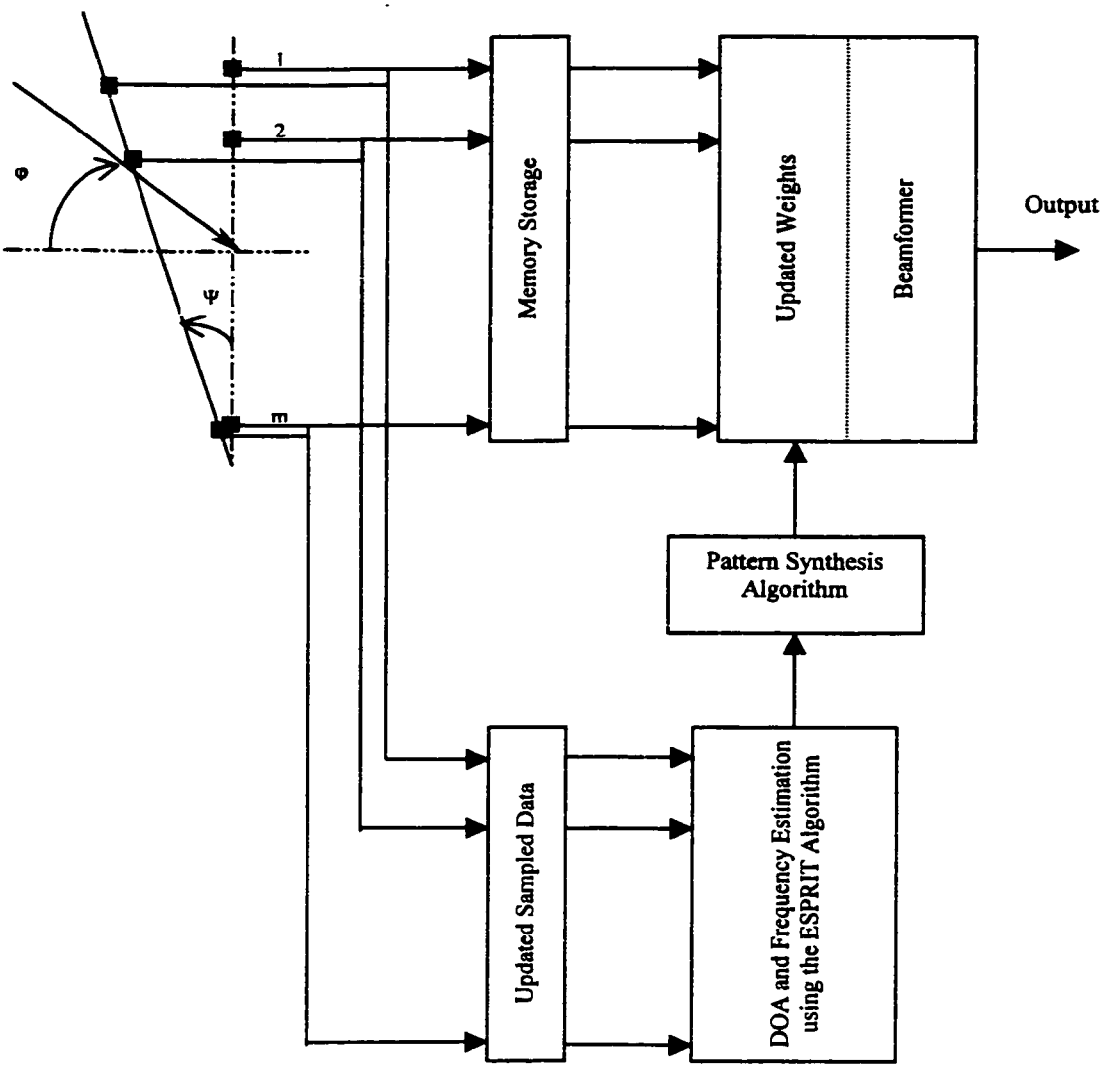

Figure 4.3-1: Array Geometry and SAS Implementation to combat interference with carrier frequency adjacent to that of desired signal

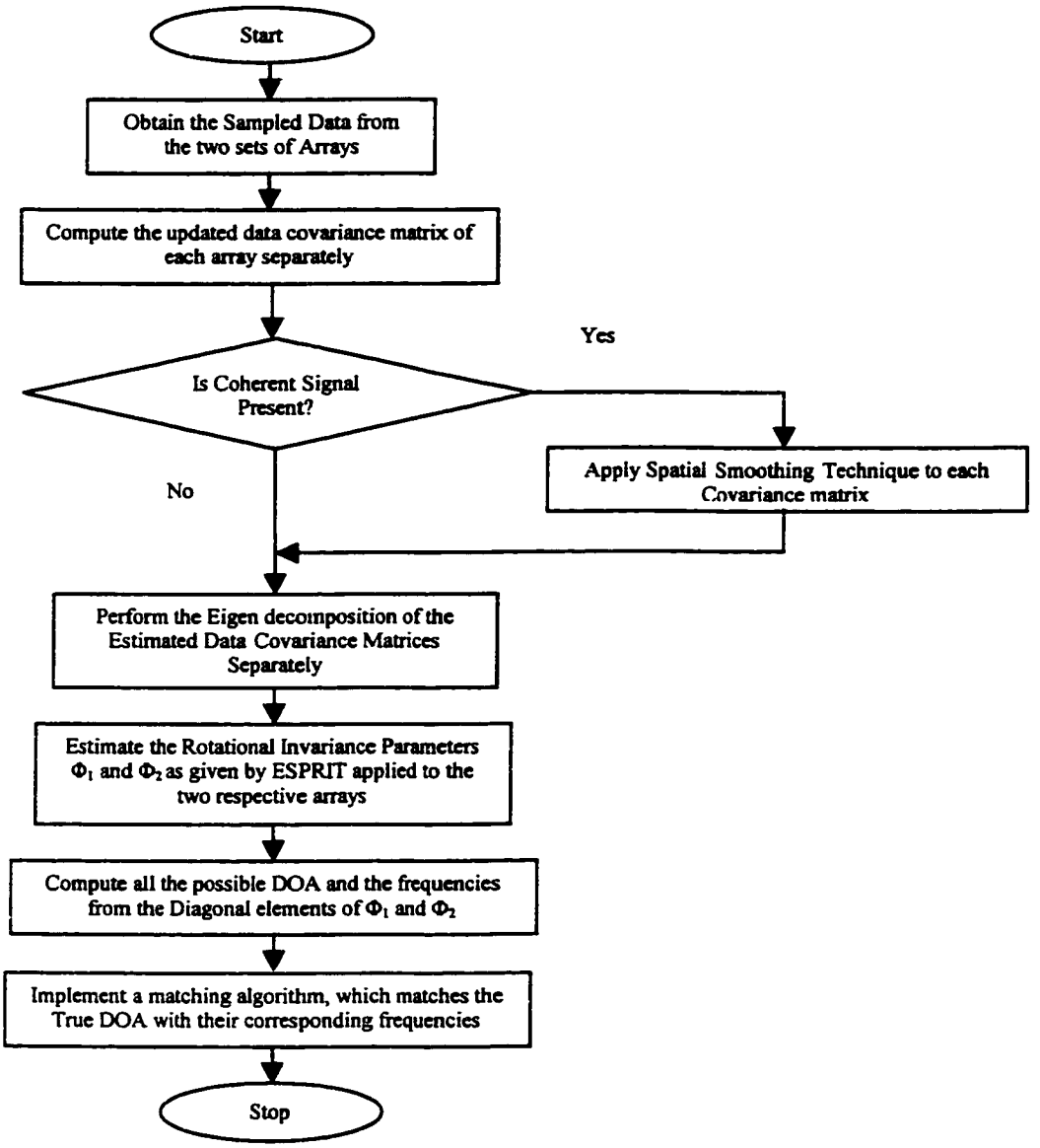

Figure 4.3-2: Flow Chart of DOA and Frequency Estimation

CHAPTER 5

RESULTS AND DISCUSSIONS

5.1 Introduction

In this chapter the simulation results for null steering and pattern synthesis in Smart Antenna Arrays are presented. Null steering aspects of Tracking Beam Smart Antenna System are dealt with in detail in Section 5.4. Null Steering in the directions of CCI, ACI and Multipath of the desired signal is carried out. A Numerical Pattern Synthesis Algorithm based on Howell-Applebaum Arrays is used for null steering and pattern synthesis. The Total Least Squares version of ESPRIT is adopted for DOA estimation. Comparison of the ESPRIT algorithm with the most popularly used MUSIC algorithm is done to illustrate the advantage of ESPRIT algorithm for real time implementation. In the DOA estimation of the signals, signal environments with only uncorrelated signals (due to CCI) and with both uncorrelated and correlated (due to multipath) signals are considered. Also heterogeneous signal environment wherein signals arrive with different carrier frequencies (giving rise to ACI) is dealt with. A study of the effect of increase in number

of elements on parameter estimates is carried out in Section 5.6. Section 5.7 demonstrates the effect of SNR of the signals on the resolution of ESPRIT estimates of parameters and the effect of separation between the signals on DOA estimation is shown in Section 5.8.

The array is assumed to be a linear array with 10 isotropic elements. The spacing between the elements is taken as 0.5 times the wavelength (corresponding to the carrier frequency of the signal). The array factor is plotted in 2-D plots showing azimuth angle (φ in Degrees) Vs Normalized Array Pattern (in dB). The elevation angle is assumed as 90°, which represents the horizon. DOA of the signals that lie in the Azimuth plane are measured with respect to the broad side of the array. The null depth specified is –60 dB and the iteration gain used to achieve the desired depth is K=500. Due to the high iteration gain taken, the desired pattern is obtained in a single iteration. While calculating the covariance estimates for the Direction Of Arrival estimation, the number of snapshots taken is 1000. The true values and the estimates of the Eigenvalues (Φ_i=exp (2πj (d/λ) sin (φ_i)) calculated as the rotational invariance by the ESPRIT algorithm, which corresponds to the Directions of Arrival (φ_i) are plotted. These plots show real part Vs imaginary part of such Eigen values.

5.2 Comparing ESPRIT with MUSIC

The ESPRIT algorithm outperforms the most commonly used MUSIC algorithm in computational time. As far as accuracy is concerned, it gives reasonable accuracy when compared with MUSIC.

In this Section, at first the resolution of MUSIC is taken as 1^0. A signal is incident from azimuthal angle 33.4^0. Clearly MUSIC algorithm could not resolve it accurately as shown in Figure 5.2-1 and Figure 5.2-2. But the ESPRIT estimates are acceptably good. Also as seen from Table 5.2-1 the CPU time taken by MUSIC is large compared to that taken by ESPRIT algorithm. In the second case the resolution of MUSIC algorithm is 0.1^0. Therefore the algorithm was able to resolve the signal up to first decimal place (Figure 5.2-4). And in the third case, the resolution was further improved to 0.01^0. The angle was resolved with accuracy of 0.01 degree (Figure 5.2-6) but at the expense of computational time. Finally the ESPRIT algorithm outperformed in computational time compared with MUSIC. The code is run on a Pentium Processor with clock speed of 200 MHz.

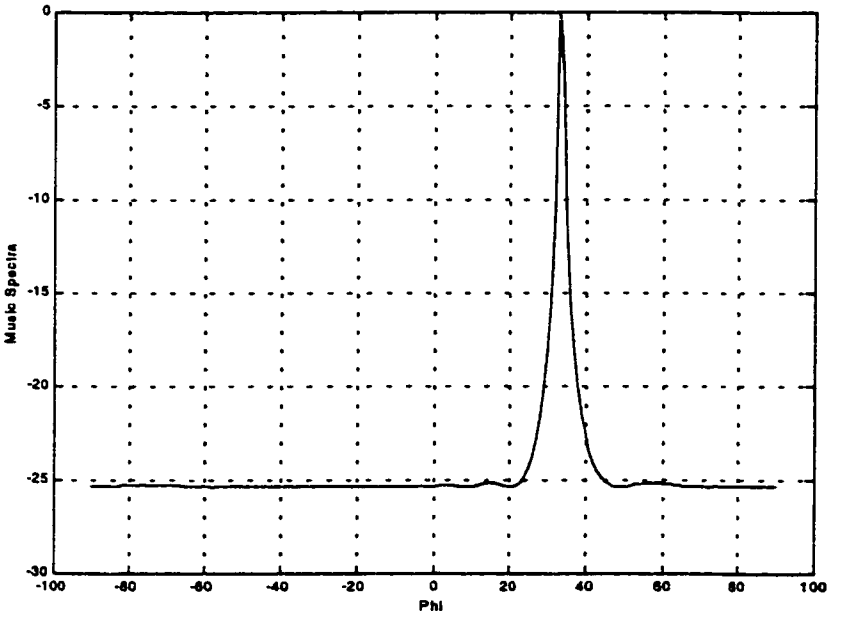

Figure 5.2-1: Estimated Direction ($\varphi = 33^0$) along the peak of the Music Spectra. Angular Resolution = 1^0

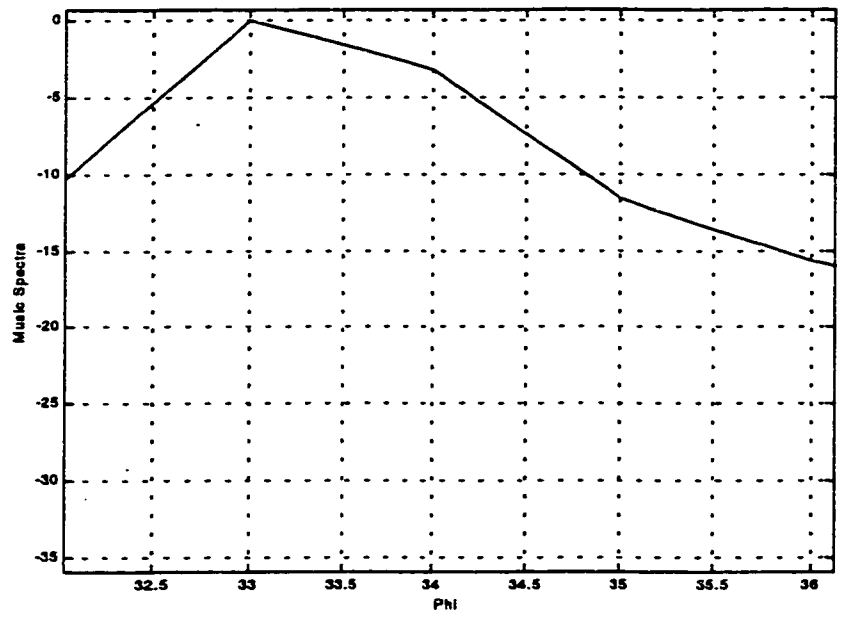

Figure 5.2-2: Peak of Figure 5.2-1 after Zooming

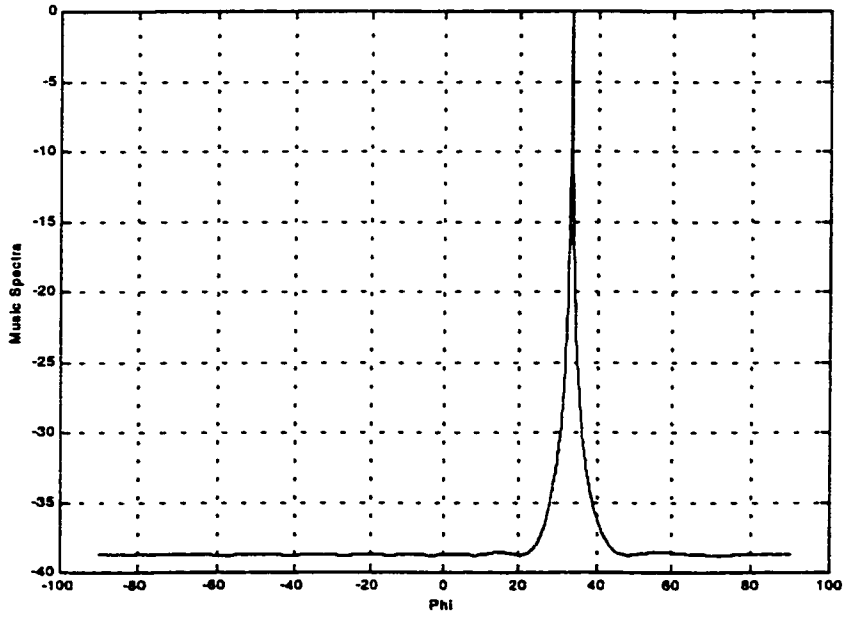

Figure 5.2-3: Estimated Direction ($\varphi = 33.3^0$) along the peak of the Music Spectra. Angular Resolution = 0.1^0

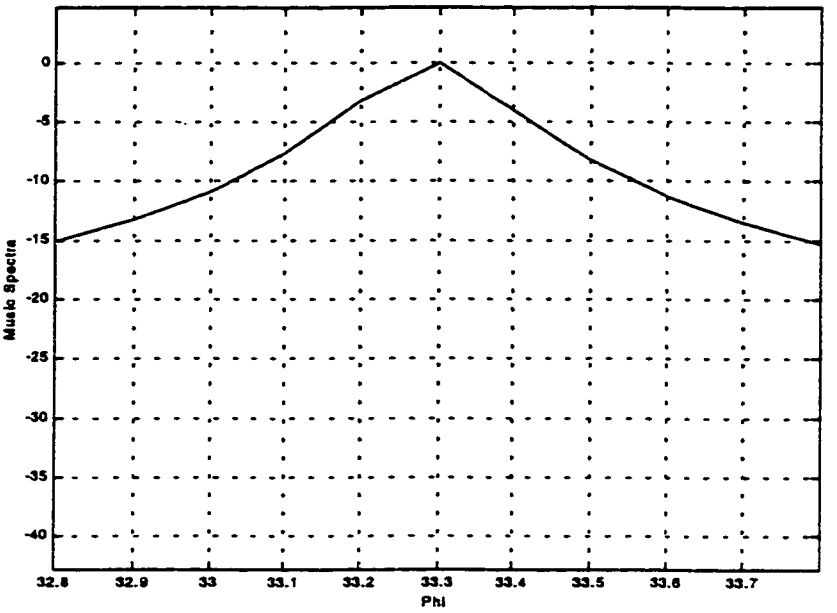

Figure 5.2-4: Peak of Figure 5.2-3 after Zooming

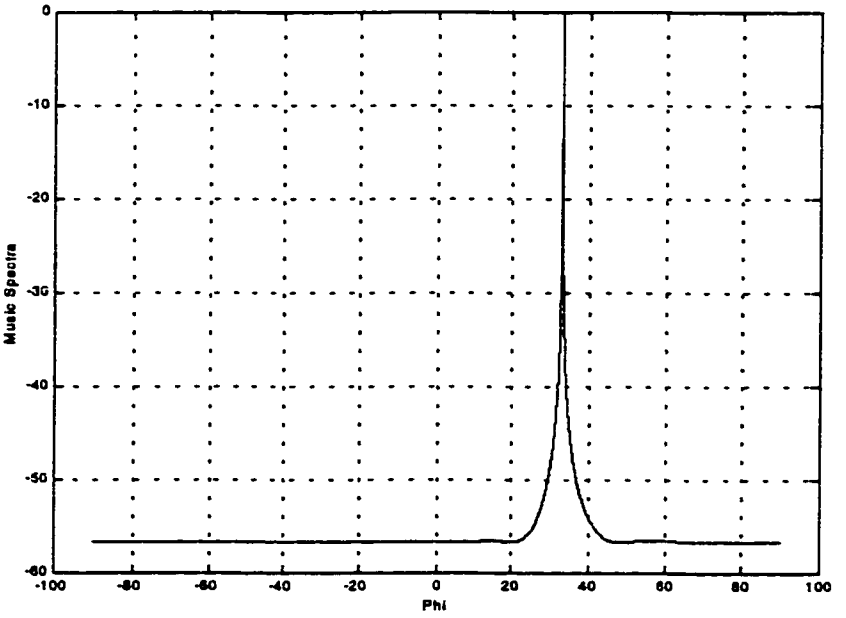

Figure 5.2-5: Estimated Direction ($\varphi = 33.33^0$) along the peak of the Music Spectra. Angular Resolution $=0.01^0$

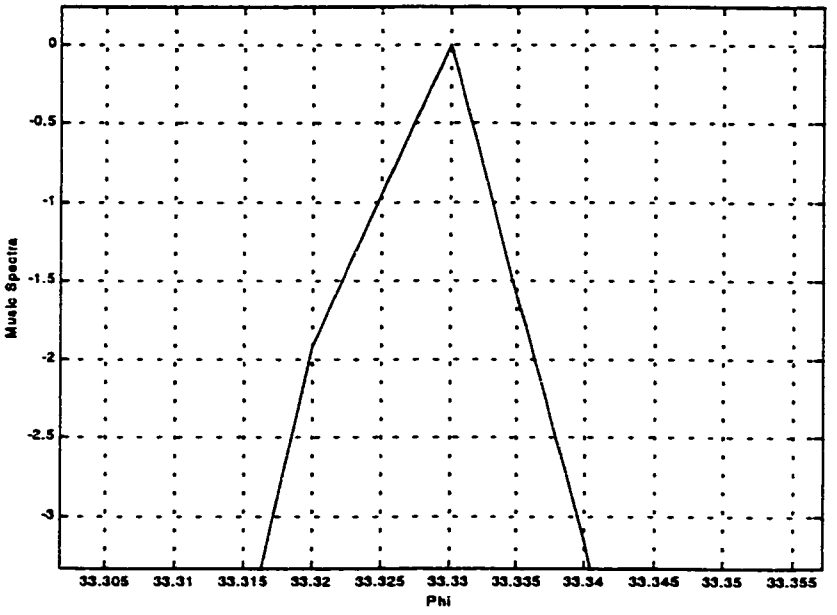

Figure 5.2-6: Peak of Figure 5.2-5 after Zooming

Table 5.2-1: Comparing CPU Time of ESPRIT and MUSIC Algorithms

True DOA	ESPRIT ANALYSIS		MUSIC ANALYSIS		
	Estimated DOA	CPU Time (milli sec)	Resolution	Estimated DOA	CPU Time (milli sec)
33.4^0	33.4006^0	1	1^0	33^0	79.5
33.3^0	33.2995^0	1	0.1^0	33.3^0	777.6
33.33^0	33.3309^0	1	0.01^0	33.33^0	7690

5.3 Pattern control in Switched Beam Smart Antenna System

A switched beam smart antenna system has a predefined number of beams pointing in specific directions. A particular beam, which fits best is selected based on the Direction of Arrival of the desired signal. When the user moves form one location to another, the selected beam also changes dynamically. The main advantage of switched beam smart antenna system is that the weights corresponding to the desired beam are calculated a priori thus avoiding complexity of the system except for a control switch. But there is a drawback of scalloping.

5.3.1 The direction of the main beam selected is exactly in the direction of the desired user

When the direction of the desired signal lies exactly along the direction of the selected beam, the performance of the switched beam smart antenna is the optimum. The array pattern then possesses maximum directivity along the desired direction. Figure 5.3-1 shows the array pattern for such a case. Here the number of predefined sectors (beams) is taken as 10 such that one of the predefined main beam points towards -18^{o}. Two uncorrelated signals with same carrier frequency, one desired signal with SNR of 15 dB and the other a Co-Channel interferer with SNR of 10 dB are considered. Their Directions of Arrival are -18^{o} and 52.5^{o}. The estimates of their directions are shown in Figure 5.3-2.

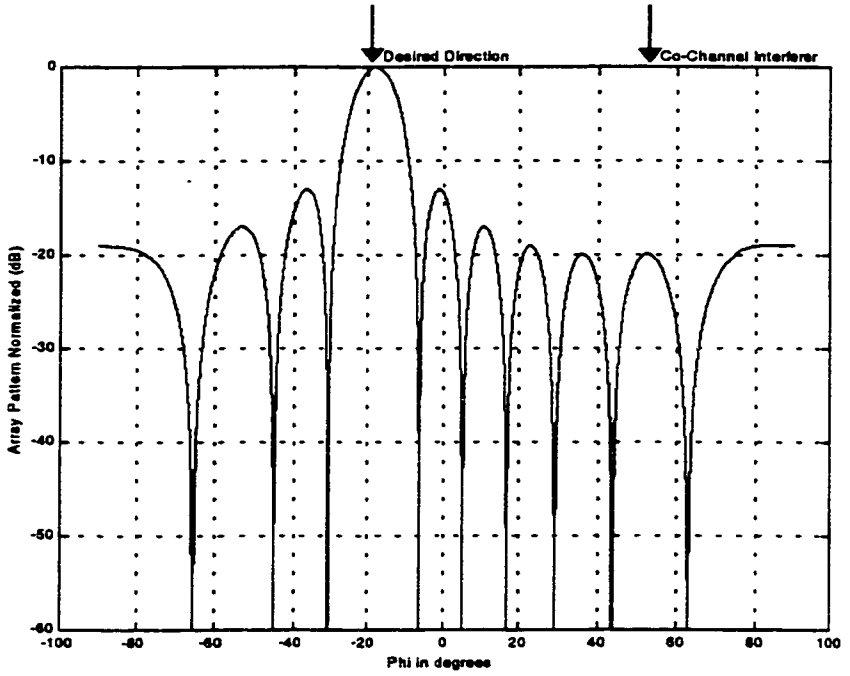

Figure 5.3-1: Array Pattern for a selected predefined main beam at –18°. Desired direction= -18.007°

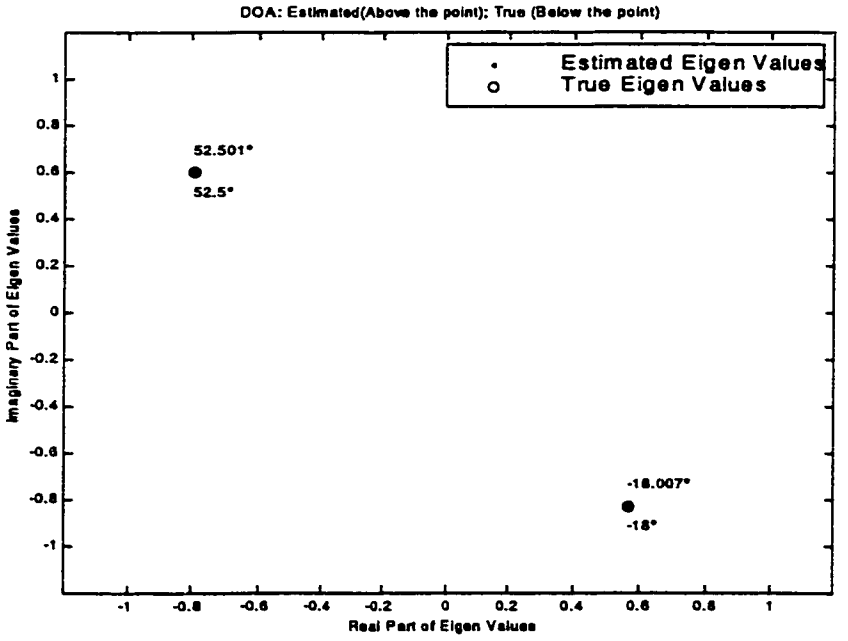

Figure 5.3-2: ESPRIT simulation results. Number of Signals = 2(Desired at-18.007^0, CCI at 52.501^0). True values and estimates of EVs Φ_i=exp (2πj(d/λ)sin (φ_i))

Table 5.3-1: Comparison of directivity along the main beam direction to that along the desired direction

Maximum Directivity (D_0)	10.0000
Directivity in Desired Direction	10.0000
HPBW	10.5653^0

Table 5.3-2: Complex weights corresponding to the selected Array Pattern

Element	Complex Weights
1	$1e^{(j0)}$
2	$1e^{(j55.6231)}$
3	$1e^{(j111.2461)}$
4	$1e^{(j166.8692)}$
5	$1e^{(-j137.5078)}$
6	$1e^{(-j81.8847)}$
7	$1e^{(-j26.2616)}$
8	$1e^{(j29.3614)}$
9	$1e^{(j84.9845)}$
10	$1e^{(j140.6075)}$

The directivity along the main beam and that along the desired direction are shown in Table 5.3-1. The complex weights used to arrive at the pattern are given in Table 5.3-2. The pattern represents that of a scanned array. As the desired direction and the main beam directions are almost same, we see that we get maximum directivity along the desired direction. But the Co-Channel interferer is not nulled.

5.3.2 Effect of Scalloping

Figure 5.3-3 shows the effect of scalloping. The desired direction is incident from –23°. As such the predefined main beam pointing towards –18° is selected. But unlike in the previous section, where the desired direction was coinciding with the direction of the main beam, the desired direction now lies on the sloping edge of the main beam. As such the directivity in the desired direction degrades rapidly as shown in Table 5.3-3. The estimates of the angles are given in Figure 5.3-4. Increasing the number of sectors, consequently achieving more closely spaced beams, can reduce scalloping effects. But the handoffs needed in such a scenario are more. A Tracking Beam Smart Antenna can overcome these shortcomings, which will be discussed in the next section.

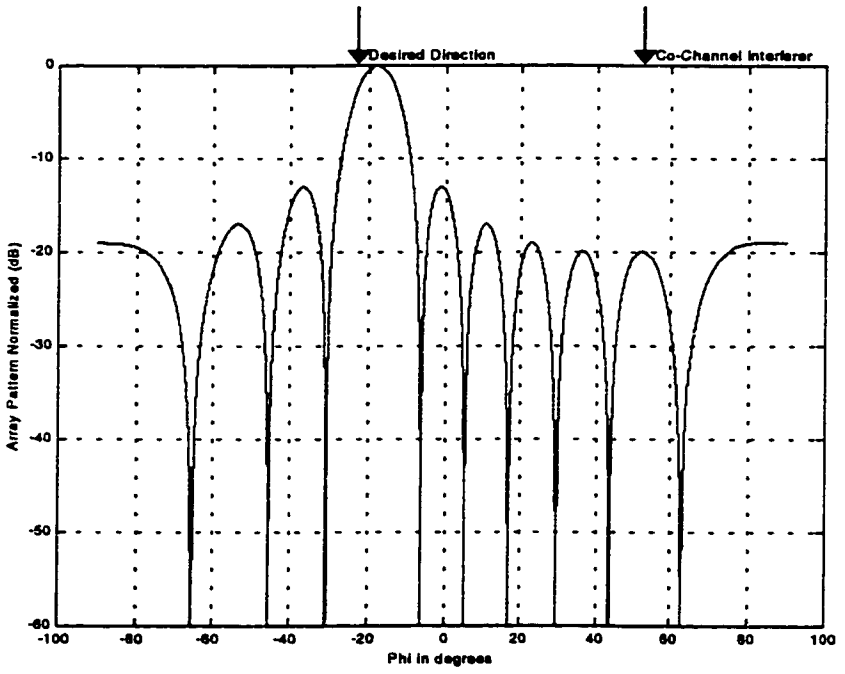

Figure 5.3-3: Array Pattern for a selected predefined main beam at –18°. Desired direction= -22.997°

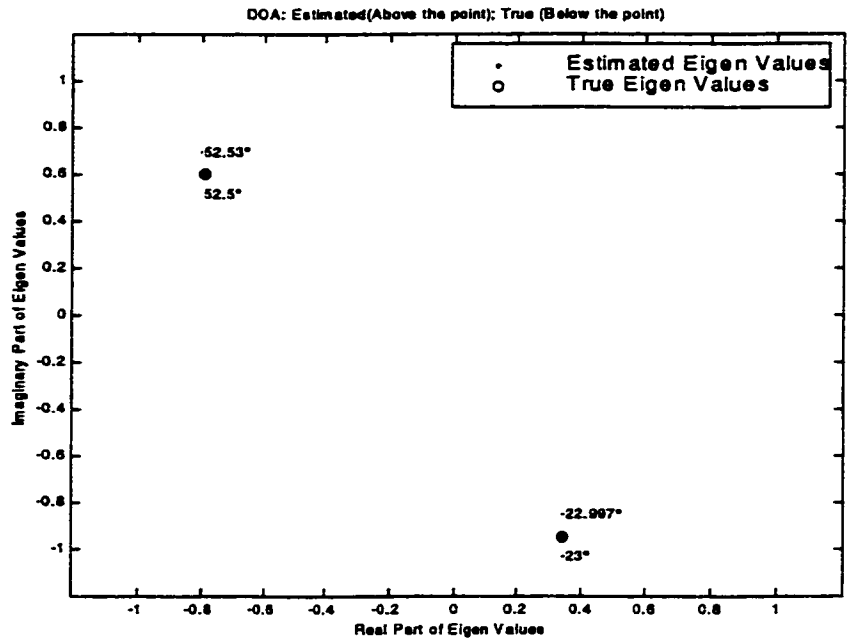

Figure 5.3-4: ESPRIT simulation results. Number of Signals = 2(Desired at -22.997^0, CCI at 52.53^0). True values and estimates of EVs $\Phi_i=exp\ (2\pi j(d/\lambda)sin\ (\varphi_i))$

Table 5.3-3: Comparison of directivity along the main beam direction to that along the desired direction

Maximum Directivity (D_0)	10.0000
Directivity in Desired Direction	5.6156

5.4 Pattern control in Tracking Beam Smart Antenna System

A Tracking Beam Smart Antenna is a fully adaptive antenna array. It dynamically adjusts its pattern based on the signal environment. It always directs the main beam in the desired direction promising maximum directivity all the time in the desired direction. The directions of the interferers can always be nulled. The interferers may be from with in the

cell where the base station is located (due to frequency re-use within the cell or due to multipath of desired signal) or Co-Channel interferers from adjacent cells separated by Re-use distance and using the same carrier frequency or Adjacent Channel Interferers with frequencies adjacent to the desired carrier frequency.

In this section, results are presented for combating these interferences in a Smart Antenna System by estimating their DOA and directing nulls in those directions.

5.4.1 Array Pattern and DOA estimation in the presence of Co-Channel interference

A signal environment is considered where in the signals are uncorrelated with each other. The desired signal in the cell of interest and Co-Channel interferers from the neighboring cells have same carrier frequencies. Also the SNR of desired signal is greater than that of interfering signals.

Case 1: Single Interferer

A single interferer is assumed coming at 52.5^0 with a SNR of 10 dB. The desired signal is at -18^0 with a SNR of 15 dB. As seen from Figure 5.4-1, the main beam is maintained at the desired direction and null of depth –60 dB at the interfering direction. Table 5.4-1 shows the final complex weights, amplitude and phase changes after steering the nulls, still maintaining the main beam in the desired direction. Figure 5.4.2 shows the estimates.

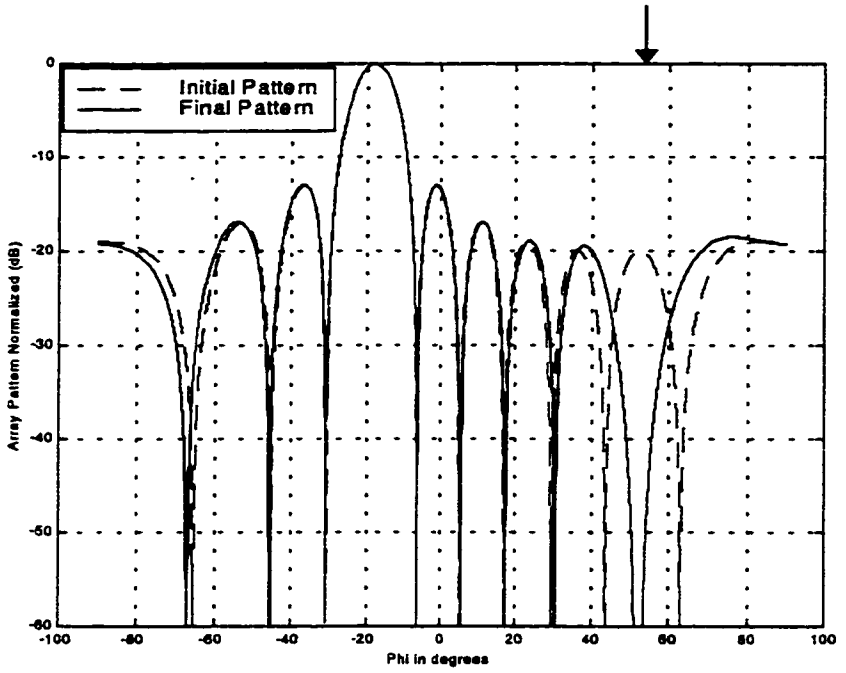

Figure 5.4-1: Array pattern showing main beam at –18.008^0 and null at 52.483^0

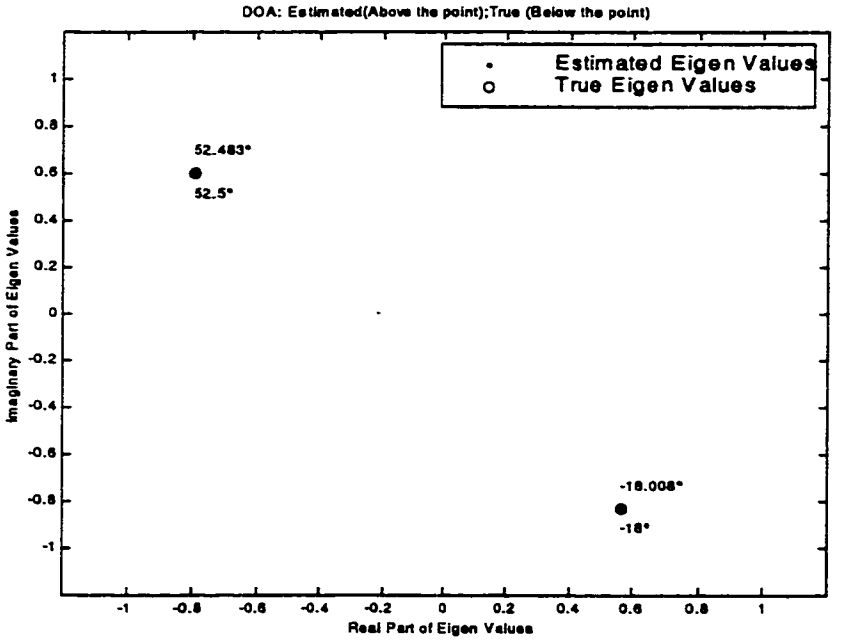

Figure 5.4-2: ESPRIT simulation results. Number of Signals = 2(Desired at-18.008^0, CCI at 52.483^0). True values and estimates of EVs Φ_i=exp $(2\pi j(d/\lambda)\sin(\varphi_i))$

Table 5.4-1: Details corresponding to the Array Patterns in Figure 5.4-1

Element	Complex Weights Before Null Steering	Complex Weights After Null Steering	Amplitude Changes after Null Steering	Phase Changes After Null Steering
1	$1e^{(j0)}$	$0.8998e^{(j0.7970)}$	-0.1002	0.7970^0
2	$1e^{(j55.6479)}$	$1.0920e^{(j53.3623)}$	0.0920	-2.2857^0
3	$1e^{(j111.2959)}$	$0.9299e^{(j115.6208)}$	-0.0701	4.3249^0
4	$1e^{(j166.9438)}$	$1.0507e^{(j162.0563)}$	0.0507	-4.8875^0
5	$1e^{(-j137.4083)}$	$0.9889e^{(-j131.6198)}$	-0.0111	5.7885^0
6	$1e^{(-j81.7603)}$	$0.9889e^{(-j87.5488)}$	-0.0111	-5.7885^0
7	$1e^{(-j26.1124)}$	$1.0507e^{(-j21.2250)}$	0.0507	4.8875^0
8	$1e^{(j29.5355)}$	$0.9299e^{(j25.2106)}$	-0.0701	-4.3249^0
9	$1e^{(j85.1835)}$	$1.0920e^{(j87.4691)}$	0.0920	2.2857^0
10	$1e^{(j140.8314)}$	$0.8998e^{(j140.0344)}$	-0.1002	-0.7970^0
HPBW		Before Null Steering		10.7640^0
		After Null Steering		10.8720^0
Directivity		Before Null Steering		10.0000
		After Null Steering		9.8979
Maximum Amplitude / Minimum Amplitude (After Null Steering)				1.2136
Maximum Phase Change				5.7885^0

Case 2: Two interferers lying in adjacent sidelobes

Main beam is steered at Desired direction of -60^0 and two interferers separated by 6^0 and lying in adjacent side lobes are nulled. All details are given in Figure 5.4-3, Figure 5.4-4 and Table 5.4-2.

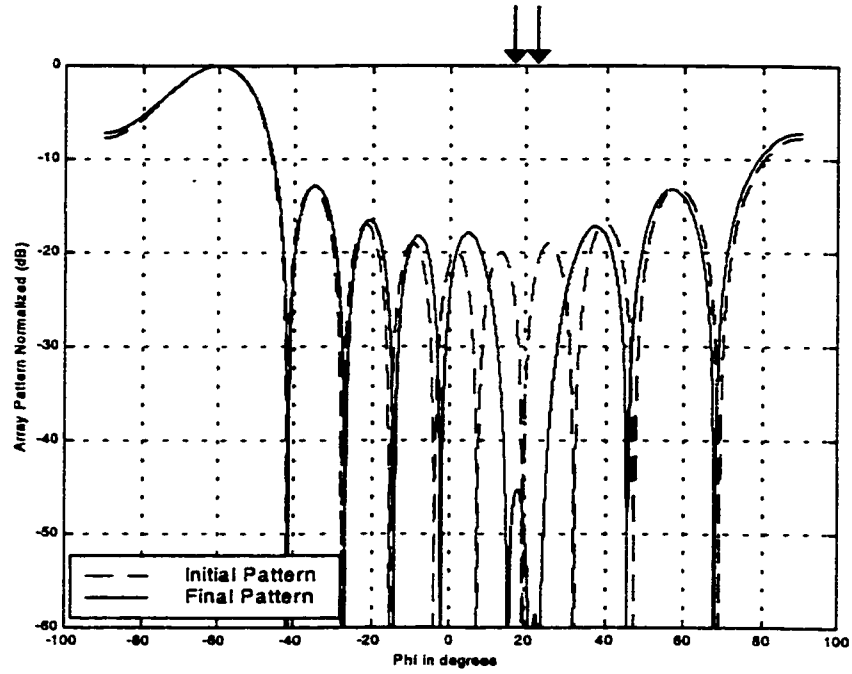

Figure 5.4-3: Array pattern showing main beam at –60.008^0 and nulls at 22.014^0 and 16.041^0

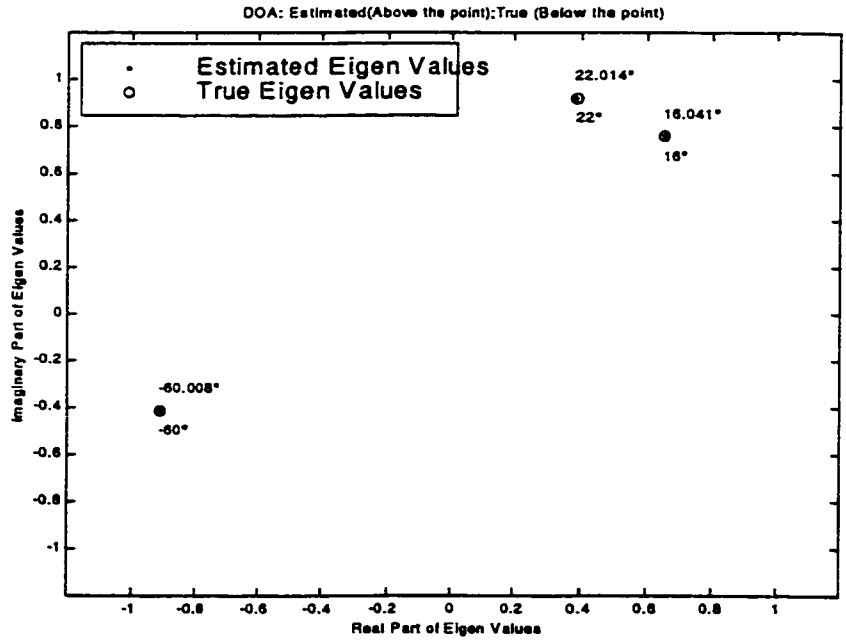

Figure 5.4-4: ESPRIT simulation results. Number of Signals = 3(Desired at –60.008^0, CCI at 22.014^0, 16.041^0). True values and estimates of EVs Φ_i=exp (2πj(d/λ)sin (φ_i))

Table 5.4-2: Details corresponding to the Array Patterns in Figure 5.4-3

Element	Complex Weights Before Null Steering	Complex Weights After Null Steering	Amplitude Changes after Null Steering	Phase Changes After Null Steering
1	$1e^{(j0)}$	$0.7651e^{(j7.7484)}$	-0.2349	7.7484^0
2	$1e^{(j155.8974)}$	$1.1293e^{(j146.8677)}$	0.1293	-9.0297^0
3	$1e^{(-j48.2053)}$	$1.0129e^{(-j39.4104)}$	0.0129	8.7948^0
4	$1e^{(j107.6921)}$	$0.9525e^{(j102.8773)}$	-0.0475	-4.8148^0
5	$1e^{(-j96.4105)}$	$1.0275e^{(-j95.3655)}$	0.0275	1.0450^0
6	$1e^{(j59.4869)}$	$1.0275e^{(j58.4418)}$	0.0275	-1.0450^0
7	$1e^{(-j144.6158)}$	$0.9525e^{(-j139.8010)}$	-0.0475	4.8148^0
8	$1e^{(j11.2816)}$	$1.0129e^{(j2.4867)}$	0.0129	-8.7948^0
9	$1e^{(j16\ 7.1790)}$	$1.1293e^{(j176.2087)}$	0.1293	9.0297^0
10	$1e^{(-j36.9237)}$	$0.7651e^{(-j44.6720)}$	-0.2349	-7.7484^0
HPBW		Before Null Steering		21.7400^0
		After Null Steering		22.4640^0
Directivity		Before Null Steering		10.0000
		After Null Steering		9.7049
Maximum Amplitude / Minimum Amplitude (After Null Steering)				1.4760
Maximum Phase Change				9.0297^0

Case 3: Multiple Interferers along successive side lobes

While maintaining the main beam still at -60^0 all the interferers coming along side lobes at -10^0, 0^0, 10^0, 20^0 and 25^0 are nulled to the depth of –60 dB. Thus even with 5 interferers with two of them separated by just 5^0, as seen form Figure 5.4-6 accurate estimates can be carried out. Details are in Table 5.4-3. But due to the fact of steering multiple nulls, the directivity decreases compared to previous cases. Array Pattern is given in Figure 5.4-5.

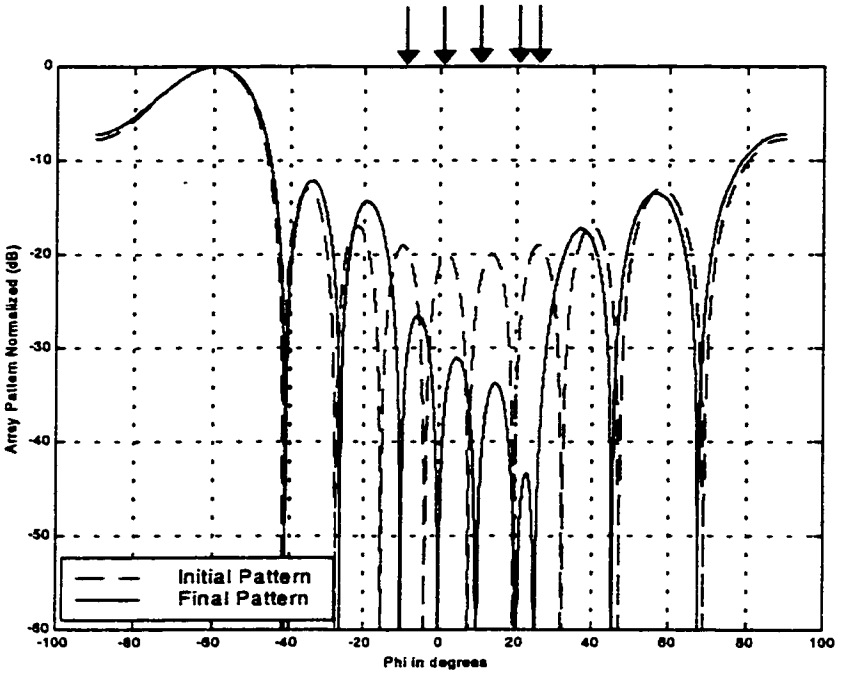

Figure 5.4-5: Array pattern showing main beam at -59.988^0 and nulls at 25.057^0 and 20.155^0, 9.966^0, 0.008^0, -10.071^0,

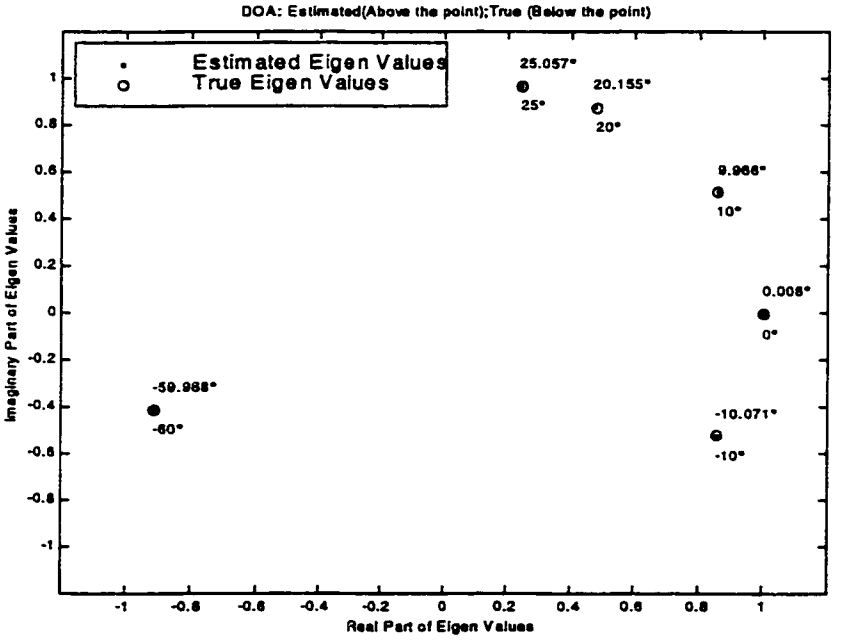

Figure 5.4-6: ESPRIT simulation results. Number of Signals = 6(Desired at -59.9880^0, CCI at 25.057^0,20.155^0,9.966^0,0.008^0, -10.071^0). True values and estimates of EVs $\Phi_i=exp\ (2\pi j(d/\lambda)sin\ (\varphi_i))$

Table 5.4-3: Details corresponding to the Final Array Pattern in Figure 5.4-5

Element	Complex Weights Before Null Steering	Complex Weights After Null Steering	Amplitude Changes after Null Steering	Phase Changes After Null Steering
1	$1e^{(j0)}$	$0.6529e^{(j8.5128}$	-0.3471	8.5128^0
2	$1e^{(j155.8657)}$	$1.1882e^{(j155.1527)}$	0.1882	-0.7130^0
3	$1e^{(-j48.2685)}$	$1.0352e^{(-j49.6386)}$	0.0352	-1.3701^0
4	$1e^{(j107.5972)}$	$0.8564e^{(j108.6371)}$	-0.1436	1.0399^0
5	$1e^{(-j96.5370)}$	$1.0757e^{(-j96.1400)}$	0.0757	0.3970^0
6	$1e^{(j59.3287)}$	$1.0757e^{(j58.9317)}$	0.0757	-0.3970^0
7	$1e^{(-j144.8055)}$	$0.8564e^{(-j145.8454)}$	-0.1436	-1.0399^0
8	$1e^{(j11.0602)}$	$1.0352e^{(j12.4303)}$	0.0352	1.3701^0
9	$1e^{(j16 6.9260)}$	$1.1882e^{(j167.6390)}$	0.1882	0.7130^0
10	$1e^{(-j37.2083)}$	$0.6529e^{(-j45.7211)}$	-0.3471	-8.5128^0
HPBW		Before Null Steering		21.7440^0
		After Null Steering		22.5720^0
Directivity		Before Null Steering		10.0000
		After Null Steering		9.6087
Maximum Amplitude / Minimum Amplitude (After Null Steering)				1.8199
Maximum Phase Change				8.5128^0

Case 4: Interferers lying in the main beam

Here a case is studied where in the interferers lie in the main beam within the HPBW. Nulls can still be placed as shown in Figure 5.4-7. The directivity is less due to uncontrolled rise in side lobe level that almost appears like grating lobes. But the major problem of interference suppression is solved. In fact more closely spaced interferences may be nulled, but to resolve two closely spaced signals requires large number of antenna elements. All results are tabulated in Table 5.4-4. From Table 5.4-4 we can see that although the phase changes are very small, much of the perturbation is done to the amplitudes. In Figure 5.4-9 is shown a much similar case, where the interferer is much closer to the desired signal. The desired signal and the interferer separated by just 3^0. As seen from Table 5.4.5, for steering single null in the main beam requires large phase

perturbations as well as amplitude perturbations. A shift in the main beam originally directed toward, 0.01^0, occurs due to the placing of a null in close vicinity of the main beam. As a result, the directivity is reduced drastically.

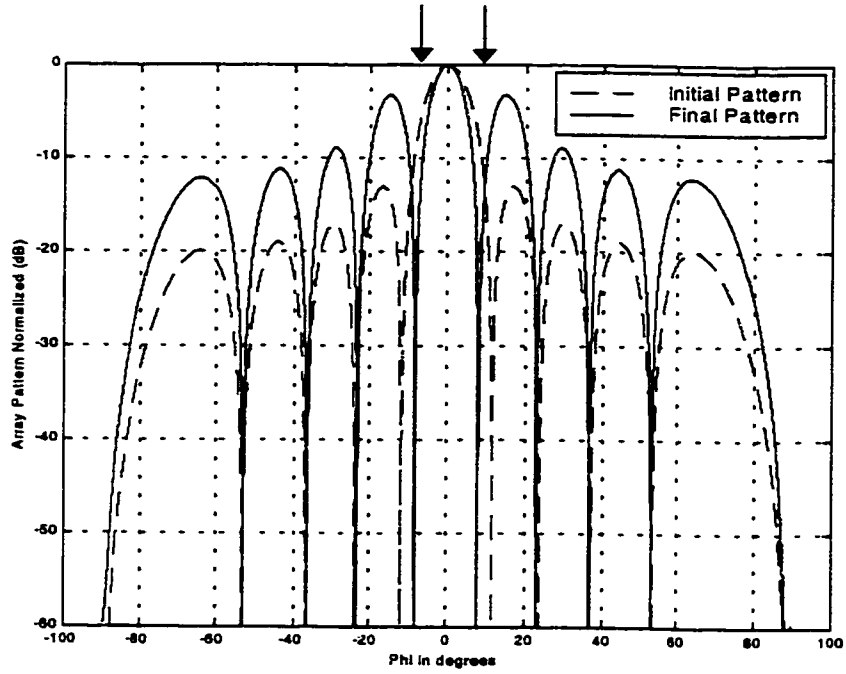

Figure 5.4-7: Array pattern showing main beam at -0^0 and null at $-8.022^0, 8.065^0$

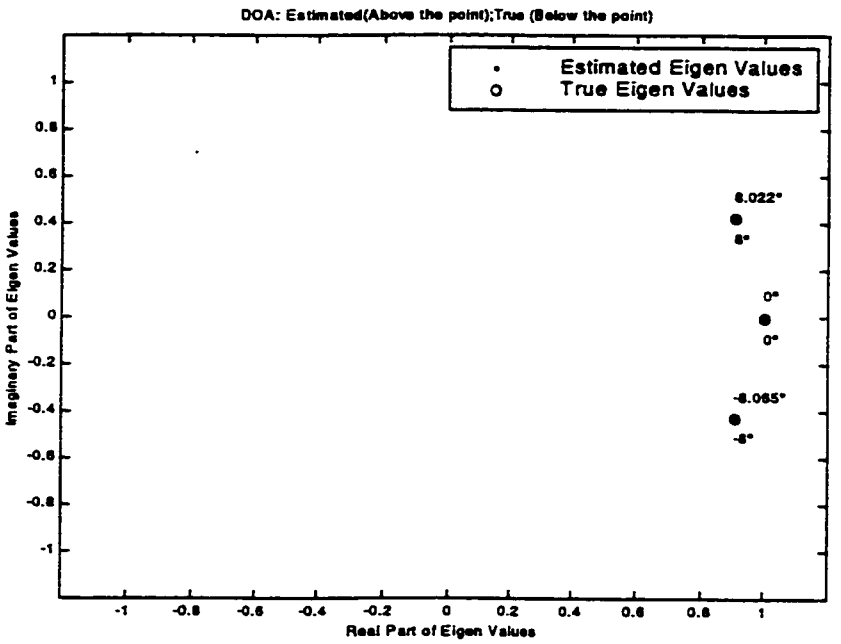

Figure 5.4-8: ESPRIT simulation results. Number of Signals=3(Desired at 0^0, CCI at -8.065^0, 8.022^0). True values and estimates of EVs $\Phi_i=exp\ (2\pi j(d/\lambda)sin\ (\varphi_i))$

Table 5.4-4: Details corresponding to the Array Patterns in Figure 5.4-7

Element	Complex Weights Before Null Steering	Complex Weights After Null Steering	Amplitude Changes after Null Steering	Phase Changes After Null Steering
1	$1e^{(j0)}$	$1.3786e^{(-j0.2361)}$	0.3786	-0.2361^0
2	$1e^{(j0.0011)}$	$0.9692e^{(-j0.2319)}$	-0.0308	-0.2330^0
3	$1e^{(j0.0023)}$	$0.5657e^{(-j0.2390)}$	-0.4343	-0.2413^0
4	$1e^{(j0.0034)}$	$0.2447e^{(-j0.2769)}$	-0.7553	-0.2804^0
5	$1e^{(j0.0046)}$	$0.0674e^{(-j0.2965)}$	-0.9326	-0.3011^0
6	$1e^{(j0.0057)}$	$0.0.0674e^{(j0.3068)}$	-0.9326	0.3011^0
7	$1e^{(j0.0069)}$	$0.2447e^{(j0.2872)}$	-0.7553	0.2804^0
8	$1e^{(j0.0080)}$	$0.5675e^{(j0.2493)}$	-0.4343	0.2413^0
9	$1e^{(j0.0092)}$	$0.9692e^{(j0.2422)}$	-0.0308	0.2330^0
10	$1e^{(j0.0103)}$	$1.3786e^{(j0.2464)}$	0.3786	0.2361^0
HPBW		Before Null Steering		10.2240^0
		After Null Steering		7.8300^0
Directivity		Before Null Steering		10.0000
		After Null Steering		6.4535
Maximum Amplitude / Minimum Amplitude (After Null Steering)				20.4695
Maximum Phase Change				0.3011^0

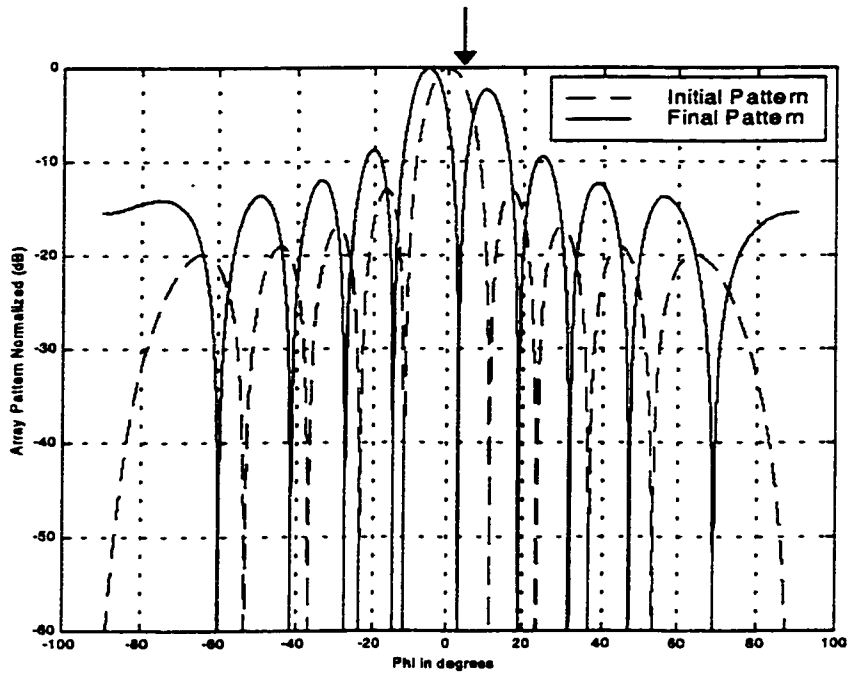

Figure 5.4-9: Array pattern showing the desired user at -0.026^0 lying with in the main beam and null at 3.043^0 placed with in the main beam

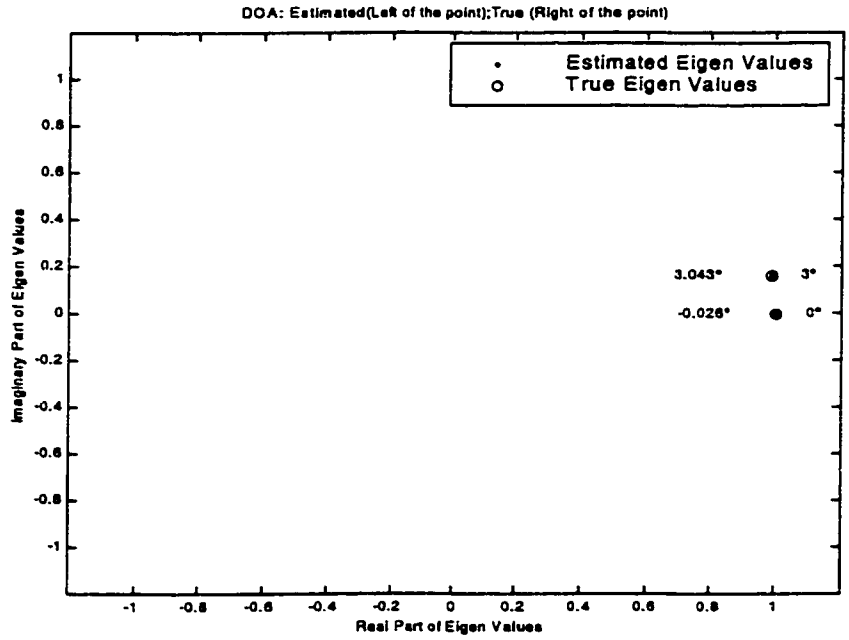

Figure 5.4-10: ESPRIT simulation results. Number of Signals=2(Desired at –0.026^0, CCI at 3.043^0). True values and estimates of EVs Φ_i=exp (2πj(d/λ)sin (φ_i)))

Table 5.4-5: Details corresponding to the Final Array Pattern in Figure 5.4-9

Element	Complex Weights Before Null Steering	Complex Weights After Null Steering	Amplitude Changes after Null Steering	Phase Changes After Null Steering
1	$1e^{(j0)}$	$0.7051e^{(-j59.7575)}$	-0.2949	-59.7575^0
2	$1e^{(j0.0830)}$	$0.5580e^{(-j61.8852)}$	-0.4420	-61.9682^0
3	$1e^{(j0.1660)}$	$0.4090e^{(-j62.1225)}$	-0.5910	-62.2885^0
4	$1e^{(j0.2489)}$	$0.2625e^{(-j57.2615)}$	-0.7375	-57.5105^0
5	$1e^{(j0.3319)}$	$0.1379e^{(-j32.3681)}$	-0.8621	-32.7000^0
6	$1e^{(j0.4149)}$	$0.1379e^{(j33.1149)}$	-0.8621	32.7000^0
7	$1e^{(j0.4979)}$	$0.2625e^{(j58.0083)}$	-0.7375	57.5105^0
8	$1e^{(j0.5808)}$	$0.4090e^{(j62.8693)}$	-0.5910	62.2885^0
9	$1e^{(j0.6638)}$	$0.5580e^{(j62.6320)}$	-0.4420	61.9682^0
10	$1e^{(j0.7468)}$	$0.7051e^{(j60.5043)}$	-0.2949	59.7575^0
HPBW		Before Null Steering		10.2060^0
		After Null Steering		8.4240^0
Directivity		Before Null Steering		10.0000
		After Null Steering		7.2763
Maximum Amplitude / Minimum Amplitude (After Null Steering)				5.1131
Maximum Phase Change				62.2885^0

Case 5: Interferer within the same cell due to Frequency reuse

One of the major advantages of the Smart Antenna is that by using the concept of SDMA, same channel (Frequency/ Time) can be used in the same cell. But it requires the signals to be separated in the spatial dimension. In this section such a case is illustrated. The user and the interferer will be of comparable SNR since they are operating in the same cell. Here a desired signal and an interferer at 0^0 and 30^0 have SNR 15 dB and 16 dB respectively. The interfering signal has a higher SNR than the desired signal. Having estimated the directions of both of them, its possible to steer the main beam in the desired direction with a null at interfering direction. From Figure 5.4-11 we see that an interferer with higher SNR than that of desired signal can be nulled. The complex weights used to achieve this are shown in Table 5.4-6.

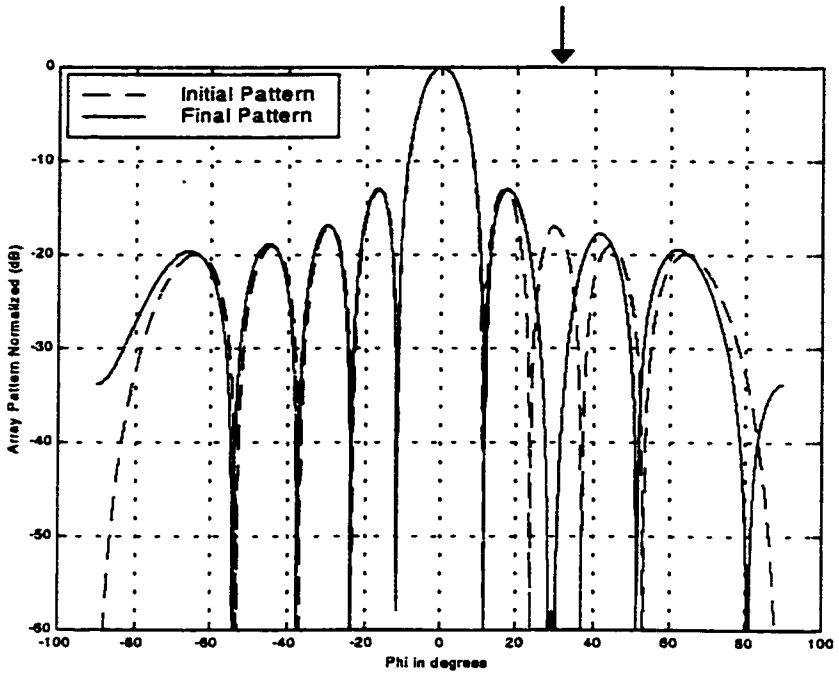

Figure 5.4-11: Array pattern showing main beam at 0^0 and null at 29.992^0

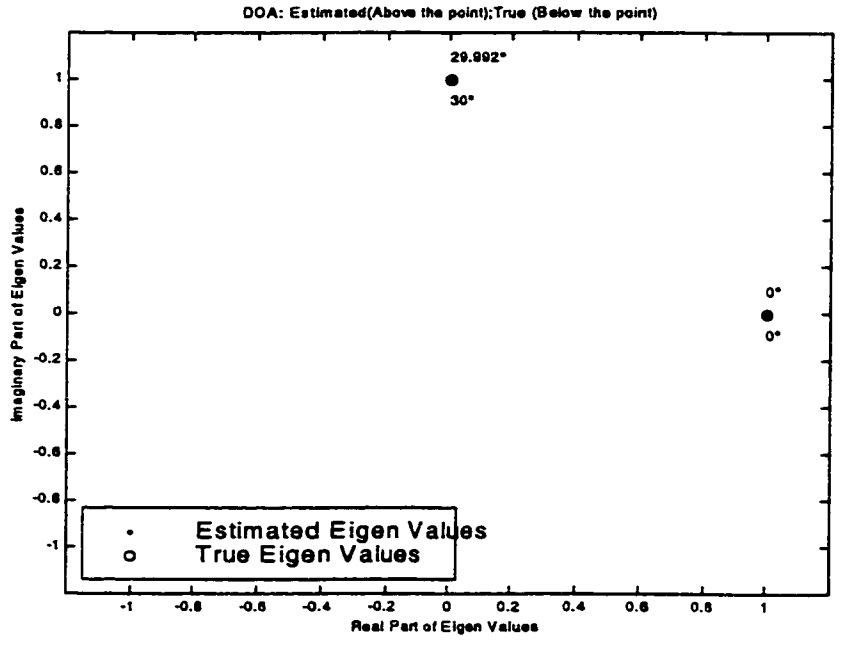

Figure 5.4-12: ESPRIT simulation results. Number of Signals=2(Desired at 29.992, Interferer at 29.992^0). True values and estimates of EVs $\Phi_i=exp\ (2\pi j(d/\lambda)sin\ (\varphi_i))$

Table 5.4-6: Details corresponding to the Final Array Pattern in Figure 5.4-11

Element	Complex Weights Before Null Steering	Complex Weights After Null Steering	Amplitude Changes after Null Steering	Phase Changes After Null Steering
1	$1e^{(j0)}$	$0.9054e^{(-j6.3214)}$	-0.0946	-6.3214^0
2	$1e^{(-j0.0012)}$	$0.9058e^{(j6.3384)}$	-0.0942	6.3396^0
3	$1e^{(-j0.0024)}$	$1.1045e^{(j5.1806)}$	0.1045	5.1830^0
4	$1e^{(-j0.0036)}$	$1.1043e^{(-j5.1957)}$	0.1043	-5.1921^0
5	$1e^{(-j0.0048)}$	$0.9056e^{(-j6.3353)}$	-0.0944	-6.3305^0
6	$1e^{(-j0.0060)}$	$0.9056e^{(j6.3246)}$	-0.0944	6.3305^0
7	$1e^{(-j0.0071)}$	$1.1043e^{(j5.1850)}$	0.1043	5.1921^0
8	$1e^{(-j0.0083)}$	$1.1045e^{(-j5.1913)}$	0.1045	-5.1830^0
9	$1e^{(-j0.0095)}$	$0.9058e^{(-j6.3491)}$	-0.0942	-6.3396^0
10	$1e^{(-j0.0107)}$	$0.9054e^{(j6.3107)}$	-0.0946	6.3214^0
HPBW		Before Null Steering		10.2240^0
		After Null Steering		10.4400^0
Directivity		Before Null Steering		10.0000
		After Null Steering		9.8006
Maximum Amplitude / Minimum Amplitude (After Null Steering)				1.2198
Maximum Phase Change				6.3396^0

5.4.2 Array Pattern and DOA in the presence of coherent multipath and Co-Channel Interference

In this section, results of estimation of Direction of Arrival of correlated signals and Null steering in those directions are presented. A practical situation of correlated signals is the presence of coherent multipaths of a desired signal. The ESPRIT algorithm is used along with SS (Spatial Smoothing) technique to deal with the coherence of the signals. Array Patterns after nulling the Signals-Not-of –Interest, which include both the undesired Co-Channel users and the multipath of the desired signals, are shown. To avoid exaggeration, three cases will be dealt with. In the case 1 a desired signal and its multipath are considered. In case 2 a desired signal, its coherent multipath and a Co-Channel interferer uncorrelated with desired signal are assumed. As studied in Section 5.4.1, the desired

signal is taken to have higher SNR and the signal environment is considered similar to the one assumed there except that here correlated multipath are also included. In case 3 the number of multipaths are increased to three.

Case 1: Desired Signal and its Multipath is Present

A desired signal with 15 dB SNR coming from 60^0 and its multipath component coming from -40^0 are considered. The multipath while taking its course will suffer an amplitude reduction and a phase change, which is represented by a complex quantity $C = \rho e^{j\alpha}$, where ρ is the amplitude reduction factor which by itself may be complex and α is the phase shift. The desired signal considered here is multiplied by $C = 0.3+0.4i$, where $\rho=0.5$ and $\alpha = 53.13^0$ to give the multipath component. Clearly the desired signal and its multipath will be highly correlated. The adapted array pattern is shown in Figure 5.4-13 and the DOA estimates shown in Figure 5.4-14. All the details are listed in Table 5.4-7. While implementing the Spatial Smoothing technique to remove the effect of coherence, the length of the Spatial Smoothing sub array is taken as L=N-1 (i.e one less than the number of array elements).

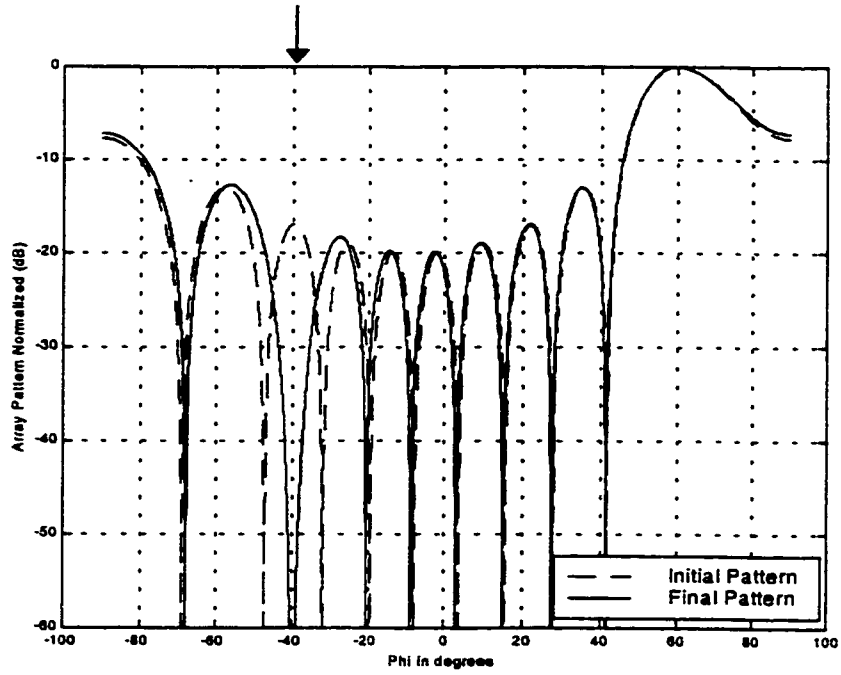

Figure 5.4-13: Array pattern showing main beam at 60.009^0 and null at –40.005^0

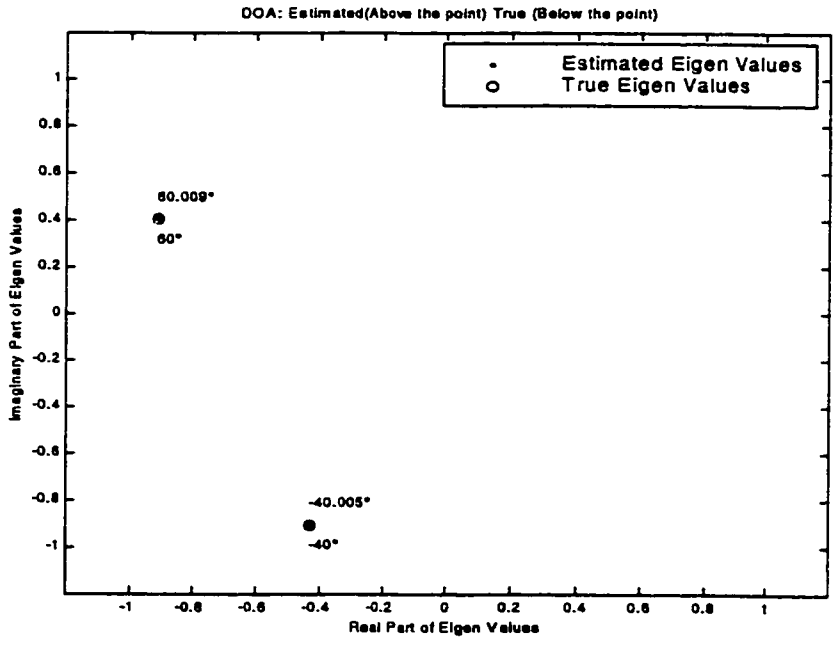

Figure 5.4-14: ESPRIT simulation results. Number of Signals=2(Desired at 60.009^0, multipath at -40.005^0). True values and estimates of EVs Φ_i=exp (2πj(d/λ)sin (φ_i))

Table 5.4-7: Details corresponding to Final Array Pattern of Figure 5.4-13

Element	Complex Weights Before Null Steering	Complex Weights After Null Steering	Amplitude Changes after Null Steering	Phase Changes After Null Steering
1	$1e^{(j0)}$	$0.8921e^{(-j5.5848)}$	-0.1079	-5.5848^0
2	$1e^{(-j155.8993)}$	$0.9166e^{(-j149.0276)}$	-0.0834	6.8716^0
3	$1e^{(j48.2015)}$	$1.1110e^{(j53.0028)}$	0.1110	4.8013^0
4	$1e^{(-j107.6978)}$	$1.1009e^{(-j113.1412)}$	0.1009	-5.4434^0
5	$1e^{(j96.4029)}$	$0.9037e^{(j90.1220)}$	-0.0963	-6.2809^0
6	$1e^{(-j59.4963)}$	$0.9037e^{(-j53.2154)}$	-0.0963	6.2809^0
7	$1e^{(j144.6044)}$	$1.1009e^{(j150.0478)}$	0.1009	5.4434^0
8	$1e^{(-11.2949)}$	$1.1110e^{(-j16.0962)}$	0.1110	-4.8013^0
9	$1e^{(-j167.1941)}$	$0.9166e^{(-j174.0658)}$	-0.0834	-6.8716^0
10	$1e^{(j36.9066)}$	$0.8921e^{(j42.4914)}$	-0.1079	5.5848^0
HPBW		Before Null Steering		21.7800^0
		After Null Steering		22.3560^0
Directivity		Before Null Steering		10.0000
		After Null Steering		9.7988
Maximum Amplitude / Minimum Amplitude (After Null Steering)				1.2454
Maximum Phase Change				6.8716^0

Case 2: Desired Signal, its Multipath and a Co-Channel Interferer are present

The analysis presented is similar to the one presented in the previous case. But here an uncorrelated Co-Channel signal is also assumed. The uncorrelated Signal is incident from azimuth direction of 20^0 with a SNR of 10 dB. The corresponding results are shown in Figure 5.4-15, Figure 5.4-16 and Table 5.4-8. Focusing on the results, particularly corresponding to Figure 5.4-16 we can conclude that by applying the Spatial Smoothing technique, the ESPRIT algorithm can resolve both uncorrelated and correlated signals.

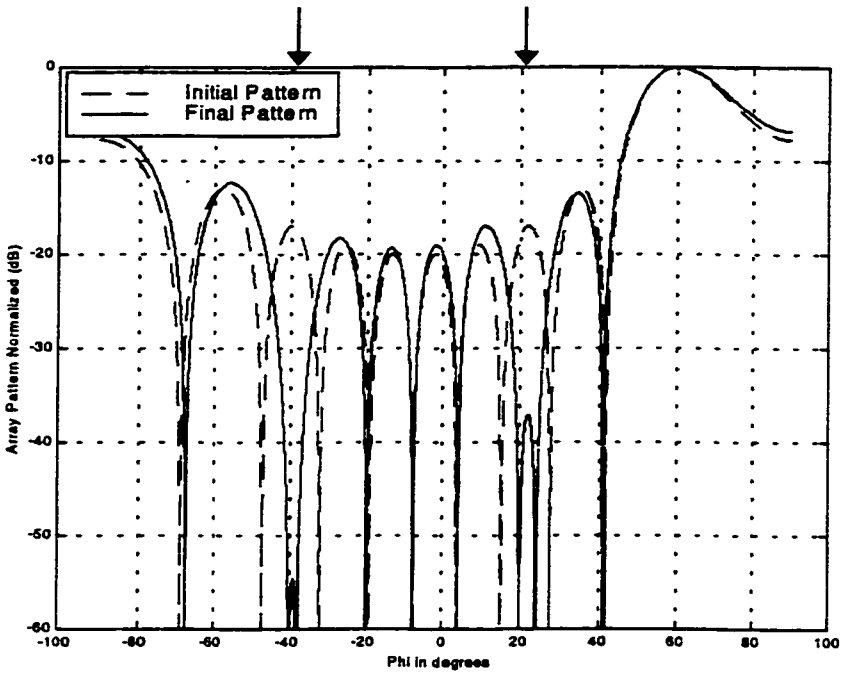

Figure 5.4-15: Array pattern showing main beam at 59.992^0 and null at –39.991^0, 20.005^0

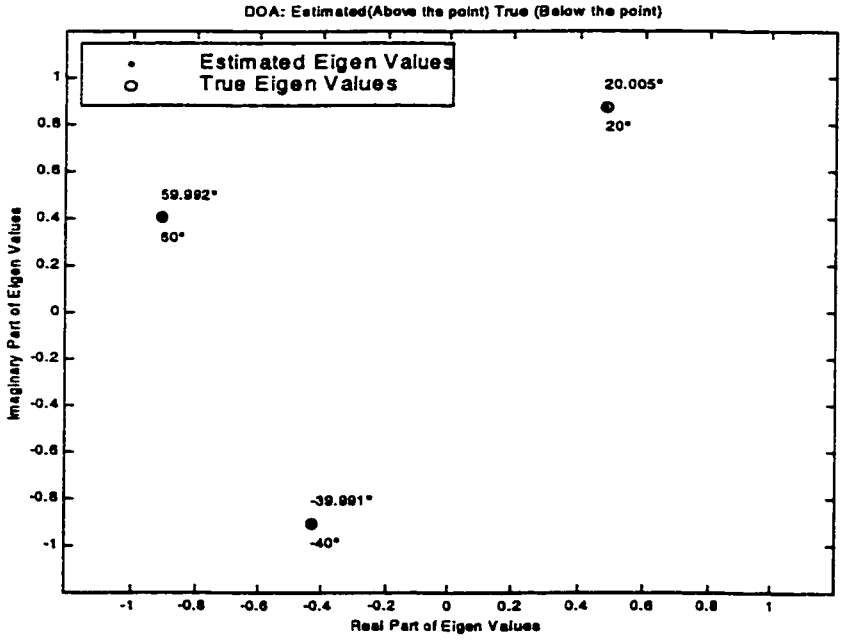

Figure 5.4-16: ESPRIT simulation results. Number of Signals=3(Desired at 59.992^0, CCI at 20.005^0, multipath at -39.991^0). True values and estimates of EVs

$\Phi_i = exp(2\pi j(d/\lambda)sin(\varphi_i))$

Table 5.4-8: Details corresponding to Final Array Pattern of Figure 5.4-15

Element	Complex Weights Before Null Steering	Complex Weights After Null Steering	Amplitude Changes after Null Steering	Phase Changes After Null Steering
1	$1e^{(j0)}$	$0.8299e^{(j1.9375)}$	-0.1701	1.9375^0
2	$1e^{(-j155.8724)}$	$0.7963e^{(-j152.5092)}$	-0.2037	3.3633^0
3	$1e^{(j48.2551)}$	$1.1825e^{(j47.6610)}$	0.1825	-0.5941^0
4	$1e^{(-j107.6173)}$	$1.2003e^{(-j108.8316)}$	0.2003	-1.2143^0
5	$1e^{(j96.5103)}$	$0.8076e^{(j96.1083)}$	-0.1924	-0.4019^0
6	$1e^{(-j59.3621)}$	$0.8076e^{(-j58.9602)}$	-0.1924	0.4019^0
7	$1e^{(j144.7654)}$	$1.2003e^{(j145.9797)}$	0.2003	1.2143^0
8	$1e^{(-11.1070)}$	$1.1825e^{(-j10.5129)}$	0.1825	0.5941^0
9	$1e^{(-j166.9794)}$	$0.7963e^{(-j170.3427)}$	-0.2037	-3.3633^0
10	$1e^{(j37.1481)}$	$0.8299e^{(j35.2106)}$	-0.1701	-1.9375^0
HPBW		Before Null Steering		21.7440^0
		After Null Steering		22.9320^0
Directivity		Before Null Steering		10.0000
		After Null Steering		9.6320
Maximum Amplitude / Minimum Amplitude (After Null Steering)				1.5074
Maximum Phase Change				3.3633^0

Case 3: Desired signal, its multipaths and Co-Channel Interfere are present

Keeping the desired signal at 60^0, Co-Channel at 20^0, three multipaths of desired signal are dealt with. Their DOAs are 0^0, -30^0 and -60^0. Their (α, ρ) factors are respectively ($0.1,10^0$), (0.05, 20^0), ($0.8,80^0$). As seen from Figure 5.4-18 and Figure 5.4-17, the multipaths are perfectly resolved and nulled.

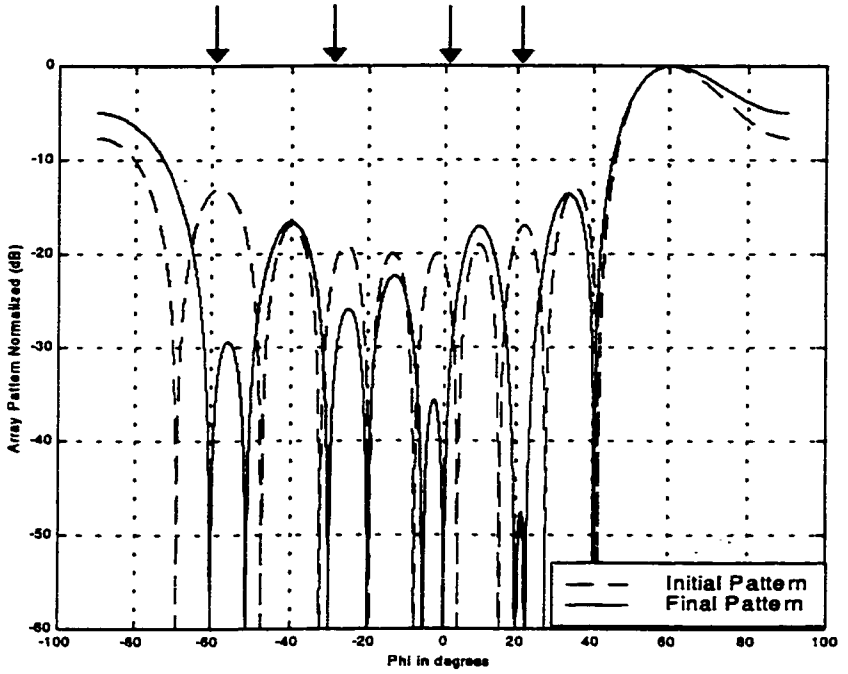

Figure 5.4-17: Array pattern showing main beam at 60.043^0 and null at 20.014^0, 0.035^0, -30.089^0, -60.044^0

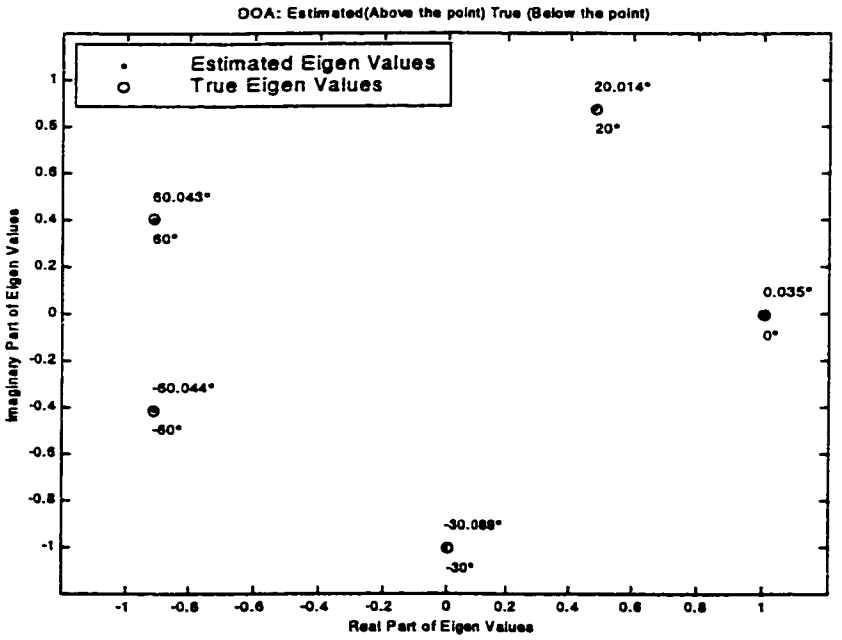

Figure 5.4-18: ESPRIT simulation results. Number of Signals=5(Desired at 60.043^0, CCI at 20.014^0, multipath at 0.035^0, -30.089^0, -60.044^0). True values and estimates of EVs $\Phi_i=exp\ (2\pi j(d/\lambda)sin\ (\varphi_i))$

Table 5.4-9: Details corresponding to Final Array Pattern of Figure 5.4-17

Element	Complex Weights Before Null Steering	Complex Weights After Null Steering	Amplitude Changes after Null Steering	Phase Changes After Null Steering
1	$1e^{(j0)}$	$0.6462e^{(-j0.3689)}$	-0.3538	-0.3689^0
2	$1e^{(-j155.9527)}$	$0.8062e^{(-j155.6111)}$	-0.1938	0.3416^0
3	$1e^{(j48.0946)}$	$0.9140e^{(j51.6074)}$	-0.0860	3.5129^0
4	$1e^{(-j107.8582)}$	$1.1808e^{(-j96.8423)}$	0.1808	11.0159^0
5	$1e^{(j96.1891)}$	$1.1585e^{(j111.7379)}$	0.1585	15.5487^0
6	$1e^{(-j59.7636)}$	$1.1585e^{(-j75.3123)}$	0.1585	-15.5487^0
7	$1e^{(j144.2837)}$	$1.1808e^{(j133.2678)}$	0.1808	-11.0159^0
8	$1e^{(-11.6690)}$	$0.9140e^{(-j15.1819)}$	-0.0860	-3.5129^0
9	$1e^{(-j167.6217)}$	$0.8062e^{(-j167.9633)}$	-0.1938	-0.3416^0
10	$1e^{(j36.4255)}$	$0.6462e^{(j36.7945)}$	-0.3538	0.3689^0
HPBW		Before Null Steering		21.7800^0
		After Null Steering		25.7760^0
Directivity		Before Null Steering		10.0000
		After Null Steering		9.3058
Maximum Amplitude / Minimum Amplitude (After Null Steering)				1.8273
Maximum Phase Change				15.5487^0

5.4.3 Array Pattern and DOA in the presence of Co-Channel Interference, Coherent multipath and Adjacent channel interference

Adjacent channel Interference (ACI) results from signals, which are adjacent in frequency to the desired signal. The cause of this is due to imperfect receiver filters that allow nearby frequencies to leak into the passband. In performing Null Steering in such a case, along with the DOA estimation, the estimation of the frequencies has to be done to extract correct information about the signal environment The array geometry for simultaneous estimation of both frequency and DOA is shown in Figure 4.3-1. The angle between the two arrays ψ is taken as 30^0. The complex weights can then be adjusted to direct the main

beam in the desired direction and nulls in the interfering directions irrespective of frequencies.

As the array at the base station is used to enhance and separate the reverse link signals in the receive mode, the frequency specifications of the reverse link (uplink) have to be focused. For the purpose of analysis wireless systems GSM and DCS-1900 belonging to the ANSI J-STD- 007 standard is taken. The typical reverse link (uplink) frequencies in such a system are 890 MHz to 915 MHz. This uses TDMA Multiple Access Technology with a carrier separation of 200KHz (0.2 MHz).

Case 1: Only ACI is present

The desired signal is impinged from the azimuthal direction 20^0 with respect to the normal of the array with SNR 30 dB and a frequency of 914.8 MHz. The interferers are uncorrelated with desired signal and assumed to be at -37^0 and 0^0 with SNR of 20 dB. Their frequencies are 915 MHz and 914.6 MHz respectively. Thus the interferers are separated by 200KHz with desired carrier frequency. Their estimates of DOA as shown in Figure 5.4-20 are quite promising. Figure 5.4-19 shows the resultant array pattern.

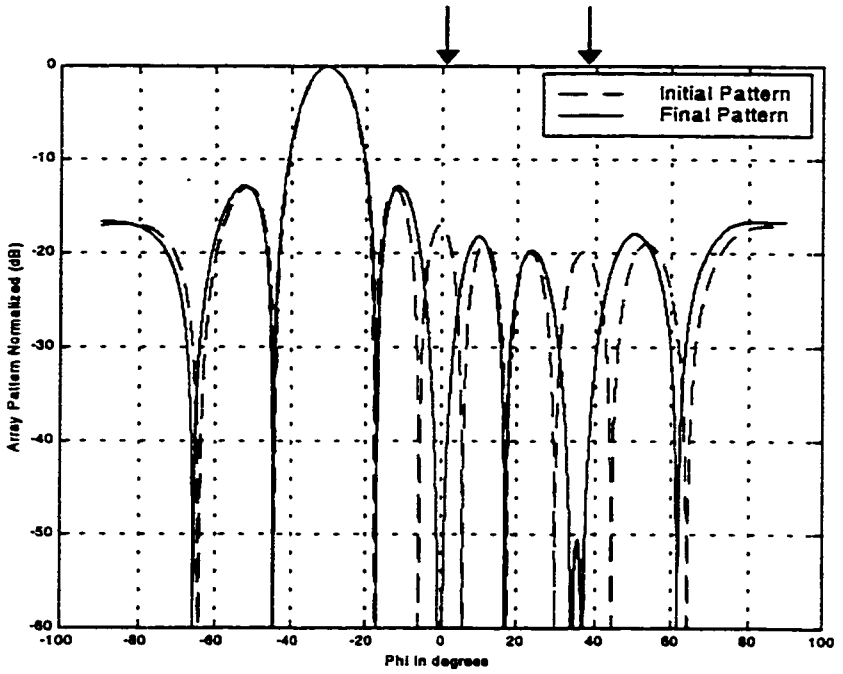

Figure 5.4-19: Array pattern showing main beam at -30^0 and null at 37.002^{0}and 0^0

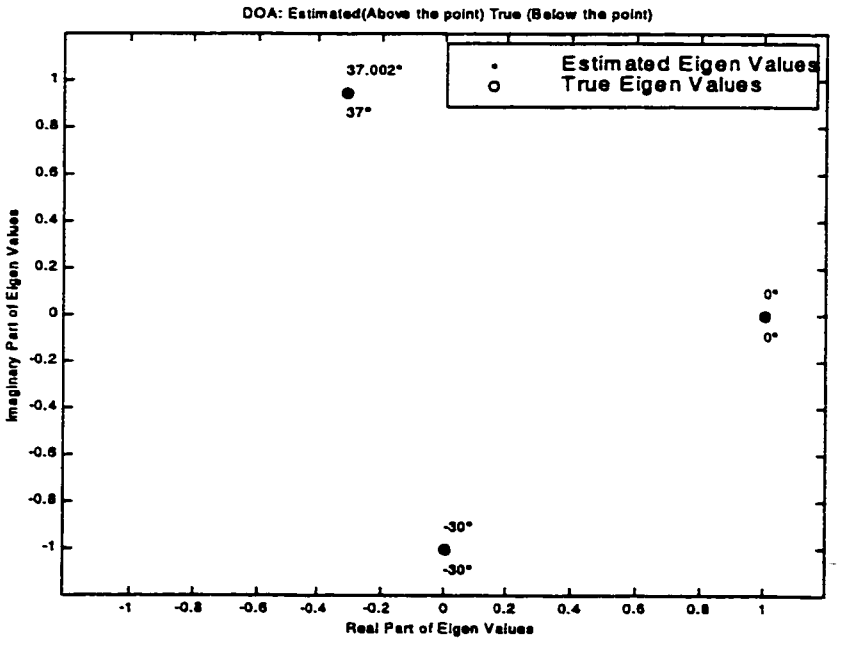

Figure 5.4-20: ESPRIT simulation results. Number of Signals=3(Desired at -30^0, ACI at 37.002^0 and 0^0). True values and estimates of EVs Φ_i=exp (2πj(d/λ)sin (φ_i))

Table 5.4-10: Details corresponding to Final Array Pattern of Figure 5.4-19

Element	Complex Weights Before Null Steering	Complex Weights After Null Steering	Amplitude Changes after Null Steering	Phase Changes After Null Steering
1	$1e^{(j0)}$	$0.8054e^{(-j6.1633)}$	-0.1946	-6.1633^0
2	$1e^{(j89.9995)}$	$0.9925e^{(j93.2218)}$	-0.0075	3.2223^0
3	$1e^{(j179.9989)}$	$1.0414e^{(-j170.6248)}$	0.0414	9.3762^0
4	$1e^{(-j90.0016)}$	$1.1615e^{(-j99.3563)}$	0.1615	-9.3547^0
5	$1e^{(-j0.0021)}$	$0.8844e^{(-j0.0242)}$	-0.1156	-0.0221^0
6	$1e^{(j89.9974)}$	$0.8844e^{(j90.0195)}$	-0.1156	0.0221^0
7	$1e^{(j179.9968)}$	$1.1615e^{(-j170.6485)}$	0.1615	9.3547^0
8	$1e^{(-j90.0037)}$	$1.0414e^{(-j99.3799)}$	0.0414	-9.3762^0
9	$1e^{(-j0.0042)}$	$0.99258e^{(-j3.2265)}$	-0.0075	-3.2223^0
10	$1e^{(j89.9952)}$	$0.8054e^{(j96.1586)}$	-0.1946	6.1633^0
HPBW		Before Null Steering		11.8440^0
		After Null Steering		12.2040^0
Directivity		Before Null Steering		10.0000
		After Null Steering		9.6996
Maximum Amplitude / Minimum Amplitude (After Null Steering)				1.4422
Maximum Phase Change				9.3762^0

Table 5.4-11:True Frequencies and Estimated Frequencies

True DOA	-30^0	37^0	0^0
Estimated DOA	-30^0	36.002^0	0^0
True Frequency (MHz)	914.8	914.6	915
Estimated Frequency (MHz)	914.8189	914.5415	914.9721

Case 2: CCI, ACI and Multipath of desired signal are present

A more generalized scenario is studied wherein the desired signal at -30^0 has a multipath component ($\varphi = 53.5^0$, $\alpha = 0.6$, $\rho = 10^0$). Also a CCI with same frequency as that of desired signal and an ACI with a different carrier frequency are dealt with. The directions of CCI and ACI are 0^0 and 37^0 respectively. Figure 5.4-21, Figure 5.4-22 and Table 5.4-12, Table 5.4-13 contains all the details.

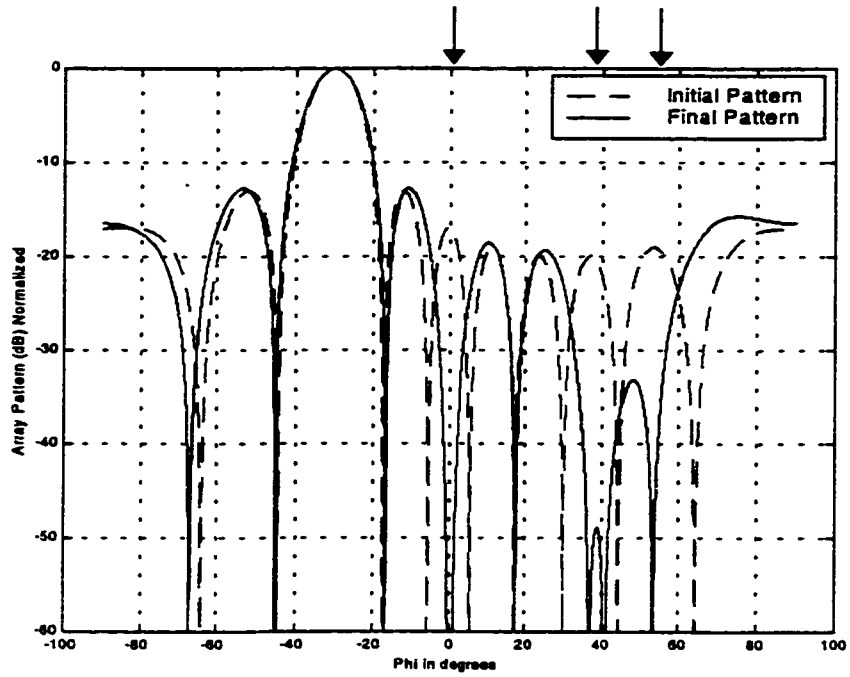

Figure 5.4-21: Array pattern showing main beam at -30^0 and null at.0^0, 37.005^{0}and 53.503^0

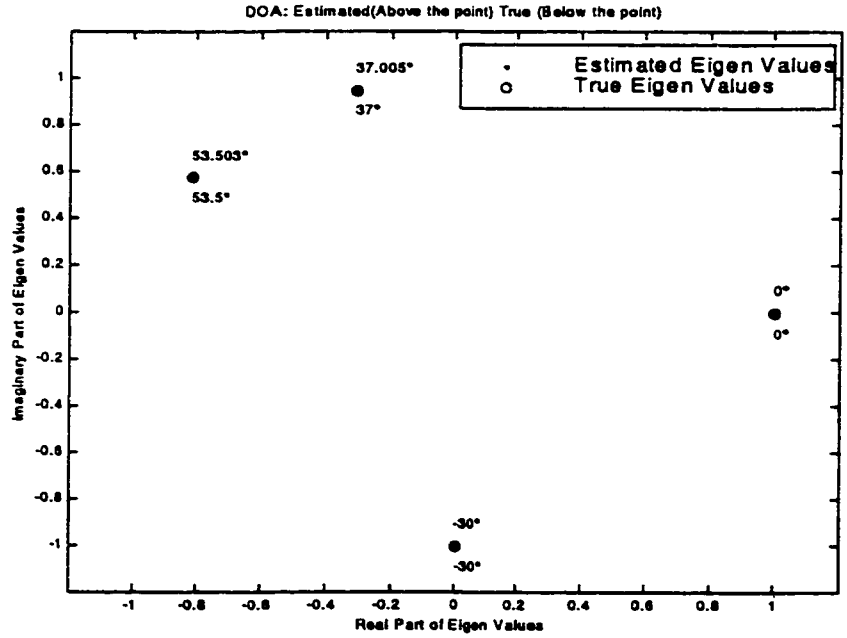

Figure 5.4-22: ESPRIT simulation results. Number of Signals=4(Desired at -30^0, ACI at 37.005^0, CCI at 0^0, Multipath at 53.503^0). True values and estimates of EVs Φ_i=exp $(2\pi j(d/\lambda)\sin(\varphi_i))$

Table 5.4-12: Details corresponding to Final Array Pattern of Figure 5.4-21

Element	Complex Weights Before Null Steering	Complex Weights After Null Steering	Amplitude Changes after Null Steering	Phase Changes After Null Steering
1	$1e^{(j0)}$	$0.7027e^{(-j3.3918)}$	-0.2973	-3.3918
2	$1e^{(j90.0001)}$	$1.0136e^{(j87.0438)}$	0.0136	-2.9563
3	$1e^{(-j179.9998)}$	$1.1310e^{(-j167.2979)}$	0.1310	12.7019
4	$1e^{(-j89.9997)}$	$1.0500e^{(-j99.4299)}$	0.0500	-9.4301
5	$1e^{(j0.0003)}$	$0.9409e^{(-j6.0329)}$	-0.0591	-6.0332
6	$1e^{(j90.0004)}$	$0.9409e^{(j96.0337)}$	-0.0591	6.0332
7	$1e^{(-j179.9995)}$	$1.0500e^{(-j170.5694)}$	0.0500	9.4301
8	$1e^{(-j89.9994)}$	$1.1310e^{(-j102.7013)}$	0.1310	-12.7019
9	$1e^{(j0.0007)}$	$1.0136e^{(j2.9570)}$	0.0136	2.9563
10	$1e^{(j90.0008)}$	$0.7027e^{(j93.3925)}$	-0.2973	3.3918
HPBW		Before Null Steering		11.8440^0
		After Null Steering		12.3840^0
Directivity		Before Null Steering		10.0000
		After Null Steering		9.5780
Maximum Amplitude / Minimum Amplitude (After Null Steering)				1.6096
Maximum Phase Change				12.7019^0

Table 5.4-13: True Frequencies and Estimated Frequencies

True DOA	-30^0	0^0	37^0	53.5^0
Estimated DOA	-30^0	0^0	37.005^0	53.503^0
True Frequency (MHz)	915	915	914.8	915
Estimated Frequency (MHz)	915.0004	914.9728	914.7900	914.9611

5.5 Consistency of the ESPRIT parameter estimate

5.5.1 Estimating DOA

The consistency of estimating DOA is carried out in this section. Signals are all considered at same SNR of 15 dB and with same carrier frequencies. Mean Values and Standard Deviation of the estimates is carried out for 100 runs. Details are shown in Table 5.5-1.

Table 5.5-1: Mean and Standard Deviation of Estimated DOA. Number of runs = 100

Number of DOA	True DOA	Mean of Estimated DOA	Standard Deviation of Estimated DOA
2	-30^0	-30.0018^0	0.0062^0
	30^0	29.9997^0	0.0109^0

5.5.2 Estimating Frequency

The signals arriving at -30^0 and 30^0 with same SNR have their carrier frequencies centered at 890.4 MHz and 890.2 MHz. For 100 runs the standard deviation and mean values of the estimated frequencies are shown in Table 5.5-2

Table 5.5-2: Mean and Standard Deviation of Estimated Frequencies. Number of runs = 100

Number of DOA	True Frequencies (MHz)	Mean of Estimated Frequencies (MHz)	Standard Deviation of Estimated Frequencies (MHz)
2	890.4	890.4087	0.0758
	890.2	890.2278	0.0671

5.6 Effect of increasing the number of elements on the accuracy of the ESPRIT parameter estimate

5.6.1 Estimation of DOA

The effect of Number of Elements on estimation of Direction of Arrival is studied in this section. The accuracy of the estimates improves as the number of elements is increased. Figure 5.6-1 shows the Standard Deviation in estimated DOA for 300 runs. Figures 5.6-2 and Figures 5.6-3 shows the mean values. The signals are considered to be with SNR 15dB.

Focusing our attention on the variation of standard deviation with number of elements, if the number of elements is taken more than 10, then the standard deviation of the estimates is less than 0.01^0. Also from Figures 5.6-2 and Figure 5.6-3 we can observe that for higher number of elements, the mean values settled within one tenth of a degree.

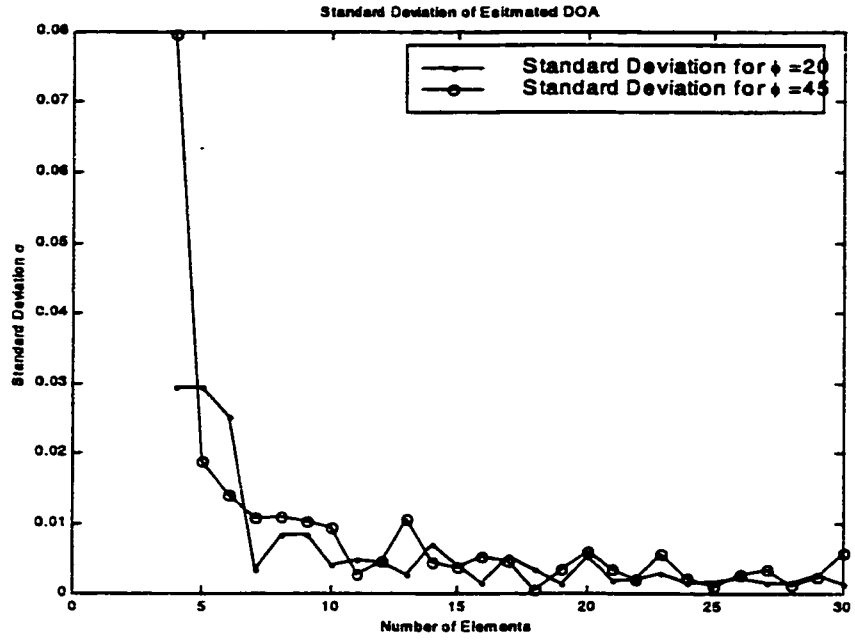

Figure 5.6-1: Effect of increasing Number of Elements on the standard deviation of the estimated DOA.

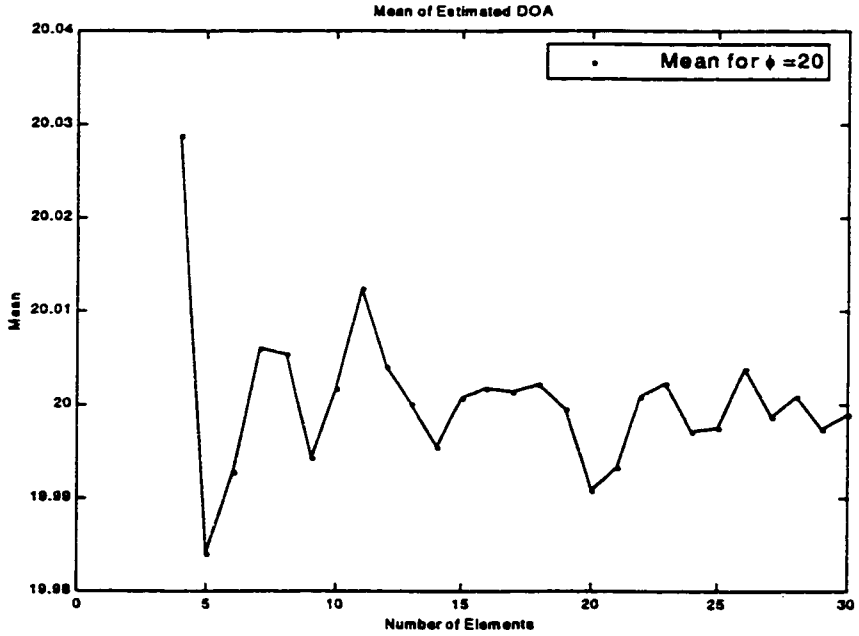

Figure 5.6-2: Effect of increasing Number of Elements on the mean of the estimated DOA

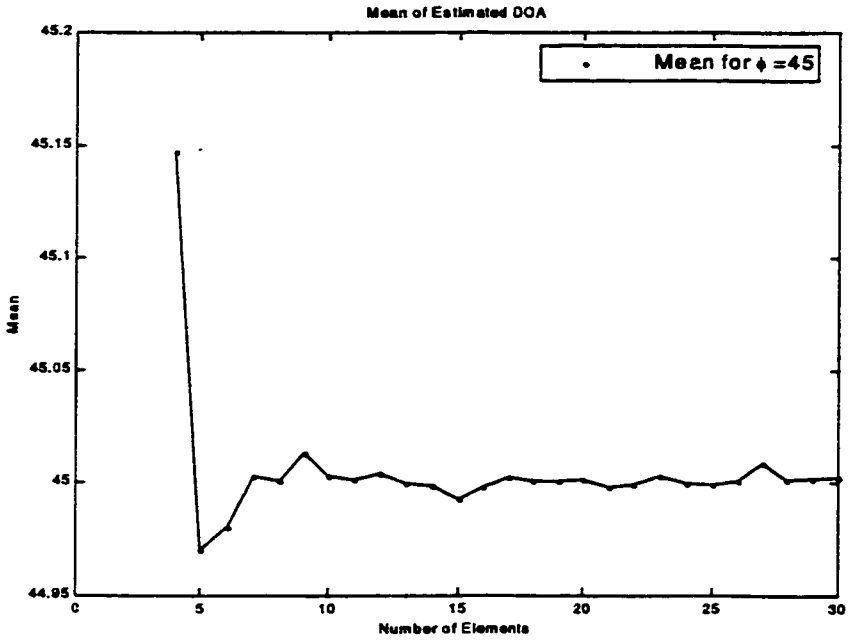

Figure 5.6-3: Effect of increasing Number of Elements on the mean of the estimated DOA

5.6.2 Estimation of Frequency

The carrier frequencies of the signals assumed in Section 5.5.1 are changed to 915 MHz and 914.8 MHz for -30^0 and 30^0 degrees respectively. The statistical analysis is carried out for the estimated frequencies. Figure 5.5-4 to Figure 5.5-6 gives the details about the Standard Deviation and Mean values. Again for higher values of number of elements the estimates are consistent and more accurate.

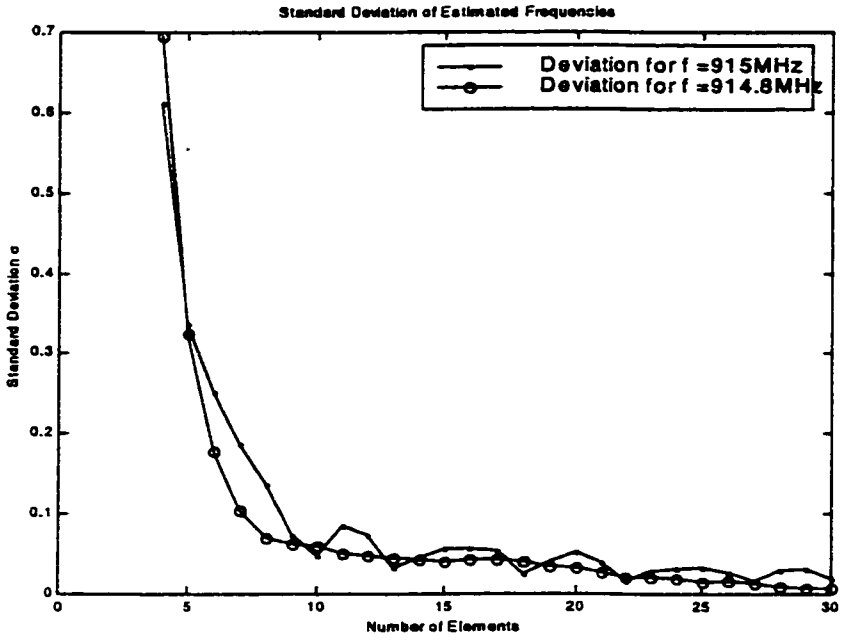

Figure 5.6-4: Effect of increasing Number of Elements on the standard deviation of the estimated Frequencies

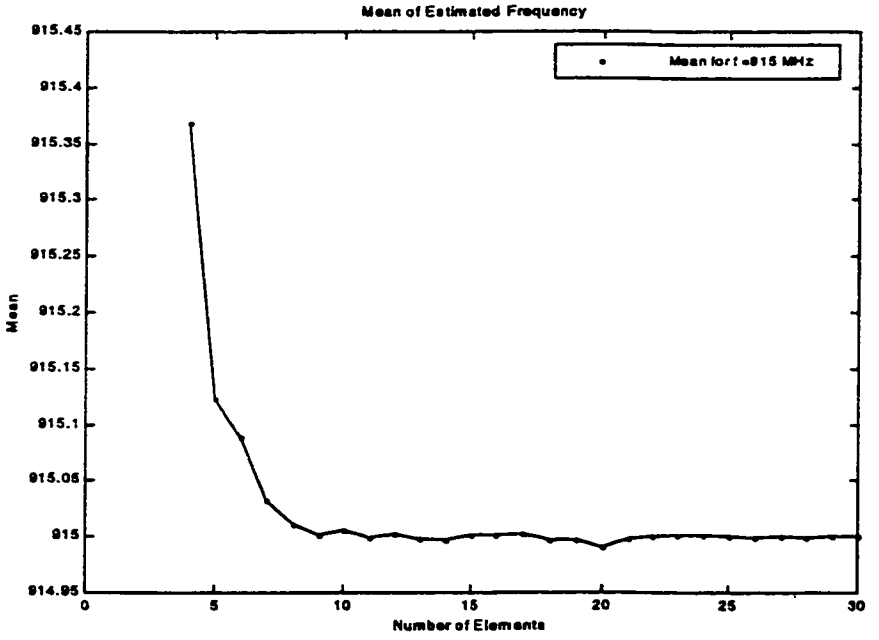

Figure 5.6-5: Effect of increasing Number of Elements on the mean of the estimated Frequency

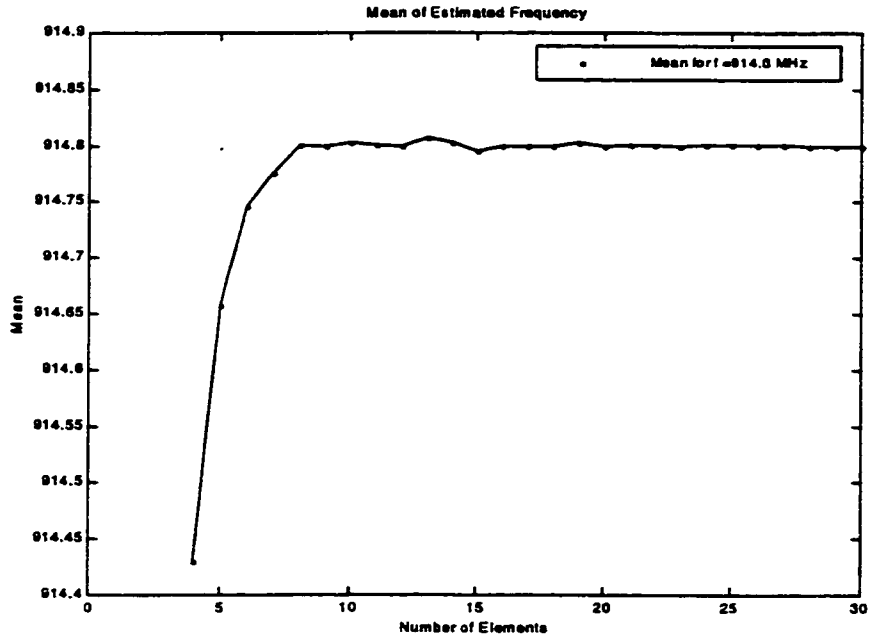

Figure 5.6-6: Effect of increasing Number of Elements on the mean of the estimated Frequency

5.7 Effect of SNR on ESPRIT parameter estimate

5.7.1 Effect on estimating DOA

The standard deviation of the estimated DOA is carried out for 300 runs for each increasing value of SNR. As seen from Figure 5.7-1, the standard deviation values decreases with increasing SNR. Case is studied for two DOA (at -30^0 and 30^0) with same carrier frequencies. The corresponding mean values for the same number of runs are given in Figure 5.7-2 and Figure 5.7-3. From these observations we see that the mean values settle near to the True values for higher SNR. As such higher the SNR, more accurate is the estimate.

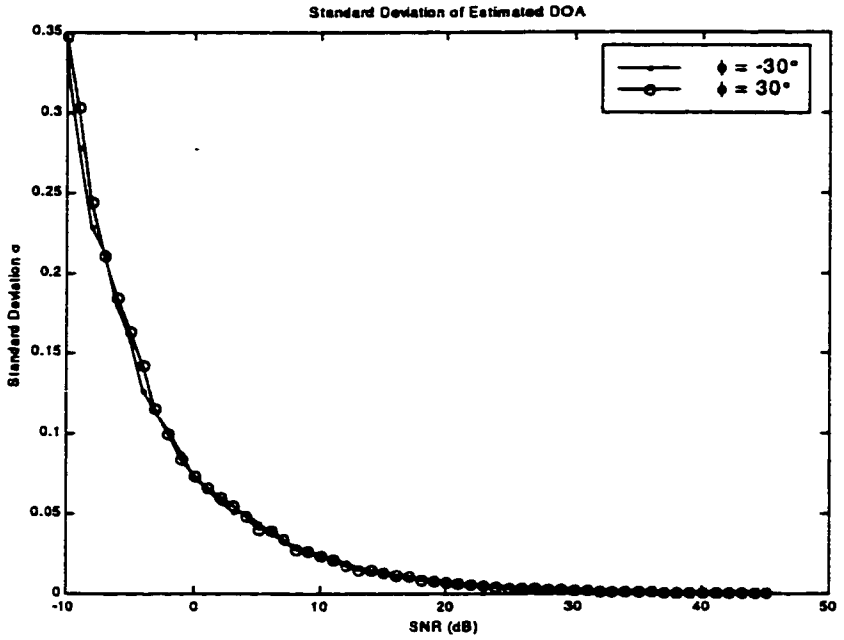

Figure 5.7-1: Standard Deviation of Estimated angle ($\varphi = -30^0$, $\varphi = 30^0$) with increasing SNR. Number of Runs = 300.

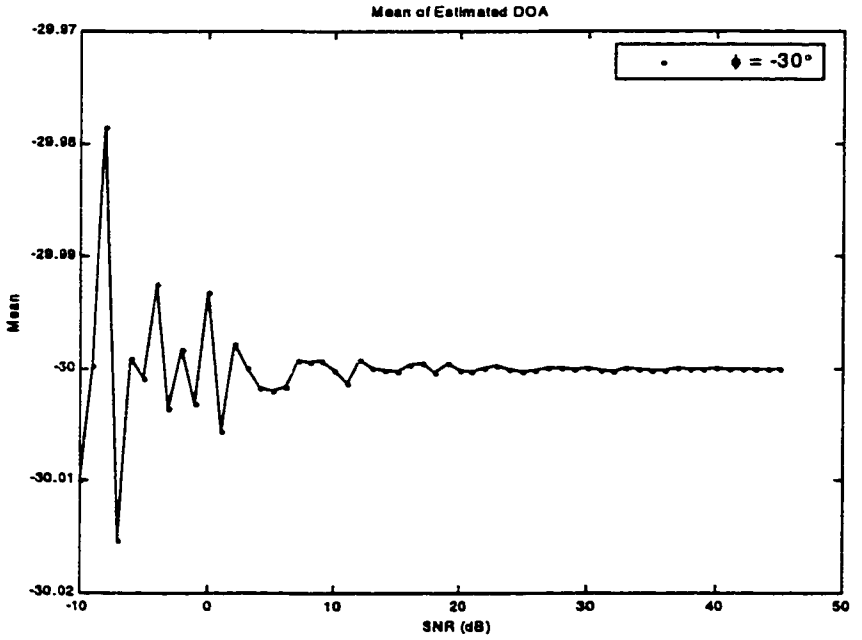

Figure 5.7-2: Mean of Estimated angle ($\varphi = -30^0$) with increasing SNR (σ given in Figure 5.7-1). Number of Runs = 300.

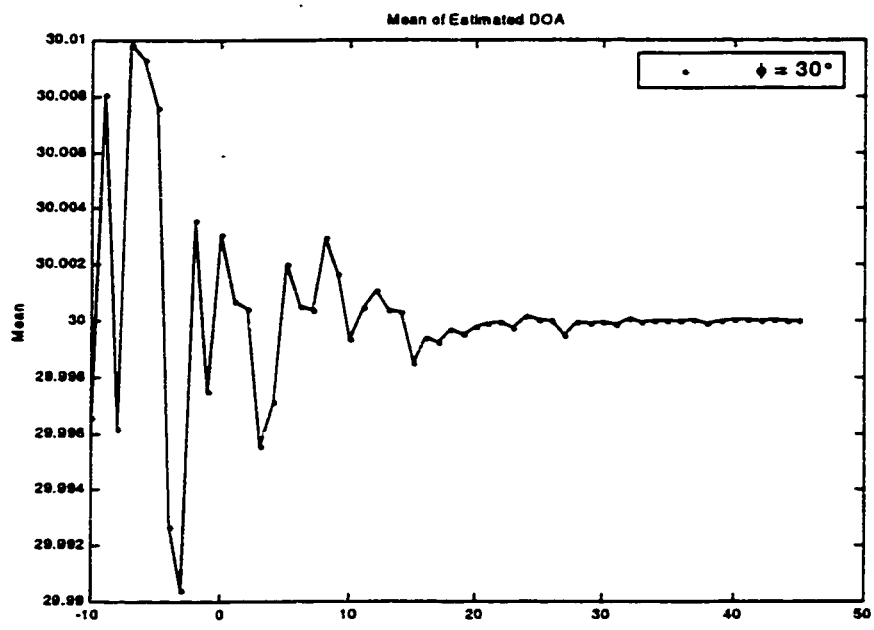

Figure 5.7-3: Mean of Estimated angle ($\varphi = 30^0$) with increasing SNR (σ given in Figure 5.7-1). Number of Runs = 300.

5.7.2 Effect on estimation of Frequency

With the assumptions of the previous section, the effect of SNR on estimation of frequency is studied. The carrier frequencies of the signals are 915 MHz and 914.8 MHz. Figure 5.7-4 shows the standard deviation values and Figure 5.7-5, Figure 5.7-6 shows the respective mean values.

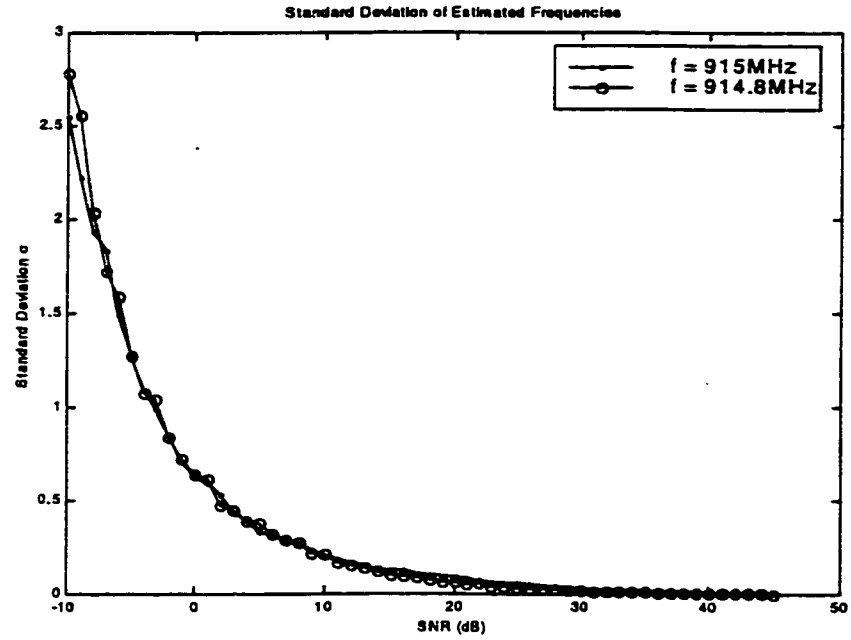

Figure 5.7-4: Standard Deviation of Estimated Frequencies (f =915 MHz, f = 914.8 MHz) with increasing SNR. Number of Runs = 300.

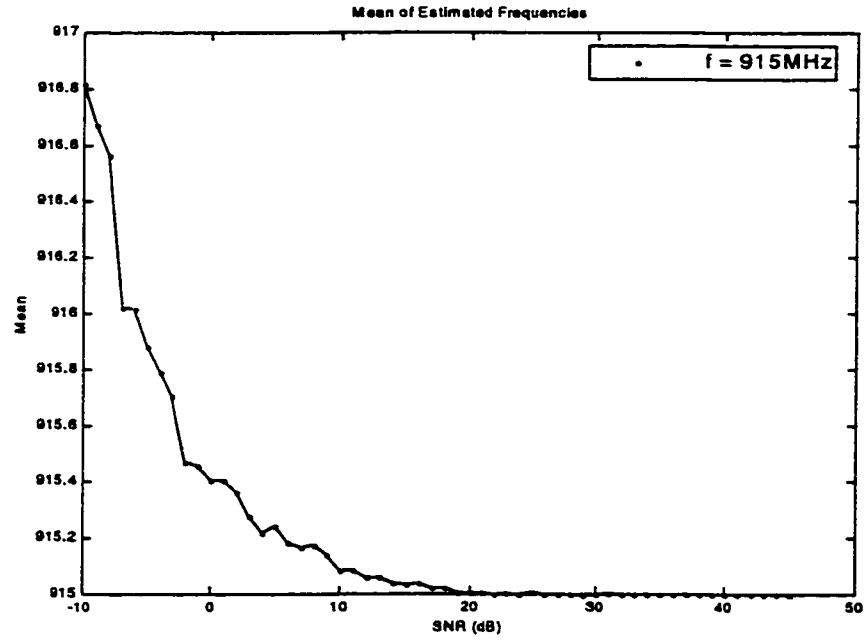

Figure 5.7-5: Mean of Estimated Frequency (f = 915 MHz) with increasing SNR (σ given in Figure 5.6-4). Number of Runs = 300.

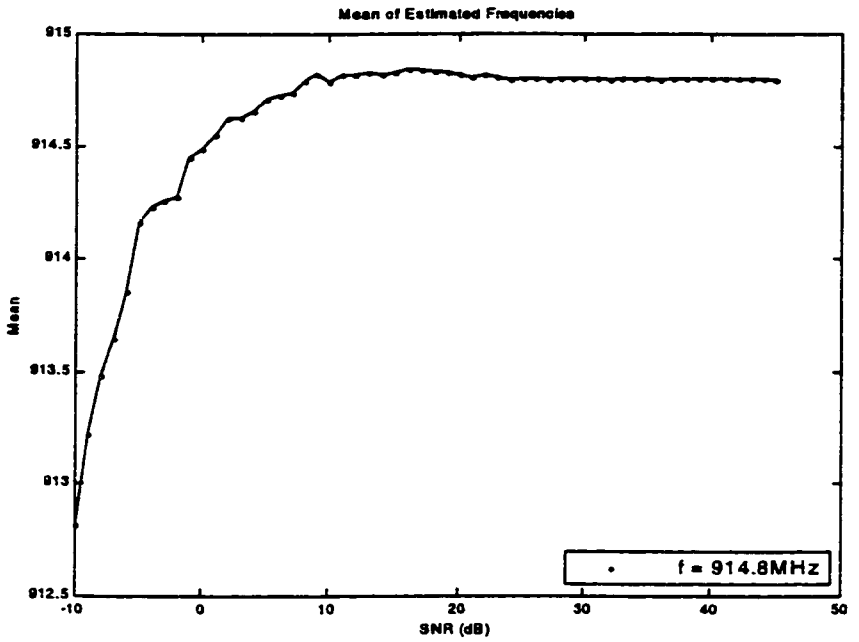

Figure 5.7-6: Mean of Estimated Frequency ($f = 914.8$) with increasing SNR (σ given in Figure 5.7-4). Number of Runs = 300.

5.8 Effect of Signal separation on ESPRIT estimate of DOA

Two signals with SNR of 20 dB each are taken for study. The separation between the signals is varied from 2^0 to 10^0. The actual DOAs of the signals are taken as -separation/2 and separation/2. For each value of separation, the standard deviation for 300 runs is calculated. Final results are presented in Figure 5.8-1. As seen from the graph, the standard deviation of the estimates is large if the separation is small. Thus two closely spaced sources are resolved with less accuracy. But as the separation is increased the standard deviation values decreases and resolution accuracy increases.

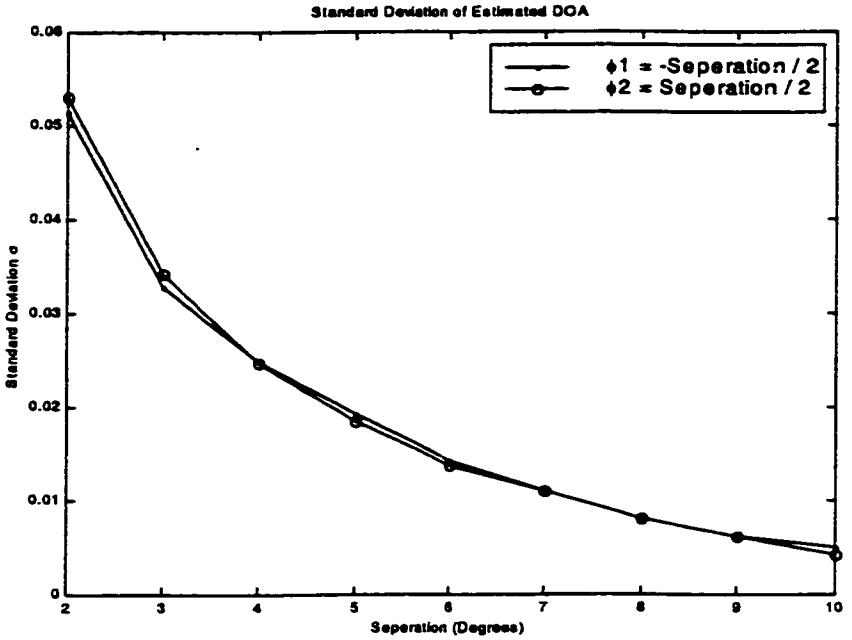

Figure 5.8-1:Standard deviation of Estimated angles with increasing separation. Number of runs for each value of separation = 300.

CHAPTER 6

CONCLUSIONS AND SUGGESTIONS

6.1 Conclusions

Null Steering and Pattern control in Smart Antenna Arrays for suppressing interference is successfully carried out. The ESPRIT algorithm for DOA estimation and the Numerical Pattern synthesis algorithm for null steering and pattern control have been implemented. Interferences like Co-Channel Interference, Multipath and Adjacent Channel Interference have been dealt with. The conclusions are summarized as below

- From this work it can be inferred that the abovementioned technique can be applied to interference suppression in an interference prone high performance mobile communication system. Having overcome with the problem of interference by nulling the same, the range and capacity of a cellular system can be greatly improved.

- In a variety of cases studied, where steering of single null to multiple nulls was carried out, the Numerical Patten Synthesis algorithm gave a set of complex weights with acceptable Amplitude and Phase Changes. Even after null steering the main-

beam remained unperturbed but for an evident increase in HPBW and a decrease in Directivity. When going from single null steering to multiple null steering, the Amplitude and Phase perturbations required gradually increased and the corresponding directivity along the desired direction showed a decrease.

- Also a calculation of Maximum Amplitude to Minimum Amplitude ratio and the Maximum Phase Change to steer the nulls were under agreeable limits which shows its practical reliability.

- It was possible to steer the main beam in any look direction with nulls in the estimated interfering direction. This makes possible for the Smart Antenna to update its pattern with each set of snapshots and adapt itself with the changing mobile environment by maintaining maximum directivity in the look direction.

- In the DOA and Frequency estimation, estimates with high accuracy were obtained even with signals closely spaced in space and frequency. As seen from Section 5.3.1, a desired signal and an interferer separated by just 3^0 were obviously resolved. Thus interferences in close vicinity of the desired user can also be mitigated. But the complex weight perturbations in such a case were large.

- Performing the statistical analysis by estimating the same DOAs for 100 trials, gave the mean values almost approaching the true values and a standard deviation of less than 0.01^0. This concludes that ESPRIT algorithm of DOA estimation is highly reliable and consistent.

- The Parameter estimates (DOA and Frequency) Of desired signal and interferences approach the true values as the SNR of the signals increases. Using the 10 element Linear Array, for two signals present, with their SNR greater than 10 dB, the mean values varied within 0.0025^0 and standard deviation was within 0.025^0 for 300 runs.

- Effect of increasing the number of elements of the array increases the resolution of the estimated parameters (DOA and Frequency).

- It is also seen that as the separation between the signals increases, more accurately the DOA of the signals can be resolved.

- Finally since the ESPRIT algorithm estimates the parameters from the computed Eigenvalues directly, it outperforms the other subspace-based algorithms, which involves a search over entire subspace. A comparison with the most popularly used MUSIC algorithm for DOA estimation shows ESPRIT algorithm to be advantageous over MUSIC algorithm for real time implementation. This is particularly important for implementation of Smart Antenna in mobile communications where, the antenna pattern has to dynamically adapt to the changing mobile environment.

6.2 Suggestions

- A real time implementation of Null Steering in Smart Antenna System can be attempted based on the results of this work. A proper hardware design can be carried out to emulate the signal processing for DOA and Null Steering.

- Instead of using the isotropic antenna elements, the use of different element patterns and its effect on Null Steering and Direction of Arrival can be investigated

- The use of planar arrays to be implemented in mobile satellite communication to achieve more directed beam is also an apt idea. In such a case both azimuth and elevation angles can be estimated and any direction in space can be accurately resolved.

- The effect of mutual coupling among the array elements can be studied and its affect on Null Steering and DOA can be investigated.

Nomenclature

$(.)^*$	Complex conjugate operator
$(.)^T$	Transpose operator
$a(\varphi_i)$	Steering Vector in the direction of φ_i
A	Steering Vector matrix
ACI	Adjacent Channel Interference
α_i	Complex amplitude of the i^{th} multipath component
CCI	Co-Channel Interference
d	Distance between elements
D_0	Maximum Directivity
DOA	Direction of Arrival
ESPRIT	Estimation of Signal Parameters via Rotational Invariance Technique
EV	Eigen Values
HPBW	Half Power Beam Width
ISI	Inter-Symbol Interference
k	$2\pi/\lambda$
K	Iteration Gain

m	Number of elements
MUSIC	MUltiple Signal Classification
n	Number of sources
φ	Azimuthal Angle
Φ	n x n matrix relating the Sub-Arrays
R_{pq}	E {p(t)*q(t)} is the covariance of the measured data obtained at sensor array p and sensor array q.
R_i^f	The covariance of the i^{th} forward Sub-Array
R_i^b	The covariance of the i^{th} backward Sub-Array
SAS	Smart Antenna System
θ	Elevation Angle
τ_i	Time Delay of the i^{th} multipath component

Appendix: Program Listing

```
%*************************************************************
%*    Function to calculate the Half Power Beam Width      *
%*************************************************************

function width=hpbw(power_norm_db,teta_deg, M)

  hpmax=find(power_norm_db==max(power_norm_db));

     for i1=hpmax:M+1,
          if power_norm_db(i1)<= -3
             u3db=i1;
             break
          else
          end
     end

     for i2=hpmax:-1:1,
          if power_norm_db(i2)<=-3
             l3db=i2;
             break
          else
          end
     end

  width=abs(teta_deg(i1)-teta_deg(i2));


************************** End ****************************
```

```
%*************************************************************
%*    Function to calculate the Steering Vector in a         *
%*    given Direction                                        *
%*************************************************************

function ur=pattern(angle,elements,d_by_lamda)

ur=[];

   for m=1:elements,
     ur=[ur exp(j*2*d_by_lamda*((m-1)*pi*sin(angle)))];
   end

ur=ur.';

************************** End ****************************
```

```
%*********************************************************
%*                    Esprit Function                    *
%*********************************************************
function bearing = esprit(ymat,dspace,nsource,delta)

%******************* Parameter checks *****************
[nsamp, msens] = size(ymat);
  if (msens == 1 | nsamp == 1)
    error('ymat - should be a matrix')
  end
  if (exist('dspace')  ~= 1) dspace  = 1/2; end
  if (exist('delta')  ~= 1) delta  = 1; end
  if (exist('nsource') ~= 1) nsource = 0; end
%*********************************************************

cmat = zeros(msens,msens);
ymat  = ymat - ones(nsamp,1) * mean(ymat);
cmat = conj(ymat' * ymat) / nsamp;
[umat, smat, vmat] = svd(cmat);
svec  = diag(smat);
Ksens = msens - delta;
ind1  = 1:Ksens;
ind2  = ind1 + delta;
uyy   = umat(ind1,1:nsource);
vzz   = umat(ind2,1:nsource);
aa=[uyy';vzz'];
bb=[uyy vzz];
ab=aa*bb;

  if size(ab)==[2 2]
    dvec  = eig( (uyy') * vzz);
  else
     [abvec abval]=eig(ab);
     ab1=abvec([1:nsource],[nsource+1:2*nsource]);
  ab2=abvec([nsource+1:2*nsource],[nsource+1:2*nsource])
     dvec1=-ab1*inv(ab2);
     [dval,dvec]=eig(dvec1);
     dvec=diag(dvec);
  end

     angle_vector=angle(dvec);
     dvec = angle(dvec)/(2*pi*dspace*delta);
     bearing = asin(dvec) * 180/pi;

************************* End ****************************
```

```
%*********************************************************
%* Program to find the Direction Of Arrival of signals *
%* uncorrelated with each other. The algorithm used is *
%* ESPRIT                                               *
%*********************************************************

function angles = esprit_angles_estimate(K,M,...
 samples,teta_incident,power_db)

%K - Number of sources
%M - Number of sensors
%samples - Number of snapshots
%teta_incident- Direction of Arrival of the signals
%power_db - SNR (dB) of the signals

%*********************************************************

d_over_lamda=.5;
p=10.^(power_db/10);
a=[];
psi=[];
ymat=zeros(samples,M);
ymat1=[];
angular_resolution=.1;
psi=[2*pi*d_over_lamda*sin(teta_incident)];

for source=1:K,
   for element=1:M,
      a(source,element)=exp(i*(element-1)*psi(source));
   end
   y(:,source)=randn(samples,1)*sqrt(p(source));
   ymat1=y(:,source)*a(source,:);
   ymat=ymat+ymat1;
end

for sa=1:M,
 ymat(:,sa)=ymat(:,sa)+randn(samples,1);
end

  angles=esprit(ymat,d_over_lamda,K,1);

************************* End ****************************
```

```
%*********************************************************
%*   ESPRIT function for simultaneous estimation of      *
%*   Direction of Arrival and Frequency                  *
%*********************************************************
function [angle_vector,tmat] = esprit2(ymat,nsource,...
 delta)

%******************* Parameter checks *****************
[nsamp, msens] = size(ymat);
if (msens == 1 | nsamp == 1)
 error('ymat - should be a matrix')
end
if (exist('delta')  ~= 1) delta  = 1; end
if (exist('nsource') ~= 1) nsource = 0; end
%*********************************************************

cmat = zeros(msens,msens);
ymat  = ymat - ones(nsamp,1) * mean(ymat);
cmat = conj(ymat' * ymat) / nsamp;
[umat, smat, vmat] = svd(cmat);
tmat  = vmat(:,1:msens);

Ksens = msens - delta;
ind1  = 1:Ksens;
ind2  = ind1 + delta;
uyy   = umat(ind1,1:nsource);
vzz   = umat(ind2,1:nsource);
aa=[uyy';vzz'];
bb=[uyy vzz];
ab=aa*bb;

if size(ab)==[2 2]
  dvec  = eig( (uyy') * vzz);
else
[abvec abval]=eig(ab);
ab1=abvec([1:nsource],[nsource+1:2*nsource]);
ab2=abvec([nsource+1:2*nsource],[nsource+1:2*nsource]);
dvec1=-ab1*inv(ab2);
[dval,dvec]=eig(dvec1);
dvec=diag(dvec);
end

angle_vector=angle(dvec);

************************ End ****************************
```

```
%*********************************************************
%* Function to find the Direction Of Arrival and         *
%* Frequency of signals uncorrelated from each other     *
%*********************************************************

function [finalangle,finallamda]=esprit_ang_freq...
   (M,K,samples,teta_incident,freq,power_db,freq_desired)

% M -  Number of sensors
% K - Number of sources
% samples - Number of snapshots
% teta_incident - Assumed directions of arrival
% freq - Frequency of the signals

%****************** Variable Declarations ***************
K1=K;
c=3*10^8;
lamda=c./freq;
max_freq=freq_desired;
min_lamda=c/max_freq;
d_xy=0.5*min_lamda;
d_xz=0.5*min_lamda;
p=10.^(power_db/10);
a_xy=[];
a_xz=[];
psi_xy=[];
ymat_xy=zeros(samples,M);
ymat1_xy=[];
psi_xz=[];
ymat_xz=zeros(samples,M);
ymat1_xz=[];
teta_disp=30*pi/180;
%*********************************************************
psi_xy=[2*pi*(d_xy./lamda).*sin(teta_incident)];
psi_xz=[2*pi*(d_xz./lamda).*sin(teta_incident +
teta_disp)];

for source=1:K,
 for element=1:M,
  a_xy(source,element)=exp(i*(element-1)*psi_xy(source));
  a_xz(source,element)=exp(i*(element-1)*psi_xz(source));
 end
  y(:,source)=randn(samples,1)*sqrt(p(source));
  ymat1_xy=y(:,source)*a_xy(source,:);
  ymat1_xz=y(:,source)*a_xz(source,:);
```

```
  ymat_xy=ymat_xy+ymat1_xy;
  ymat_xz=ymat_xz+ymat1_xz;
end

rand_samp_xy=[];
rand_samp_xz=[];
for sa=1:M,
  rand_samp_xy(:,sa)=randn(samples,1);
  rand_samp_xz(:,sa)=randn(samples,1);
end

ymat_xy=ymat_xy + rand_samp_xy;
ymat_xz=ymat_xz + rand_samp_xz;
[samp, sens] = size(ymat_xy);

[eig_vec1,tmatxy]=esprit2(ymat_xy,K,1);
[eig_vec2,tmatxz]=esprit2(ymat_xz,K,1);

for prim1 =1:K,
   eta1=eig_vec1(prim1);
 for prim2=1:K,
   eta2=eig_vec2(prim2);
   lamda_est(prim1,prim2)=(2*pi*d_xy*sin(teta_disp)) /...
    sqrt((((d_xy/d_xz)*eta2-eta1*cos(teta_disp))^2) + ...
       (eta1*sin(teta_disp))^2);
   angles_all(prim1,prim2)=asin(eta1 /...
       (2*pi*(d_xy / lamda_est(prim1,prim2))))*180/pi;
 end
end

int_lamda=lamda_est;
int_angle=angles_all;
st=[];
sm=[];
for pp=1:K,
  for p1=1:K1,
     for p2=1:K,
        st= exp(sqrt(-1)*(2*pi*(d_xy/lamda(pp)))...
           *sin(angles_all(p1,p2)*pi/180)*[0:sens-1]');
       sm(p1,p2) =(st'*tmatxy(:,K+1:M)*tmatxy...
          (:,K+1:M)'*st);
       smt(p1,p2)=abs(sm(p1,p2));
    end
 end
 done=1;
 min_sm1=min(min(smt));
 [ro1,co1]=find(smt==min_sm1);
```

```
max_sm=max(max(smt));
max_sm=max_sm+1;
while done==1;
   lamda_diff=abs(lamda(pp)-lamda_est);
   min_lamda_diff=min(min(lamda_diff));
   min_sm=min(min(smt));
   [ro,co]=find(smt==min_sm);
   if abs(lamda(pp)-lamda_est(ro,co))==...
         min_lamda_diff
      finalangle(pp)=angles_all(ro,co);
      finallamda(pp)=lamda_est(ro,co);
      break
   else
      smt(ro,co)=max_sm;
      if smt/max_sm==1
         finalangle(pp)=angles_all(ro1,co1);
         finallamda(pp)=lamda_est(ro1,co1);
         break
      end
   end
end
lamda_est1=[];
angles_all1=[];
for del_row=1:K1,
   if del_row ~= ro
      lamda_est1=[lamda_est1;...
            lamda_est(del_row,:)];
      angles_all1=[angles_all1;...
            angles_all(del_row,:)];
   else
   end
end
K1=K1-1;
lamda_est=lamda_est1;
angles_all=angles_all1;
sm=[];
smt=[];
end
```

```
%*********************************************************
%* Program to find the Direction Of Arrival of signals *
%* in the signal environment of both correlated and    *
%* uncorrelated signals. Spatial Smoothing technique   *
%* is used to deal with correlated case                *
%*********************************************************

function bearing = esprit_coherent_power(N,KD,KR,...
 samples,teta_incident_direct,...
 teta_incident_reflected,power_db_direct,attn)

%KD - Number of direct signals
%KR - Number of reflected signals
%N - Number of sensors
%samples - Number of snapshots
%teta_incident- Direction of Arrival of the signals
%power_db - SNR (dB) of the signals
%attn - Attenuation of the reflected coherent signals

%***************  Variable Declarations ***************

L=N-1;                          %length of the subarray
d_over_lamda=.5;                %Element seperation
pd=10.^(power_db_direct/10);
row_desired=find(pd==max(pd));
pr=pd(row_desired).*attn;
p=[pd pr];
teta_incident=[teta_incident_direct...
      teta_incident_reflected];
K=KR+KD;
a=[];
psi=[];
ymat=zeros(samples,N);
ymat1=[];

%*********************************************************

psi=[2*pi*d_over_lamda*sin(teta_incident)];
dist_from_ref=[0:1:N-1];

for source=1:K,
  aa1(source,:)=exp(i*dist_from_ref*psi(source));
end
```

```
yy1=randn(samples,1);

for source=1:K,
 if (source>KD)|(source==1)
    y(:,source)=yy1*sqrt(p(source));
    ymat1=y(:,source)*aa1(source,:);
    ymat=ymat+ymat1;
 else
    y(:,source)=randn(samples,1)*sqrt(p(source));
    ymat1=y(:,source)*aa1(source,:);
    ymat=ymat+ymat1;
 end
end

for sa=1:N,
 ymat(:,sa)=ymat(:,sa)+randn(samples,1);
end

rf=zeros(L);
for fo=1:(N-(L-1))
  ri = conj(ymat(:,fo:(fo+(L-1)))'*...
    ymat(:,fo:(fo+(L-1)))) / samples;
 rf=rf+ri;
end

rb=zeros(L);
ymat=conj(ymat);

for fb=N:-1:L
 rj=conj(ymat(:,fb:-1:fb-(L-1))'*...
    ymat(:,fb:-1:fb-(L-1))) / samples;
 rb=rb+rj;
end

rr= (rf+rb) / L;
[umat, smat, vmat] = svd(rr);
Ksens = L-1;
ind1  = 1:Ksens;
ind2  = ind1 + 1;
uyy   = umat(ind1,1:K);
vzz   = umat(ind2,1:K);

 aa=[uyy';vzz'];
bb=[uyy vzz];
ab=aa*bb;
if size(ab)==[2 2]
dvec  = eig( (uyy') * vzz);
```

```
else
   [abvec abval]=eig(ab);
 ab1=abvec([1:K],[K+1:2*K]);
 ab2=abvec([K+1:2*K],[K+1:2*K]);
 dvec1=-ab1*inv(ab2);
 [dval,dvec]=eig(dvec1);
 dvec=diag(dvec);
end

dvec = angle(dvec)/(2*pi.*d_over_lamda*1);
bearing = asin(dvec) * 180/pi;
```

********** **End** **********

```
%*********************************************************
%* Function to find the Direction Of Arrival of the     *
%* signals along with their respective frequencies in   *
%* an environment where both correlated and             *
%* uncorrelated signals are present. Spatial smoothing  *
%* technique is used to deal with correlated case       *
%*********************************************************

function [angles,lamdas]=esprit_coherent_freq(N,KD,...
   KR,samples,teta_incident_direct,...
   teta_incident_reflected,freq_direct,freq_reflected,...
   desired_freq,power_direct,attn)

% N - Number of sensors
% KD - Number of direct signals
% KR - Number of indirect signals
% samples - Number of snapshots
% teta_incident_direct - DOA  of direct signals
% teta_incident_reflected - DOA of reflected signals
% freq_direct - frequency of the direct signals
% freq_reflected - frequency of the reflected signals
% desired_freq - desired frequency
% power_direct - power in db of direct signals
% attn - attenuation of the reflected signals

%**************  Variable Declarations *****************

K=KD+KR;
K1=K;
L=N-1;
teta_incident=[teta_incident_direct...
      teta_incident_reflected]*pi/180;
c=3*10^8;
freq=[freq_direct freq_reflected]*10^6;
lamda=c./freq;
desiredlamda=c/(desired_freq*10^6);
d_xy=0.5*(c/max(freq_direct*10^6));
d_xz=0.5*(c/max(freq_direct*10^6));
row_desired=find(freq_direct==desired_freq);
pd=10.^(power_direct/10);
pr=pd(row_desired).*attn;
p=[pd pr];
a_xy=[];
```

```
a_xz=[];
psi_xy=[];
ymat_xy=zeros(samples,N);
ymat1_xy=[];
psi_xz=[];
ymat_xz=zeros(samples,N);
ymat1_xz=[];
teta_disp=30*pi/180;

%*********************************************************

psi_xy=[2*pi*(d_xy./lamda).*sin(teta_incident)];
psi_xz=[2*pi*(d_xz./lamda).*sin(teta_incident+teta_disp)];

yy1=randn(samples,1);
for source=1:K,
   for element=1:N,
      a_xy(source,element)=...
         exp(i*(element-1)*psi_xy(source));
      a_xz(source,element)=...
         exp(i*(element-1)*psi_xz(source));
   end
   if (source > KD)|(source==1)
      y(:,source)=yy1*sqrt(p(source));
   else
      y(:,source)=randn(samples,1)*sqrt(p(source));
   end

   ymat1_xy=y(:,source)*a_xy(source,:);
   ymat1_xz=y(:,source)*a_xz(source,:);
   ymat_xy=ymat_xy+ymat1_xy;
   ymat_xz=ymat_xz+ymat1_xz;
end

rand_samp_xy=randn(samples,N);
rand_samp_yz=randn(samples,N);
ymat_xy=ymat_xy+rand_samp_xy;
ymat_xz=ymat_xz+rand_samp_yz;

[samp, sens] = size(ymat_xy);

rfxy=zeros(L);
rfxz=zeros(L);
for fo=1:(N-(L-1))
   rixy = conj(ymat_xy(:,fo:(fo+(L-1)))'*...
      ymat_xy(:,fo:(fo+(L-1)))) / samples;
   rixz = conj(ymat_xz(:,fo:(fo+(L-1)))'*...
```

```
      ymat_xz(:,fo:(fo+(L-1)))) / samples;
   rfxy=rfxy+rixy;
   rfxz=rfxz+rixz;
end

rbxy=zeros(L);
rbxz=zeros(L);

ymat_xy=conj(ymat_xy);
ymat_xz=conj(ymat_xz);

for fb=N:-1:L
   rjxy=conj(ymat_xy(:,fb:-1:fb-(L-1))'*...
      ymat_xy(:,fb:-1:fb-(L-1))) / samples;
   rjxz=conj(ymat_xz(:,fb:-1:fb-(L-1))'*...
      ymat_xz(:,fb:-1:fb-(L-1))) / samples;
   rbxy=rbxy+rjxy;
   rbxz=rbxz+rjxz;
end

 rrxy= (rfxy+rbxy) / L;
 rrxz= (rfxz+rbxz) / L;

[eig_vec1, tmatxy]=esprit2(rrxy,K,1);
[eig_vec2, tmatxz]=esprit2(rrxz,K,1);

spec=[];

   for prim1 =1:K,
      eta1=eig_vec1(prim1);
      for prim2=1:K,
         eta2=eig_vec2(prim2);
         lamda_est(prim1,prim2)=(2*pi*d_xy*...
            sin(teta_disp))/sqrt(((d_xy/d_xz)*...
            eta2-eta1*cos(teta_disp))^2) +...
          (eta1*sin(teta_disp))^2);
         angles_all(prim1,prim2)=asin(eta1 /...
            (2*pi*(d_xy /lamda_est(prim1,prim2))));
          d_xy_by_lamda=d_xy/lamda(prim1);
          est_vector=pattern(angles_all(prim1,prim2), ...
            N,d_xy_by_lamda);
          angles_all(prim1,prim2)= ...
            angles_all(prim1,prim2)*180/pi;
      end
   end

   int_angle=angles_all;
```

```
int_lamda=lamda_est;

st=[];
sm=[];
for pp=1:K,
   for p1=1:K1,
      for p2=1:K,
         st= exp(sqrt(-1)*(2*pi*(d_xy/lamda(pp)))*...
            sin(angles_all(p1,p2)*pi/180)*[0:L-1]');
         sm(p1,p2) =(st'*tmatxy(:,K+1:L)*...
            tmatxy(:,K+1:L)'*st);
         smt(p1,p2)=abs(sm(p1,p2));
      end
   end
   done=1;
   min_sm1=min(min(smt));
   [ro1,co1]=find(smt==min_sm1);
   max_sm=max(max(smt));
   max_sm=max_sm+1;

   while done==1;
      lamda_diff=abs(lamda(pp)-lamda_est);
      min_lamda_diff=min(min(lamda_diff));
      min_sm=min(min(smt));
      [ro,co]=find(smt==min_sm);
      if abs(lamda(pp)-lamda_est(ro,co))==min_lamda_diff
         finalangle(pp)=angles_all(ro,co);
         finallamda(pp)=lamda_est(ro,co);
         break
      else
         smt(ro,co)=max_sm;
         if smt/max_sm==1
            finalangle(pp)=angles_all(ro1,co1);
            finallamda(pp)=lamda_est(ro1,co1);
            break
         end
      end
   end

   lamda_est1=[];
   angles_all1=[];
   for del_row=1:K1,
      if del_row ~= ro
         lamda_est1=[lamda_est1;lamda_est(del_row,:)];
         angles_all1=[angles_all1;...
               angles_all(del_row,:)];
      else
```

```
      end
   end
   K1=K1-1;
   lamda_est=lamda_est1;
   angles_all=angles_all1;

   sm=[];
   smt=[];

end

directangle=[];
directlamda=[];

for ks=1:KD
   for kall=1:K
      selectdirect=int_angle(ks,:)-finalangle(kall);
      if all(selectdirect)==0
         directangle=[directangle finalangle(kall)];
         directlamda=[directlamda finallamda(kall)];
      else
      end
   end
end

difference=abs(directlamda-desiredlamda);
mindifference=min(difference);
row_lamda=find(difference==mindifference);
mainbeamangle=directangle(row_lamda);
mainbeamlamda=directlamda(row_lamda);

interfer_angle=finalangle-mainbeamangle;
row_interfer=find(interfer_angle~=0);
interferangle=finalangle(row_interfer);
interferlamda=finallamda(row_interfer);

angles=[mainbeamangle interferangle];
lamdas=[mainbeamlamda interferlamda];
```

```
%*********************************************************
%*    Iterative Algorithm for Null Steering and Pattern *
%*    synthesis                                          *
%*********************************************************
clc
clear all
N=input('Enter the number of elements: ');
samples=input('Enter the number of snapshots: ');
n_sources=input('Enter the number of sources: ');
teta_incident_deg=input('Enter the DOA of signals: ');
teta_incident=teta_incident_deg*pi/180;
p_dB=input('Enter the SNR(dB)of the signals: ');

%*********** Run the estimate algorithm ***************

angles=esprit_angles_estimate(n_sources,N,...
 samples,teta_incident,p_dB)

%************** Load the estimated angles *************

angle_desired=[];
angle_interfer=[];
hpbwf=[];
dirf=[];
length_angles=length(angles);
loc_max_power=find(p_dB==max(p_dB));
teta_max_power=teta_incident(loc_max_power);
angles_diff=abs(angles-teta_max_power*180/pi);

for sort_teta=1:n_sources
 if angles_diff(sort_teta)==min(angles_diff)
    angle_desired=angles(sort_teta);
 else
    angle_interfer=[angle_interfer angles(sort_teta)];
 end
end

angles=[angle_desired angle_interfer];

%*************** Variable Declarations ******************

variance=1;        %Variance of noise(Noise Power)
spacing=0.5;       %Spacing between elements in lamda
M=1000;            %No of divisions of teta
D=-60;             %Desired null depth
```

```
K=500;              %Iteration gain
teta_interfer_deg=[];

%*********************************************************

ang_desired_deg=angles(1);
ang_desired_rad=ang_desired_deg*pi/180;
u_desired =pattern(ang_desired_rad,N,spacing);

%***Interference directions with zero power initially ***

teta_interfer_deg=angles([2:length_angles]);
nos_interfer=length(teta_interfer_deg);
teta_interfer=teta_interfer_deg*pi/180;
zeta=zeros(1,nos_interfer);
iteration=2;
stop=0;

%****************** Iteration loop *********************

while stop==0

%************* Calculation of weight vector ************

cov_interfer=zeros(N);

for t=1:nos_interfer,
 ui(:,t)=pattern(teta_interfer(t),N,spacing);
cov_interfer=cov_interfer+zeta(t)*conj(ui(:,t))*ui(:,t).'
end

phi=variance*(eye(N)+cov_interfer);
weight(:,iteration)=inv(phi)*conj(u_desired);

%************* Directivity Calculation ******************

for teta=1:M+1,
 teta_rad(teta)=-((M/2)-(teta-1))*pi/M;
 u=pattern(teta_rad(teta),N,spacing);
 power(teta)=abs((weight(:,iteration).')*u);
 u1(teta)   =power(teta)*power(teta);
 u2(teta)=u1(teta)*cos(teta_rad(teta));
end

yd=trapz(teta_rad,u2);
pow=2*pi*yd;
u1_max=max(u1);
```

```
dirf=[dirf 4*pi*ul_max/pow];

%Normalising the pattern w.r.t to the desired direction

   power_max=max(power);
   power_norm=power/power_max;
   power_norm_dB=20*log10(power_norm);

   for teta=1:M+1,
       teta_deg(teta)=-((M/2)-(teta-1))*180/M;
      if power_norm_dB(teta)<-60
         power_norm_dB(teta)=-60;
      end
   end

   if iteration==2,
      init_pattern=power_norm_dB;
      hpbwi=hpbw(power_norm_dB,teta_deg,M);
   end

     hpbwf=[hpbwf hpbw(power_norm_dB,teta_deg,M)];

      condition=[];

   for t=1:nos_interfer,
       p(t)=abs((weight(:,iteration).')*pattern(...
        teta_interfer(t),N,spacing))/power_max;
      d=10^(D/20);
      power_net(t)=zeta(t)+K*(p(t)-d);
      zeta(t)=max(0,power_net(t));
      p_dB1(t)=20*log10(p(t));
   end

for t=1:nos_interfer,
 condition=[condition (p_dB1(t)<=D)];
end

if (condition==1)
 nos_iterations=iteration
 break
else
end

if ((weight(:,iteration-1)==weight(:,iteration)))
 nos_iterations=iteration
 break
else
```

```
end

iteration
iteration=iteration+1;

end

amplitude_change=abs(weight(:,iteration))-...
 abs(weight(:,2))
initialamp=abs(weight(:,2))
initialphase=angle(weight(:,2))*180/pi
finalamp=abs(weight(:,iteration))
finalphase=angle(weight(:,iteration))*180/pi
phases_rad=angle(weight);
phases_deg=phases_rad*180/pi;
phase_changes=phases_deg(:,iteration)-phases_deg(:,2);
phase_changes1=unwrap(phase_changes*pi/180,pi)*180/pi
complex=weight(:,nos_iterations);

figure(1)
plot(teta_deg,init_pattern,'b:',teta_deg,...
  power_norm_dB, 'k-');
legend('Initial Pattern','Final Pattern',0)
xlabel('Phi in degrees');
ylabel('Array Pattern Normalized (dB)');
text([teta_interfer_deg],[1*ones(1,length_angles-1)],...
   '\downarrow');
grid on;

figure(2)
gev_est=exp(sqrt(-1)*2*pi*(spacing)*sin(angles*pi/180));
gev_true=exp(sqrt(-1)*2*pi*(spacing)*sin(teta_incident));
real_gev_est=real(gev_est);
imag_gev_est=imag(gev_est);

real_gev_true=real(gev_true);
imag_gev_true=imag(gev_true);

plot(real_gev_est,imag_gev_est,'k.',real_gev_true,...
 imag_gev_true,'bo');
title('DOA: Estimated(Above the point);True(Below the
point)')
legend('Estimated Eigen Values','True Eigen Values',0)
xlabel('Real Part of Eigen Values');
ylabel('Imaginary Part of Eigen Values');

for pl=1:n_sources
```

```
  display1=num2str(teta_incident_deg(pl));
 text(real_gev_true(pl),imag_gev_true(pl)-.09,...
    [display1 '\circ']);
end

angles=round(angles*1000)/1000;
for pl=1:n_sources
 display2=num2str(angles(pl));
 text(real_gev_est(pl),imag_gev_est(pl)+.09,...
    [display2 '\circ']);
end

xlim([-1.2 1.2]);
ylim([-1.2 1.2]);
```

Bibliography

[1] Theodore S. Rappaport, "Future Trends of Mobile and Personal Communications", *IEEE Proceedings of IMOC,* Vol. 1, pp. 387-395, 1995.

[2] Joseph C. Liberti. Jr and Theodore S. Rappaport, "Smart Antennas for Wireless Communications: IS–95 and Third Generation CDMA Applications", *Prentice Hall Inc,* New Jersey, 1999.

[3] Mark Goldburg and Mike Lynd, "Tutorial on Smart Antennas", *http://news.wirelessdesignonline.com/design-features/19980127-92.html,* January 1998.

[4] L. C Godara, "Application of Antenna Arrays to Mobile Communications, Part I: Performance improvement, Feasibility and System considerations", *Proceedings of the IEEE,* Vol. 85, No. 7, pp. 1031-1060, July 1997.

[5] L. C Godara, "Application of Antenna Arrays to Mobile Communications, Part II: Beam-Forming and Direction Of Arrival considerations", *Proceedings of the IEEE,* Vol. 85, No. 8, pp. 1195-1245, August 1997.

[6] R. T Compton Jr, "Adaptive Antennas", *Prentice Hall Inc,* New Jersey, 1988.

[7] R. Mozingo and T. Miller, "Introduction to Adaptive Arrays", *John Wiley and Sons,* New York, 1980.

[8] Hudson J. E., "Adaptive Array Principles", *Peter Peregrinus Ltd.,* New York, 1981.

[9] William F. Gabriel, "Adaptive Processing Array Systems", *Proceeding of the IEEE,* Vol. 80, No. 1, pp. 152-162, January 1992.

[10] Richard H. Roy, "Application of Smart Antenna Technology in Wireless Communication Systems", *http://www.arraycomm.com* ,

[11] Roy Richard H., "Overview of Smart Antenna Technology: The Next Wave in Wireless Communications", *Proceedings of the IEEE Aerospace Conference,* Vol. 3, pp. 339-345, 1998.

[12] R. Kohno, "Spatial and Temporal Communication Theory Using Adaptive Antenna Arrays", *IEEE Personal Communications,* Vol. 5, No. 1, pp. 28-35, February 1998.

[13] Arogyaswami J Paulraj and Boon Chong Ng, "Space Time Modems for Wireless Personnel Communications", *IEEE Personal Communications,* Vol. 5, No. 1, pp. 36-35, February 1998.

[14] Jack H. Winters, "Smart Antennas for Wireless Systems", *IEEE Personal Communications,* Vol. 5, No. 1, pp. 23-27, February 1998.

[15] S. Choi, D. Shim, T. K. Sarkar, "A Comparison of Tracking Beam Array and Switching Beam Array operating in a CDMA Mobile Communication Channel", *IEEE Antennas and Propagation Magazine,* Vol. 41, No. 6, pp. 10-56, December 1999.

[16] B. Pattan, "Robust Modulation Methods and Smart Antennas in Wireless Communications", *Prentice Hall Inc,* New Jersey, 2000.

[17] M. H. Er, and Y. H. Sng, "A New GSC Beamformer Employing DOA Estimation and Null Steering", *ICCS / ISITA 'Communications on the move',* Vol. 2, pp. 816-820, 1990.

[18] A. H. El-Zooghby, C. G. Christodoulou, Michael Georgiopoulos, "A Neural Network Based Smart Antenna for Multiple Source Tracking", *IEEE Transactions on Antennas and Propagation,* Vol. 48, No 5, pp. 768-776, May 2000.

[19] A. H. El-Zooghby, Southall, H. L., Christodoulou C. G., "Experimental Validation of a Neural Network Direction Finder", *IEEE Antennas and Propagation Society, AP-S International Symposium (Digest),* Vol. 3, pp. 1592-1595, 1999.

[20] Per Zetterberg and Björn Ottersen, "The Spectrum Efficiency of a Base Station Antenna Array System for Spatially Selective Transmission", *IEEE Transactions on Vehicular Technology,* Vol. 44, No. 3, August 1995.

[21] S. Ponnikanti, and S. Sali, "Application of Antenna Arrays for Spatial Separation in Wireless Systems", *IEEE International Conference on Personal Wireless Communications,* pp. 243-246. 1996.

[22] Y. H. Sng, M. H. Er, Y. C. Soh, "Partially Adaptive Array Design using DOA estimation and Null Steering", *IEE Proceedings of Radar, Sonar Navigation,* Vol. 142, No. 1, February 1995.

[23] Richard J. Kozick, Frank J. Elmer and Vahakn Nalbandian, "Phased Arrays composed of Antennas with Steerable Patterns", *IEEE International Radar Conference,* pp. 737-741, 1995.

[24] S. Choi, Hyeongdong Kim and Byungcho Choi, "An Adaptive Algorithm for Computing the Primary Eigenvector with a Linear Complexity for a Smart Antenna System in a CDMA Channel, *http://dsplab.hanyang.ac.kr/cgi/index.cgi?7,*

[25] Xu B., Vu T. B., "Effective Interference Cancellation Scheme based on Smart Antennas", *Electronic Letters,* Vol. 33, No. 13, pp. 1114-1116, June 1997.

[26] Haimovic A. M. and Shah, "Performance of Space-Time Processing for Suppressing Narrow Band Interference in CDMA Communications", *Wireless Personal communications,* Vol. 7, No 2-3, pp. 233-255, August 1998.

[27] Ibars C., Bar-Ness and Yeheskel, "Interference Cancellation for Downlink TDMA Systems using Smart Antennas", *IEEE Global Telecommunications Conference,* Vol. 4, pp. 2233-2237, 1999.

[28] Saleeb Adel A., "Design of a Smart Antenna for reducing Co-Channel Interference in cellular mobile communications", *IEEE Antennas and Propagation Society, AP-S International Symposium (Digest),* Vol. 3, pp. 1620-1623, 1999.

[29] D. H. Johnson, "The Application of Spectral Estimation methods to Bearing Estimation Problems", *Proceedings of the IEEE,* Vol. 70, pp. 1018-1028, 1982.

[30] S. V. Shell and W. A. Gradner, "High Resolution Direction Finding", Chapter 17, K. Base and C. R. Rao, pp. 755-817, 1993.

[31] M. S. Barlett, "An Introduction to Stochastic Process", *Cambridge University press,* New York, 1956.

[32] J. Capon, "High Resolution Frequency-Wavenumber Spectral Analysis", *Proceedings of the IEEE,* Vol. 57, No. 8, pp. 1408-1418, August 1969.

[33] J. P. Burg, "Maximum Entropy Spectral Analysis", *37th Annual Meeting, Society Exploration Geophysics,* Oklahoma, 1967.

[34] R. O. Schmidt, " Multiple Emitter Location and Signal Parameter Estimation", *Proceedings of RADC Spectrum Estimation Workshop,* Griffiss AFB, New York, pp. 243- 258, 1979.

[35] R. O. Schmidt, "Multiple Emitter Location and Signal Parameter Estimation", *IEEE Transactions on Antennas and Propagation,* Vol. AP-34, No. 3, March 1986.

[36] R. O. Schmidt and R. E. Franks, "Multiple Source DF Signal Processing: An Experimental System", *IEEE Transactions on Antennas and Propagation,* Vol. AP-34, No. 3, pp. 281-290, March 1986.

[37] S. V. Schell, Calabretta, W. A. Gardner and B. G. Agee, "Cyclic MUSIC Algorithms for Signal Selective DOA Estimation', *Proceedings of the International Conference on Acoustics, Speech and Signal Processing-89,* pp. 2278-2281.

[38] A. J. Barabell, "Improving the Performance of Eigenstructure Based Direction Finding Algorithms", *Proceedings of the International Conference on Acoustics, Speech and Signal Processing-83,* pp. 336-339, 1983.

[39] A. Paulraj, R. Roy and T. Kailath, "A Subspace Rotation Approach to Signal Parameter Estimation", *Proceedings of the IEEE,* Vol. 74, No. 7, pp. 1044-1045, July 1986.

[40] A. Paulraj, R. Roy and T. Kailath, "Estimation of Signal Parameters via Rotational Invariance Techniques-ESPRIT", *Proceedings of the 19th Asilomar Conference on Circuits and Systems,* pp. 83-89, 1985.

[41] R. Roy and T. Kailath, "ESPRIT-Estimation of Signal Parameters via Rotational Invariance Techniques", *IEEE Transactions on Acoustics, Speech and Signal Processing,* Vol. 37, No. 7, pp. 984-995, July 1986.

[42] R. Roy and T. Kailath, "ESPRIT-Estimation of Signal Parameters via Rotational Invariance Techniques", *Optical Engineering,* Vol. 29, No 4, pp. 296-313, April 1990.

[43] J. E. Evans, J. R. Johnson, D. F. Sun, "High Resolution Angular Resolution Spectrum Estimation Techniques for Terrain Scattering Analysis and Angle of Arrival Estimation in ATC Navigation and Surveillance System", *M.I.T Lincoin Lab., Lexington, MA,* Rep. 582, 1982.

[44] T. J. Shan, M. Wax and T. Kailath, "On Spatial Smoothing for Estimation of Coherent Signals, *IEEE Transactions on Acoustics, Speech and Signal Processing,* Vol. ASSP-33, pp. 802-811, August 1985.

[45] K. Takao and N. Kikuma, "An Adaptive Array Utilizing an Adaptive Spatial Averaging Technique for Multipath Environments", *IEEE Transactions on Antennas and Propagation,* Vol. AP-35, No. 12, pp. 1389-1396, December 1987.

[46] F. Haber and M. Zoltowski, "Spatial Spectrum Estimation in a Coherent Signal Environment Using an Array in Motion", *IEEE Transactions on Antennas and Propagation,* Vol. AP-34, pp. 301-310, March 1986.

[47] J. Li and R. T. Compton, "Angle of Arrival Estimation of Coherent Signals Using and Array Doublet in Motion", *IEEE Transactions on Aerospace and Electronic Systems,* Vol. 30, No. 1, pp. 126-133, January 1994.

[48] Y. H. Chen and C. H. Chen, "Direction Of Arrival and Frequency estimation for Narrowband sources using two Single Rotation Invariance Algorithms with the Marked Subspace", *IEEE Proceedings of Radar and Signal Processing,* Vol. 139. No. 4, pp. 297-300, August 1992.

[49] S. U. Pillai and B. H. Kwon, "Forward/ Backward Spatial Smoothing Techniques for Coherent Signal Identification", *IEEE Transactions on Acoustics, Speech and Signal Processing,* Vol. 37, 1989.

[50] R. Roy, A. Paulraj and T. Kailath, "A Subspace Rotation Approach to Estimation of Parameters of Cisoids in Noise", *IEEE Transactions on Acoustics Speech and Signal Processing,* Vol. ASSP-34, No. 5, October 1986.

[51] T. H. Ismail and M. M. Dawoud, "Null Steering in Phased Arrays by Controlling the Element Positions ", *IEEE Transactions on Antennas and Propagation,* Vol. AP-39, No 11, pp. 1561-1566, November 1991.

[52] T. H. Ismail, M. M. Dawoud, "Experimental Verificatoin of Null Steering by Element Position Perturbations", *IEEE Transactions on Antennas and Propagation,* Vol. AP-40, No 11, pp. 1431-1434. November 1992.

[53] A. Tennant, M. M. Dawoud, A. P. Anderson, "Array Pattern Nulling by Element Position Perturbation using a Genetic Algorithm", *Electronic Letters,* Vol. 30, No. 3, pp. 174-176, February 1994.

[54] M. M. Dawoud, "Null Steering in Scanned Linear Arrays by Element Position Perturbations", *International Journal of Electronics,* Vol. 78, No. 4, pp. 743-757, 1995.

[55] C. A. Olen and R. T. Compton, "A Numerical Pattern Synthesis Algorithm for Arrays", *IEEE Transactions on Antennas and Propagation,* Vol. 38, No. 10, pp. 1666-1676, October 1990.

[56] W. P. Liao and F. L. Chu, "Application of Genetic Algorithms to Phase only Null Steering of Linear Arrays", *Electromagnetics,* pp. 171-183, 1997.

[57] W. P. Liao and F. L. Chu, "Null Steering in Planar Arrays by controlling only Current Amplitudes using Genetic Algorithms", *Microwave and Optical Technology Letters,* pp. 97-103, 1997.

[58] R. J. Mitchell, B. Chambers and A. P. Anderson, "Array Pattern control in the complex plane Optimized by a Genetic Algorithm", *IEE 10th International Conference on Antennas and Propagation,* No. 436, pp. 1330-1333, April 1997.

[59] M. J. Mismar and T. H. Ismail, "Null Steering using Minimax Approximation by controlling only the Current Amplitudes", *International Journal of Electronics,* Vol. 78, No. 2, pp. 409-415, February 1995.

[60] T. H. Ismail and M. J. Mismer, "Null Steering with Arbitrary Phase Perturbations using Dual Phase Shifters", *Journal of Electromagnetic Waves and Applications,* Vol. 13, No. 8, pp. 1021-1029, 1999.

[61] H. Steyskal, "Simple Method for Pattern Nulling by Phase Perturbations", *IEEE Transactions on Antennas and Propagation,* Vol. AP-31, pp. 163-166, January 1983.